SESSION III

FUEL AND TARGET FABRICATION AND CROSS-SECTION DATA

CHAIRMAN: S. PILATE

CO-CHAIRMAN: R.J.M. KONINGS

SESSION III
CHAIRMAN: S. PILATE

New concrete achievements were obtained in fabrication and irradiation of americium and technetium. In the frame of the EFTTRA programme, an americium target was fabricated and irradiated. However, as the target was not sufficiently homogeneous, under irradiation it swelled substantially. Improved methods of fabrication are needed to eliminate this disadvantage.

It is interesting to note that the Americium Laboratory is planned to be operational at ITU in the year 2000. As there will be extra-shielding, targets containing some curium mixed with americium will also be handled. Further irradiation is planned in the High Flux Reactor with Am and Tc targets in order to achieve higher burnup.

In the progress of research work on the nitride fuel cycle at JAERI, an important aspect was mentioned: the recycling of ^{15}N could probably be done on an industrial scale with a good recovery yield (90 %), thus providing minimised costs linked to ^{15}N.

The knowledge of the physical characteristics of Tc metal and of Tc-Ru alloys was progressively enlarged.

The merits of the high thermal flux reactor at Grenoble (ILL) were shown; it was capable of determining with high accuracy the cross-section data of minor actinides. This reactor has D_2O as coolant and moderator. The example of the capture cross-section of $^{242}Am_{gs}$ was given showing the JEF 2.2 file was largely in error; however, this discrepancy was recently resolved.

Recent results were then presented from two major experimental facilities; IRMM in Geel and at CERN in Geneva. In the linac of Geel, GELINA, in close co-operation between CEA-Saclay and IRMM scientists, two investigations were recently conducted; one on the total cross-section of ^{237}Np, and the other on the total and capture cross-sections of ^{99}Tc in the resonance region. The quality of the measurements in GELINA is well known, as measurement of cross-sections is frequently done on the request of JEF2.

The TARC experiment measuring ^{99}Tc and ^{129}I capture cross-sections was described. Small samples were irradiated in the centre of a large block of pure lead with neutrons produced by spallation. While these results are of high quality, one should not extrapolate the transmutation yields on small samples to the case of the Energy Amplifier, where large quantities of Tc and I should be loaded and dispersed. One difficulty will be to minimise self-shielding effects in the targets.

FEASIBILITY OF THE FABRICATION OF AMERICIUM TARGETS

D. Haas, J. Somers
European Commission
Institute for Transuranium Elements
Postfach 2340
76125 Karlsruhe
Germany

A. Renard, A. La Fuente
Belgonucleaire
Avenue Ariane 4
1200 Bruxelles,
Belgium

Abstract

The paper compares the processes used at ITU for the fabrication of americium targets for transmutation: powder mixing process, sol-gel method and the infiltration by an active solution of inactive pellets. The advantages of the latter processes, related mainly to the lower level of dust formation, are stressed. Moreover, the radiological constraints on the fabrication as a function of Am content and of selected fabrication process are evaluated. As conclusion, the feasibility of Am target fabrication has been demonstrated on a laboratory scale, based on experimental results evaluation. The penalties due to radiological constraints in a semi-industrial process are acceptable. The future developments consist in the construction of a laboratory fully dedicated to minor actinides fuel pins or targets fabrication.

Introduction

In the frame of the P&T programme, the transmutation of separated minor actinides and fission products requires the necessary step of manufacturing targets to be irradiated in specific reactors.

Fabrication of Pu-bearing fuels (MOX) both for LWR's or FBR's has now been mastered industrially, in Belgium, France, Germany, and Great Britain using powder blending processes. However, when fabrication of much more radioactive materials, like americium, curium or long-lived fission products is considered, dust production and consequent radiation exposure to personnel could limit the applicability of these mechanical processes. Therefore, alternative fabrication routes have been envisaged. The final selection of the fabrication routes relies on following evaluation parameters:

- Their technical feasibility.
- The quality and quantity of wastes produced.
- The accumulation of the dose to the personnel during fabrication and handling of the materials.
- The irradiation behaviour of the fuels and targets produced.
- The economical feasibility

In this paper, the first three aspects will be dealt with.

For the fabrication of fuels or targets containing highly radioactive elements, the following alternative processes can be compared with the mechanical blending of powders.

Gelation techniques

Gelation techniques have been developed and are still in use, in particular in Switzerland (PSI), Germany (ITU), and Russia.

These methods involve the dissolution of the starting materials (alternatively, if located at the reprocessing plant, the active solutions are readily available) followed by controlled droplet to particle conversion for the production of flowable microspheres. These are then pressed into pellets. The process produces little dust and can be automated readily.

These methods are particularly well suited in the frame of P&T strategies because of the high radio-toxicity of the active materials, but also of the limited capacity required in the manufacturing chains.

Hybrid gelation-blending methods

With hybrid methods we consider the combination of gelation techniques and mechanical mixture, for example particles made by gelation are mixed with inert matrices in the form of powders. These hybrid methods present similar advantages to the pure gelation methods, and allow larger output capacities.

Novel techniques

Advanced techniques are being developed. One of them is called INRAM (Infiltration of Radioactive Materials) [1,2]. It has been used for other applications in non-nuclear ceramics and for isolation of radioactive wastes, and has recently been applied for Am target fabrication. This process involves the dissolution of the active material and its infiltration into a porous (non-active) medium. Infiltration into porous green pellets drastically reduces the number of production steps involving handling of highly radioactive materials.

Americium Target Fabrication at ITU

General Requirements and Specifications

The term "Americium targets for transmutation" does not define the product to be manufactured, even in general manner. Today, it just means that cylindrical pellets containing a (variable) amount of americium diluted in a preferably non-uranium matrix have to be manufactured and loaded in fuel pins, in geometries of either LWR's or FBR's! There are no well defined specifications for the pellet, but well a series of criteria (neutronic and materials properties, solubility, reaction with coolant …) that should lead to the selection of the dilution materials.

It is not the aim of this paper to review all alternatives of supporting matrices examined in the world. Let us just state that ITU, in the field of transmutation research, concentrates its efforts on following materials:

- Oxides of Am (stabilised with Zr), diluted in inert matrices of the types spinel ($MgAl_2O_4$), MgO, or stabilised ZrO_2. The type of microstructure (homogeneous mixture, or so-called macro-masses of Am-rich particles in the matrix) is a parameter that must be considered in the development stage.
- A mixed oxide of AmO_{2-x} and ThO_2 chosen per analogy with UO_2, which presents the advantage of an easier licensability of the product.
- Nitrides, for their good thermal conductivity. However, this subject, based on specific processes, will not be discussed in this paper.

The elaboration of specifications of such new materials is made following continuous exchanges between the designers, the manufacturers, and the final users, namely today the operators of the experimental facilities like PHENIX or Material Testing Reactors.

In case of Am targets, a particular difficulty exists in the quality control of the fuel, because of the specific nature of the compounds.

Sol-gel method

The sol-gel coprocessing process (Fig. 1), developed originally at ITU for the production of MOX fuels, has also been used to fabricate U-Pu-Am-Np oxide fuels for the transmutation and incineration of americium and neptunium. In this procedure, a droplet to particle conversion process is used to produce beads (ϕ = 20 - 300 μm) with high mechanical stability, so that dust formation is eliminated. Furthermore, the free flowing beads reduce the fabrication steps and facilitate automation of the process.

At the heart of the sol-gel beads production step is an ammonia precipitation of the metal hydroxides from an aqueous solution, which requests the need of the active solution preparation. Waste solutions can be recovered and recycled.

Today, the sol-gel method is used for the development work on the fabrication of $(ZrAm)O_2$ + inert matrices, using cerium as a simulant for Am. The fabrication parameters have to be adopted to obtain good quality pellets (dimensions, stability, density, visual aspect ...), and taking into account the wishes of the designer to have the Am particles distributed heterogeneously in the matrix (to the contrary of all present requests for industrial MOX fabrication!). This is therefore a particular challenge.

Figure 1. **Pellet fabrication procedures**

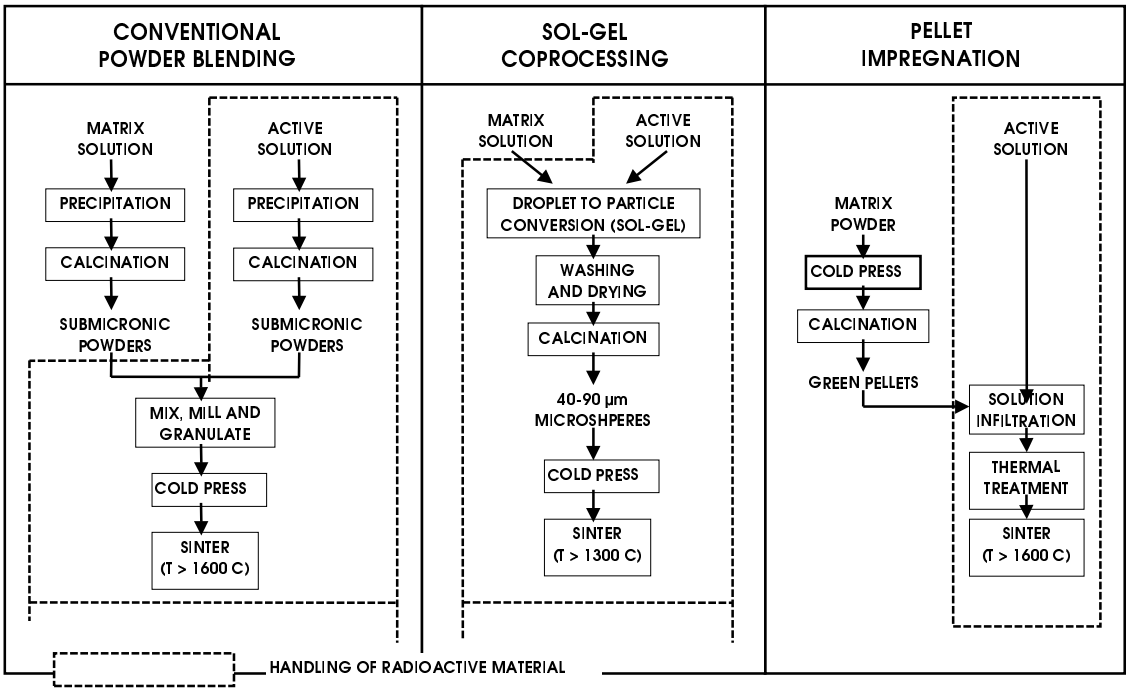

INRAM method

The flow sheet for the fabrication of INRAM pellets is shown and compared with the sol-gel and mechanical blending methods in Figure 1. The main advantage of this method is that matrices with low or zero activity can be fabricated and formed into the required shape in an unshielded facility. The matrix material is then introduced into the shielded glove-box and immersed in a solution of the infiltrant in a controlled way. Thereafter the resulting material is treated thermally to convert the infiltrant into the desired chemical form, and sintered to produce the product pellets. As no precipitation or washing steps are required within the shielded area, the radioactive wastes produced in the process are negligible. The fabrication process can also be performed in facilities combining remote handling for the fabrication steps and standard glove-box technology should intervention be required.

The infiltration process relies on the action of capillary forces to draw the solution into the pores of the host material. The application of this process to the fabrication of transmutation and incineration targets requires that the pellet is insoluble in the solution containing the infiltrant and that the infiltrant should be easily convertible into its desired chemical form.

The concentration of the second phase introduced into the pellet can be controlled by adjusting the concentration of the infiltrant solution to the porosity of the pellet. Immersion of green spinel pellets with 50% porosity in a 400 g/L Am solution yielded a final product with 11 $^{w}/_{o}$ Am. Tailored distributions of the infiltrant can be obtained by complete immersion of the pellet and control of the immersion time and/or by sealing selected surfaces of the pellet.

The infiltration of radioactive materials (INRAM) method was used to produce two fuel pins, containing 11 $^{w}/_{o}$ Am in spinel for the EFTTRA-T4 [3] irradiation in HFR Petten, which is now completed. In the pre-fabrication phase, test pellets with 9 $^{w}/_{o}$ Am were fabricated. A relatively uniform Am distribution throughout the pellets was obtained for the pre-fabrication test pellets. The pellets for the EFTTRA-T4 irradiation were produced in exactly the same way, but the total Am content was 11 $^{w}/_{o}$. The Am distribution within the pellet was not as uniform as in the pre-fabrication tests. In particular, α-autoradiography showed a roughly cylindrical symmetric shell (200 μm thick) within the pellet in which the Am content was higher than the surrounding regions. EPMA revealed an Am concentration of 14 $^{w}/_{o}$ within this band and 9 $^{w}/_{o}$ elsewhere. This is most probably due to a diffusion process during the thermal treatment in the steps involving liquid to solid Am nitrate and/or nitrate to oxide conversion. The guaranteed homogeneity requires further investigations of these effects. Optical microscopy of the samples has shown that using the INRAM method, the Am containing particles have a diameter of 2 - 3 μm.

Technical feasibility of the fabrication

Handling of highly radioactive materials and the fabrication of targets containing minor actinides should be considered at both laboratory and industrial scales. At the ITU a minor actinide laboratory is being developed to cover the needs of the ITU and its partners for the fabrication of fuels and targets in the framework of test irradiation programmes (e.g. EFTTRA and CAPRA) and to make tests for future industrial applications. The handling facilities (see Fig. 2) consist of shielded cells combining the protection of a hot cell with the flexibility of a glove-box. These hybrid cells are equipped with manipulators and biological protection (water and lead) for direct handling of minor actinide containing fuels and targets. When the minor actinides are removed from the box, or shielded *in situ*, access to the boxes can be obtained using conventional glove-box procedures. In this way, equipment can be exchanged or modified within the cell or even the entire glove-box behind the protection wall can be replaced. Thus the high level of flexibility necessary for research and development can be maintained. The laboratory is currently being modified and cells incorporating powder preparation (sol-gel and INRAM methods), pellet pressing, sintering, control and pin fabrication are being built.

Fabrication methods based on sol-gel or infiltration (INRAM) could provide alternative means for the preparation of targets for transmutation and incineration. Due to the low levels of dust formation, both processes are compatible with the handling facilities in use at the ITU. Further investigations are required to provide process data for these procedures which would permit their scaling up for industrial production. A possible flow sheet for an industrial scale application of the INRAM process is shown in Fig. 3, which shows a rough evaluation of the flow of materials required for each step, corresponding to the quantity of americium which would be available annually from 50 LWR's [3] in a strategy that would produce about 1 ton Am/year. In this flow sheet, assumptions have been made regarding the Am content in the fuel (10 $^{w}/_{o}$), fuel length and equipment capacities. The number of different equipment required is given on the flow sheet. Only one immersion tank would be required. Industrial application will require extensive if not complete automation and adequate shielding, and further evaluation assessments of the radiation dose. A similar evaluation could be done for a plant relying on sol-gel method.

Figure 2. **Minor actinide laboratory: lay-out**

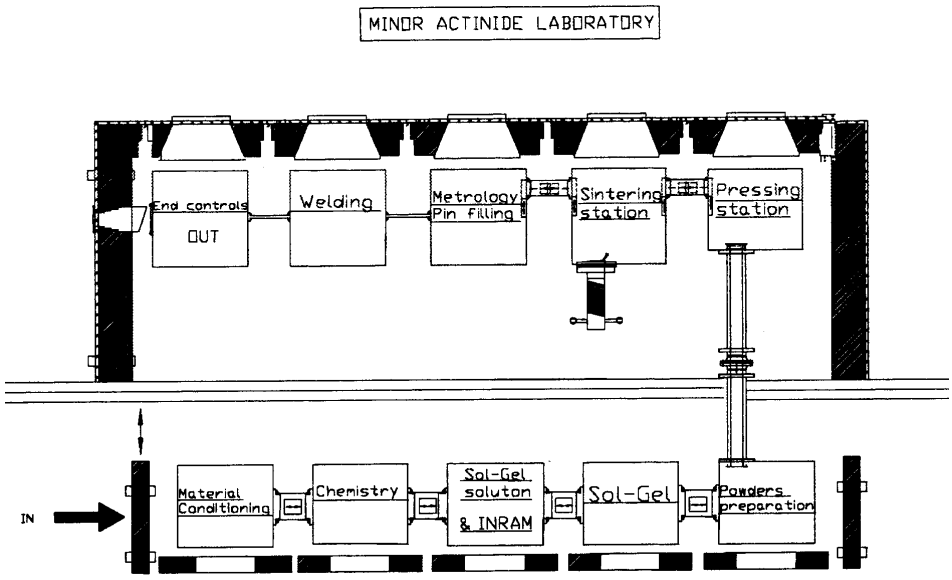

Figure 3. **Flow sheet for americium target fabrication INRAM process 1 ton Am/year**

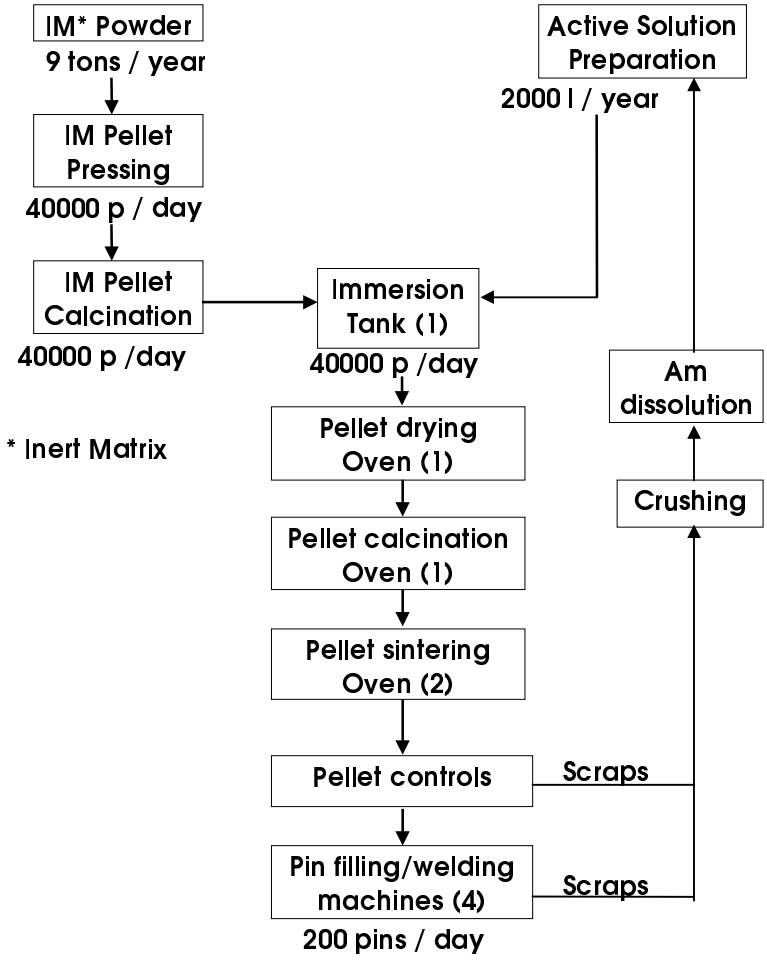

Radiological constraints

Due to the high activity of the minor actinide materials, the feasibility of the fabrication of Am targets depends very much on the additional radiation protection measures necessary for each process step as well as for the storage of the primary Am material and the transport of the fabricated product.

The semi-industrial process implies, in comparison with the laboratory techniques:

- The handling of bigger quantities of materials which induces higher dose rates and the need of increased automation of the process.
- The adoption of maintenance procedures due to production constraints.
- Additional costs associated with the radioprotection and automation equipment.

The radiological constraints are a function of the content of americium in the targets and of the density of the support material.

Comparison with standard MOX fuel

Specific conditions of fabrication and transport of Am target pins for recycling in LWR cores are analysed by comparison with the current (U-Pu) MOX fuel fabrication at BELGONUCLEAIRE - Dessel (Belgium). The equivalent dose rates are evaluated by means of 3D calculation techniques validated on benchmarks and experimental results obtained in the fabrication chain and around a transport container as well as from some measurements performed on a SUPERFACT pellet [6].

The front-end stages of the fabrication process are the most critical ones because the heat and radiation sources are concentrated in the primary material. One example is the comparison of the storage of the same amount of pure PuO_2 and AmO_2 powders in a shielded cavity of a typical MOX fabrication plant, which shows an increase of the total dose rate in front of the doors by a factor 82, for the americium oxide case.

Further in the process, the handling of a target pin, designed for insertion in a PWR fuel assembly with 20% AmO_2 in an inert matrix for instance, induces a total dose rate behind a 10 mm thick Plexiglas layer, which is about 1500 times higher than when handling a PWR MOX pin with 7.8% Pu. Indeed, the dose due to PWR MOX is weak, but for any case of AmO_2 content higher than about 2% in such a target pin, a reinforced protection made of lead glass (or steel) is necessary to fulfil the current dose rate limit criteria at some distance from the glove box. The reduction of the autoabsorption of gamma rays in the inert matrix compared to an UO_2 matrix plays an important role.

At the back-end stage, the transport of a large number of target pins, either towards the fuel assembly mounting hall or already grouped in a Am-dedicated assembly, would require a big reinforcement of the lead shielding of the cask licensed for fresh MOX fuel, so that it could be more appropriate to use a cask designed for irradiated fuel, but it would be oversized and very heavy.

Feasibility evaluation

The comparison with the MOX fuel fabrication conditions applies to the Am-target pin fabrication by the conventional powder blending process. The conclusion is that it is preferable to establish a fabrication chain dedicated to Am targets in shielded cells with some automation equipment, using specific transport containers, instead of adapting standard MOX fuel equipment.

The required additional protections are quite feasible, although they are cumbersome and they increase the costs. However, the penalties due to these constraints in a semi-industrial process seem quite acceptable.

As the radioprotection constraints are mostly conditioned by the radioactive sources, proportional to the Am content of the pellets, and by the density of the pellet matrix, the fabrication technique has only a very limited influence on the order of magnitude of the dose rate due to a target rod during handling and transport. Consequently, the additional protections for those operations are similar for each technique.

But the fabrication technique has an important effect on the secondary radiations due to dust, waste, and possible contamination. The advantages of the INRAM technique are namely due to the reduced number of fabrication steps involving highly radioactive materials and to the liquid nature of the infiltrant, so that the hazard of radioactive dusts can be minimised, as well as the risk of contamination within the glove boxes.

Conclusion

For the fabrication of fuels and targets containing Minor Actinides (in particular Am), processes that produce minimal quantities of dust and waste are recommended.

In particular, ITU has demonstrated on a laboratory scale, the feasibility of the infiltration (INRAM) technique consisting of the infiltration of the active solution (Am nitrate solution) into a non-active matrix (a porous pellet in this case) by capillary forces. Tests are still required to permanently avoid the heterogeneity sometimes observed in the americium distribution, which were probably due to diffusion during thermal treatment.

Theoretical studies performed during the last years, as well as experimental results on ion-bombardment of inert matrices, however, predict that for Am-containing targets macro-dispersions of the fissile phase are to be preferred to micro-dispersions, in order to limit radiation damage in the matrix due to alpha-decay and stopping of fission products [3].

The current research at ITU in this field is as follows:

- improvement of INRAM methods: to apply this method on porous beads instead of pellets to obtain higher actinide contents (up to 40 $^{w}/_{o}$) and guaranteed homogeneous distributions
- macro-dispersion fuels: to fabricate inert matrix fuels containing Am in inclusions of sizes > 50 μm by mixing Am containing spheres (produced by gelation methods) with inert matrix powders.

Both processes are the reference for the minor actinides fabrication laboratory currently under construction.

REFERENCES

[1] K. Richter, A. Fernandez, and J. Somers, J. Nucl. Mater. 249 (1997) 121-127.

[2] A. Fernandez, K. Richter, J. C. Closset, S. Fourcaudot, C. Fuchs, J. F. Babelot, R. Voet, and J. Somers, Proceedings of CIMTEC'98, Florence, 1998.

[3] R. J. M. Konings *et al.,* Proceedings of OECD/NEA Workshop on Advanced Reactors with Innovative Fuels, 21-23 Oct. 1998.

[4] L. H. Baetslé, Proceedings of Global 97 Conference, p. 207.

[5] A. Renard *et al*., Proceedings of Global'97 Conference, p. 484.

[6] A. Renard, A. La Fuente, S. Pilate, A. Harislur, H. Mouney, and M. Rome, Proceedings of the 4th International Information Exchange Meeting on Actinide and Fission Product Partitioning and Transmutation (1996) p. 189.

TRANSMUTATION OF AMERICIUM AND TECHNETIUM: RECENT RESULTS OF EFTTRA

R.J.M. Konings
Nuclear Research and Consultancy Group
P.O. Box 25, 1755 ZG Petten,
The Netherlands

G. Mühling
Forschungszentrum Karlsruhe,
Postfach 3640, 76125 Karlsruhe,
Germany

R. Conrad
European Commission,
Joint Research Centre,
Institute for Advanced Materials,
P.O. Box 2, 1755 ZG Petten,
The Netherlands

J. Rouault
Commisariat à l'Énergy Atomique,
Centre de Cadarache,
13108 Saint-Paul-Lez-Durance Cedex,
France

D. Haas
European Commission,
Joint Research Centre,
Institute for Transuranium Elements,
Postfach 2340, 76125 Karlsruhe,
Germany

G. Vambenepe
Electricité de France,
SEPTEN,
12-14 Avenue Dutrievoz,
69628 Villeurbanne Cedex,
France

Abstract

The results of irradiation experiments of the transmutation of technetium and americium, performed by the EFTTRA group, are described. First the results of the recent tests, T1 and T2, for technetium in the HFR are discussed. In two subsequent experiments targets of metallic technetium were transmuted to an extent of about 6% and 16%. Post-irradiation examination of the targets revealed an excellent in-pile behaviour. Secondly, the results of the T4 test, the transmutation of americium in a spinel-based fuel (micro-dispersed), are presented. It is shown that extensive swelling of the fuel took place, probably due to the damage of the matrix by fission product and/or accumulation of helium as a result of alpha decay. A more promising concept for an inert matrix fuel for transmutation of americium, based on a macrodispersion of a host phase in the inert matrix is discussed.

Introduction

EFTTRA, which is the acronym for Experimental Feasibility of Targets for Transmutation, is a network of research organisations in France, Germany and the Netherlands that was formed in 1992 [1]. The goal of EFTTRA is the study of transmutation of americium as well as of the long-lived fission products technetium (^{99}Tc) and iodine (^{129}I). The work of the partners of the EFTTRA group is focused on the development and testing of targets and fuels, taking into account the scenario's developed in Europe for possible P&T strategies. To that purpose fabrication routes are being investigated, irradiation tests are performed, and post-irradiation examinations are made in the various facilities of the EFTTRA partners. In Table 1 an overview is given of the EFTTRA irradiation experiments that are completed or ongoing at present.

In the present paper the results of the EFTTRA irradiations test on the transmutation of technetium and americium performed in the High Flux Reactor at Petten are described. A more detailed version of this paper has recently been presented at the OECD/NEA Workshop on Advanced Reactors with Innovative Fuels [3].

Table 1. **EFTTRA irradiation experiments**

Name[a]	Reactor	Description	State of the art	Refs
T1	HFR	Technetium and iodine	completed	3-6
T2	HFR	Technetium	completed	7
		Neutron damage in inert matrices	completed	8
T2bis	HFR	Neutron damage in inert matrices	completed	
T3	HFR	Neutron damage in inert matrices	PIE to be started	
		Dispersion inert matrix fuel using enriched UO_2	PIE to be started	
T4	HFR	Americium in spinel	PIE ongoing	9,10
T4bis	HFR	Americium in spinel	irradiation ongoing	
T4ter	HFR	Central fuel temperature of spinel/UO_2	irradiation ongoing	11
F1	Phénix	Neutron damage in inert matrices	continued	12
		Dispersion inert matrix fuel using enriched UO_2	PIE ongoing	12
F1A	Phénix	Neutron damage in inert matrices	irradiation ongoing	
		Dispersion inert matrix fuel using enriched UO_2	irradiation ongoing	
F2	Phénix	Technetium and iodine	start pending	

[a] Some of the experiments are also known under different names such as RAS or MATINA.

Transmutation of Technetium

The study of the transmutation of the technetium was started in 1992 when irradiation tests of targets of ^{99}Tc metal were planned for the High Flux Reactor (HFR) at Petten as well as the Phénix fast reactor at Cadarache (see Table 1). The fabrication of the targets for these tests was studied at ITU where a technique was developed for the fabrication of cylinders/pellets by casting of liquid technetium metal in a water-cooled copper mould. The targets that were fabricated for the irradiation tests each contained two of such cylinders (4.8 mm diameter, 25 mm length).

The results of the T1 test, which was completed in 1995, have been reported extensively [3-6]. They showed good behaviour of the technetium metal at an extent of transmutation of about 6%. To study the behaviour at an higher extent of transmutation, one of the targets (2 cylinders) of the T1 test was re-encapsulated and irradiated again in the HFR. The T2 test has been completed successfully in 1997 and the results of the post-irradiation examinations have become available recently and will be summarised shortly below.

Figure 1 **Microscopic cross section of irradiated Tc target from the T2 experiment showing oriented crystal growth (diameter 4.8 mm)**

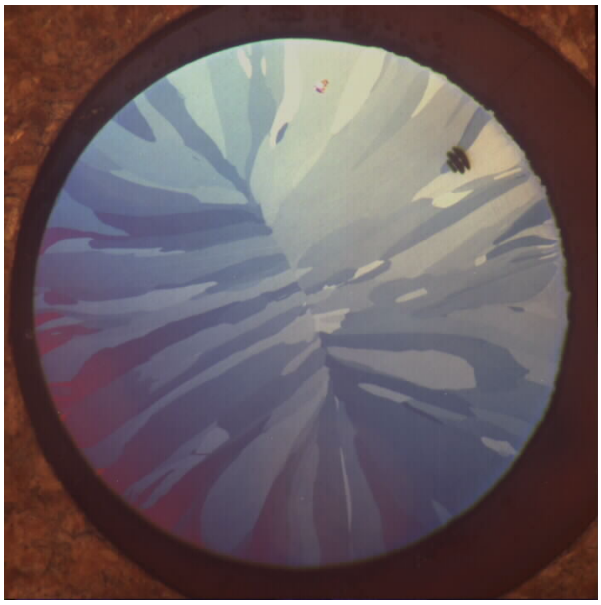

Figure 2 **A representative EPMA curve of the radial ruthenium concentration in technetium from the T2 experiment**

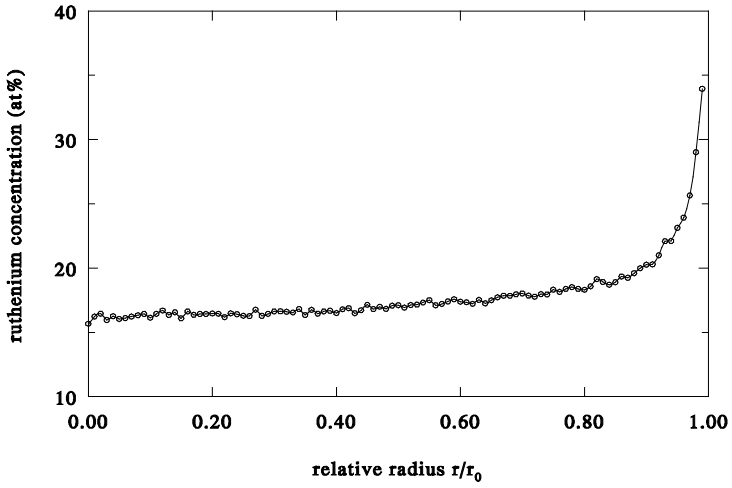

The cumulative irradiation time for the T2 experiments was 24 reactor cycles (579.3 full power days) during which the total neutron fluency accumulated to about 5.8×10^{26} m^{-2}. The post-irradiation examination (PIE) revealed an excellent in-pile behaviour of the metallic technetium rods. Metallographic examinations showed no changes in the microstructure compared to the unirradiated material. An example of a typical micrograph is given in Figure 1. Electron probe microanalysis (EPMA) of the radial distribution of ruthenium, the product of the transmutation process, showed an increase from about 15-16 % in the centre to 30-40 % near the rim of the pellets, giving a pellet-average Ru concentration of about 18 % (Figure 2). Mass spectrometric analysis of the pellet-average Ru concentration showed that the extent of transmutation is about 16 %.

From the results of the T2 test it is concluded that there are no technical limitations to the use of metallic technetium as a target for transmutation. No further EFTTRA irradiation experiments in the HFR are foreseen, but an irradiation test of the same material in the Phénix reactor (F2) is in preparation, as mentioned before.

Transmutation of Americium in an Inert Matrix

In 1995 the T4 experiment was initiated by the EFTTRA partners to study the feasibility of americium transmutation in a so-called once-through mode. In this scenario the extent of fissioning should be very high (>90%).The T4 experiment was performed as a shared cost action project in the cluster “P&T strategy studies and transmutation experiments” of the Fourth Framework Programme of the CEC (Contrat No. FI4I-CT95-0007)

For the T4 experiment pellets of magnesium aluminate spinel ($MgAl_2O_4$) containing about 10-12 ^{w}% ^{241}Am were fabricated by the newly developed infiltration method (INRAM) at ITU [9,13]. This methods yields a relatively fine distribution of the americium in the pellet [9,13]. However, it was observed that this distribution is not uniform and that the americium, intended to be present as an oxide, formed a compound during sintering, probably $AmAlO_3$. Two irradiation capsules were prepared.

Table 2 **Dimensional changes of the pellets of the T4 test derived indirectly from non-destructive examinations**

	Length (%)	Diameter (%)
Neutron radiography (mol[a])	+5.2	
Gamma spectrometry	+4.5	+6.7
Gamma tomography		+6.7

[a]Mol = mid-of-life (231.4 full power days)

The irradiation of the T4 target in the HFR at Petten has been performed from August 1996 to January 1998 (358.4 full power days), during which a burnup of 32% FIMA (value obtained from post-test burnup calculation) has been achieved. During the irradiation a neutron radiograph was made. After the irradiation the fuel was examined non-destructively in the hot-cell laboratories in Petten. The following results are now available [10]:

- Neutron radiography of the sample holder at mid-of-life shows no visible damage of the fuel pin and an increase of the length of the pellet stack (Table 2).

- Gamma-spectrometry and gamma-tomography of the fuel pin shows that the distribution of the fission products is correlated to the initial americium concentration of the pellets.
- Gamma-spectrometry and gamma-tomography of the fuel pin show an increase in length of the pellet stack and in the diameter of the pellets (Table 2).

Profilometry of the fuel pin showed an increase of the diameter of the cladding from 6.55 mm originally to 6.75 mm at maximum after irradiation (Figure 3).

Figure 3 .**The diameter of the cladding of the irradiated T4 rod (original diameter 6.55 mm)**

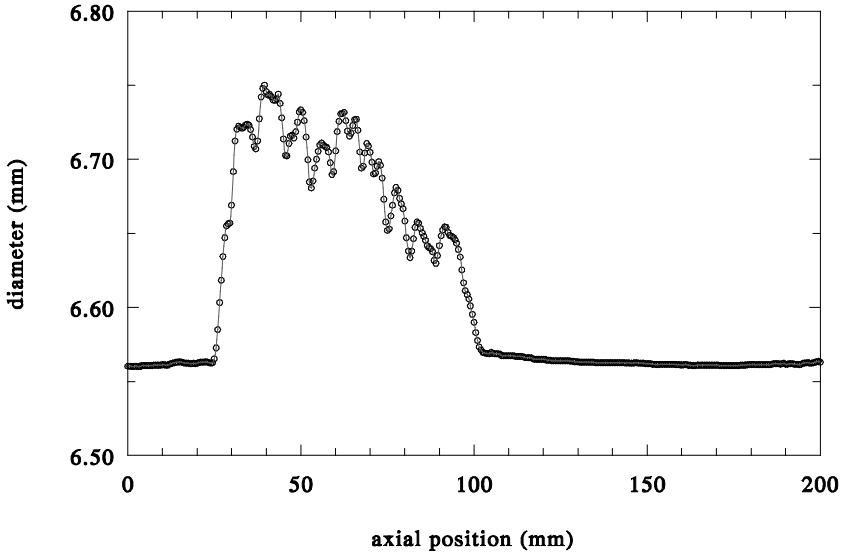

From the results it is clear that considerable swelling of the fuel occurred. From the data in Table 2 is can be calculated that the increase in volume is about 18%. This swelling can be caused by two different processes: (i) the damage of the spinel matrix by fission fragments, which can be extensive in this type of fuel due to the relatively small size of the americium dispersions, and (ii) the formation of gas bubbles containing helium that was produced by the alpha decay of ^{242}Cm, one of the isotopes in the transmutation chain of ^{241}Am. Destructive examinations to be performed at ITU have to confirm this.

The results of the T4 test, combined with results of theoretical studies and separate effect experiments, are being used to modify the design of as reported in a separate study [14]. It is proposed to use a so-called “hybrid” fuel, a dispersion of spherical inclusions (between 50 and 300 :m) of a host phase, which contains the americium, in a dense inert matrix. For the host phase the cubic solid solution $(Zr,Am)O_2$, possibly stabilised by yttrium, and for the inert matrix MgO (fast reactors) and $MgAl_2O_4$ (thermal reactors) are the most likely candidates.

REFERENCES

[1] J.F. Babelot, R. Conrad, W.M.P. Franken, J. van Geel, H. Gruppelaar, G. Mühling, C. Prunier, M. Rome and M. Salvatores, Proceedings GLOBAL'95, September 11-14, 1997, Versailles, France, Vol. 1, p. 524.

[2] J.N.C. van Geel, R. Conrad, R.J.M. Konings, G. Mühling, J. Rouault, G. Vambenepe, Proceedings OECD/NEA Workshop on Advanced Reactors with Innovative Fuels, October 21-23 1998, Villigen, Switzerland, in press.

[3] R.J.M. Konings, W.M.P. Franken, R. Conrad, J.-F. Guegnon and J.-C. Spirlet,. Nucl. Technol. 117 (1997) 293.

[4] R.J.M. Konings, J. Nucl. Mat. 244 (1997) 16.

[5] R.J.M. Konings, J.L. Kloosterman, J.A. Hendriks and H. Gruppelaar, Nucl. Sci. Eng. 128 (1998) 70.

[6] R.J.M. Konings, A.D. Stalios, C.T. Walker and N. Cocuaud, J. Nucl. Mat. 254 (1998) 122.

[7] R.J.M. Konings, K. Bakker, R. Conrad, C. Boshoven and H. Hein, J. Nucl. Mat. 254 (1998) 135.

[8] R.J.M. Konings and R. Conrad, J. Nucl. Mat., submitted.

[9] J.-F. Babelot, R. Conrad, R.J.M. Konings, G. Mühling, M. Salvatores and G. Vambenepe, J. Alloys Comp., in press.

[10] R.J.M. Konings et al., in preparation.

[11] R.J.M. Konings, K. Bakker, J. G. Boshoven, H. Hein, R. R. van der Laan, J. Nucl. Mater., submitted.

[12] N. Chauvin, T. Albiol, R. Mazoyer, J. Noirot, D. Lespieux, J. C. Dumas and J. P. Ottaviani, J. Nucl. Mater., submitted.

[13] K. Richter, A. Fernandez and J. Somers, J. Nucl. Mat., submitted.

[14] N. Chauvin, R.J.M. Konings and H.J. Matzke, J. Nucl. Mat., submitted

RECENT PROGRESS OF RESEARCH ON NITRIDE FUEL CYCLE IN JAERI

Yasufumi Suzuki, Toru Ogawa, Yasuo Arai and Takehiko Mukaiyama
Japan Atomic Energy Research Institute
Tokai-mura, Naka-gun, Ibaraki-ken, 319-1195,
Japan

Abstract

The present status of the research on the nitride fuel cycle for transmutation of minor actinides (MAs) in JAERI is described. The recent research focuses on the pyrochemical process and the database for fuel properties. As for the pyrochemical process, electrochemical studies have been carried out mainly by voltammetry to understand the electrodeposition of actinide elements in the LiCl-KCl system. The recovery of Np and Pu metals was demonstrated by electrolysis of the nitrides at gram-scale experiments. In relation to a new concept "LINEX", the evolution behaviour of N_2 gas was also examined by oxidation of NdN with $CdCl_2$ and it was confirmed that nitrogen in NdN may be recovered up to 95%. The properties of nitride fuel, such as thermal conductivity and irradiation behavior, have been investigated for the preparation of the database.

Introduction

Nitride fuel is a promising candidate for transmutation of MAs because of its excellent thermal and neutronic properties [1,2]. The advantages of nitride fuel have been confirmed through the research on the nitride fuel cycle and the recent interest focuses on the application of pyrochemical process with the LiCl-KCl eutectic melt to the nitride fuel cycle and the preparation of the database on fuel properties such as thermal conductivity and irradiation behaviour.

The pyrochemical process, which has been developed originally by the ANL laboratory [3], may be applicable to the reprocessing of nitride fuel with minor modifications as shown in Figure 1 [4], because actinide nitride is a good electric conductor and the free energy changes for the formation of chlorides from nitrides of actinides and most of FPs are similar to the case of metal fuel. This system may be convenient for recovering ^{15}N-enriched nitrogen gas, contrary to the Purex method where nitrate solution is used and the recovery of $^{15}N_2$ gas may be difficult. In order to confirm the applicability of the pyrochemical process to the nitride fuel cycle, the electrolysis of nitrides such as UN, NpN and PuN in the LiCl-KCl eutectic melt and the relating electrochemical studies have been carried out in JAERI [5-7]. In addition, a new concept, "LINEX", has been proposed as an alternative option as shown in Figure 1 [8]. In the LINEX process, actinide elements in spent nitride fuel are selectively dissolved as chlorides into the molten salt by electrolysis or oxidation and the actinide nitrides are synthesised from the chlorides by adding Li_3N, which is formed by the reaction of Li with $^{15}N_2$ gas released at the dissolution step of the spent nitride fuel.

Figure 1 **Concepts of nitride/pyroprocess for MA burning**

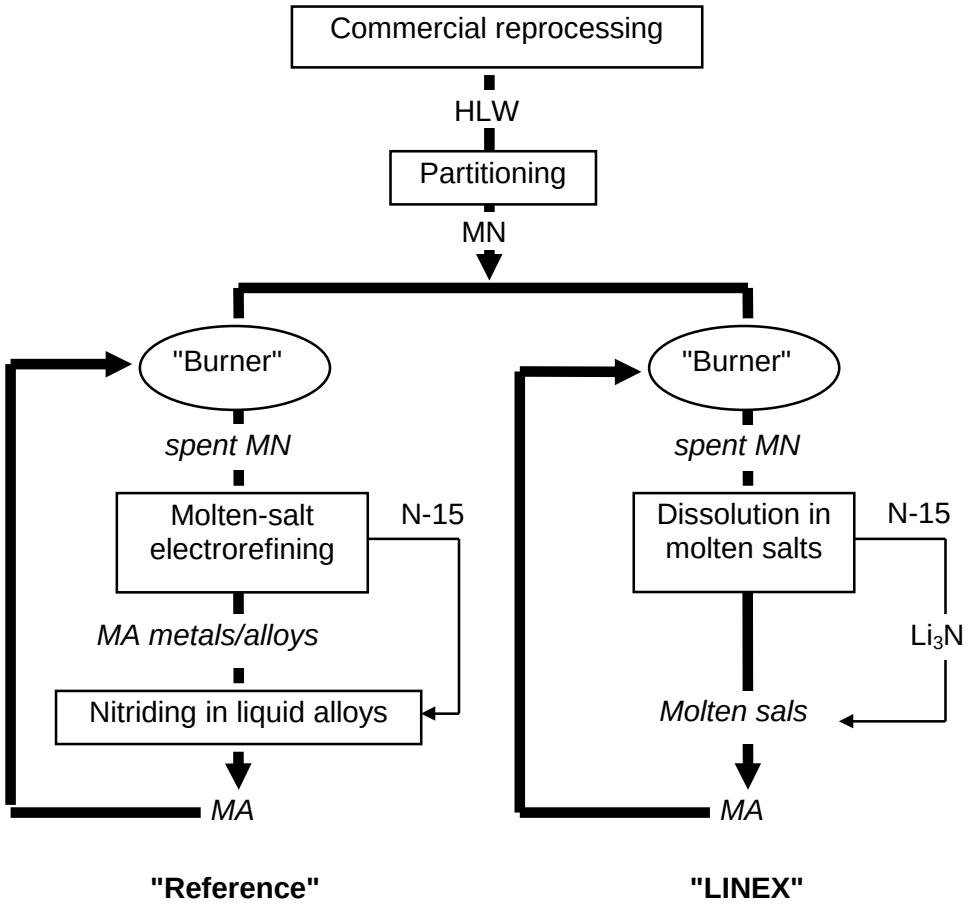

The properties of nitride solid solutions of the UN-NpN-PuN system, such as thermal conductivity and evaporation behavior, have been studied to prepare the database [9-12]. Furthermore, an equipment is being installed in the WASTEF of JAERI to study the fabrication of AmN. With regard to the irradiation behavior, the irradiation tests up to the burnup of about 5.5%FIMA in JMTR have been completed and it has been confirmed that nitride shows excellent performance, i.e., very low fission gas release of about 0.5%/%FIMA [9]. Uranium-plutonium mixed nitride fuel is under irradiation in JOYO with a collaboration with JNC up to a target burnup of about 4% FIMA to confirm the performance of nitride fuel in fast neutron circumstances.

This paper describes the present status of the research on nitride fuel cycle in JAERI, especially on the results obtained after the last meeting on P&T [13].

Pyrochemical Process of Nitride Fuel

Electrolysis of Actinide Nitrides

Electrode Reaction of Minor Actinides

The electrochemical behaviour of Np and Pu on the solid electrodes in the LiCl-KCl eutectic melt was studied by cyclic voltammetry [6] to understand the behavior of actinide elements in the molten salt and the electrodeposition on the electrodes. The chlorides of Np and Pu were prepared as the mixtures with LiCl-KCl by oxidation of $NpPt_3$ and Pu metal with $CdCl_2$ in the LiCl-KCl eutectic melt at 773 K, respectively.

The voltammogram of Pu in LiCl-KCl-0.54wt.%$PuCl_3$ with a Mo working electrode and a Ag/AgCl reference electrode was obtained in the temperature range of 773 – 973 K. The electrodeposition and dissolution of Pu can be expressed by the following equation,

$$Pu(III) + 3e^- = Pu.$$

The reaction is considered to be quasi-reversible and diffusion may be a rate-determining step. The observed potentials can be principally explained by the thermodynamic functions, but there were found some discrepancies caused perhaps from the interaction between the actinide metals and the surface of the electrode. The voltammogram of the system of LiCl-KCl-$NpCl_3$ showed similar behavior to the case of the LiCl-KCl-$PuCl_3$ system.

Recovery of actinide metals by electrolysis

The dissolution of NpN and PuN at the anode and the electrodeposition of the respective metals on the solid cathode were examined by electrolysis in gram-scale experiments [7]. The concentrations of actinide chlorides in the LiCl-KCl were about 0.54wt.%. Nitride samples were prepared by carbothermic reduction of the dioxides, NpO_2 and PuO_2, in a N_2-H_2 stream [14].

Figure 2. **Cyclic voltammogramm of NpN in LiCl-KCl**

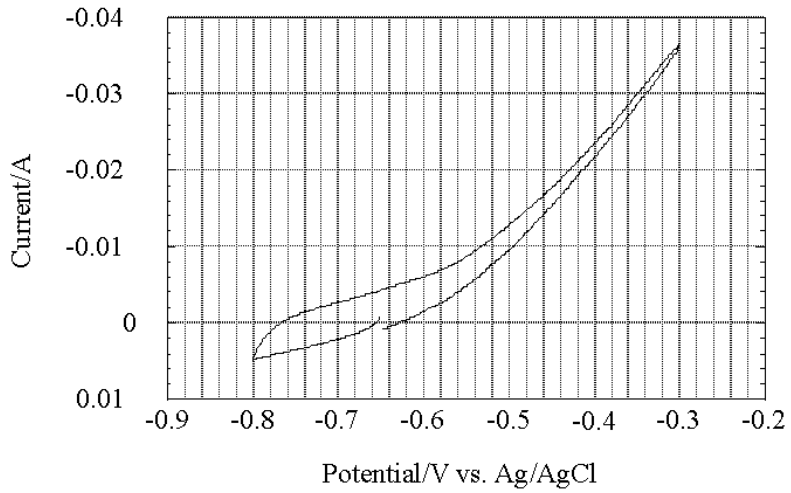

The nitrides of Np and Pu were confirmed from the cyclic voltammograms to dissolve and form the ions such as Np(III) and Pu(III) at the anode. The theoretical potential for the dissolution of PuN was evaluated from the observed one to be –0.865 V vs. a Ag/AgCl reference electrode with 1.00wt.%AgCl, which is close to that estimated from the thermodynamic functions. In case of UN, the formation of UNCl was confirmed theoretically and experimentally [4,5], but no ternary compound like UNCl was observed in cases of NpN and PuN as expected from thermodynamic considerations [4].

For the electrolysis of nitrides, a cage made of tungsten was used as an anode in which several small pieces of nitride blocks of were put. A molybdenum wire was used as a cathode. The composition of the salt was the same as above. The electrolysis of nitrides was carried out under the conditions of constant potential (-2.00V) and constant current (10-20mA) by using a potentio/galvanostat coulometer. The deposits of Np and Pu on the Mo cathodes are shown in Photo 1. In cases of the Pu experiments, it was observed that a part of the deposit was taken off from the cathode. Such tendency was also pointed out from the experiment with LiCl-NaCl-$CaCl_2$-$BaCl_2$ eutectic melt [15]. Therefore, in cases of the NpN experiments, spiral-shaped wires were used to keep the deposits on the cathode. As the concentrations of actinide chlorides in the LiCl-KCl were relatively low, the deposits included a lot of salts. Obviously, the deposits showed a paste-form and were differed from that of U, which forms a dendrite precipitation. After heating the deposits at 1073 K, the parts of metallic form were subjected to X-ray diffraction analysis and confirmed to consist of alpha Np and Pu metals, although the salts still remained.

LINEX Concept

A new concept, ”LINEX”, has been proposed as an alternative option to the ANL method [4,8] as shown in Figure 1. As for nitride fuel, the recycle of ^{15}N-enriched nitrogen is a subject to be solved to compensate the cost of ^{15}N enrichment. In the process, $^{15}N_2$ is recycled by use of Li_3N, i.e., $^{15}N_2$ gas released from spent fuel is combined with Li to form $Li_3{}^{15}N$ and $Li_3{}^{15}N$ reacts with actinide chlorides in the molten salt to form the nitride. In this case, it is important to understand the evolution behavior of nitrogen in the salt. As a preliminary test, the evolution of nitrogen gas during the oxidation of NdN by $CdCl_2$ in the LiCl-KCl eutectic melt was examined [8].

Photo 1. **Deposits of Np(right) and Pu(left) on cathodes by electrolysis of NpN and PuN in LiCl-KCl eutectic melts at 773 K**

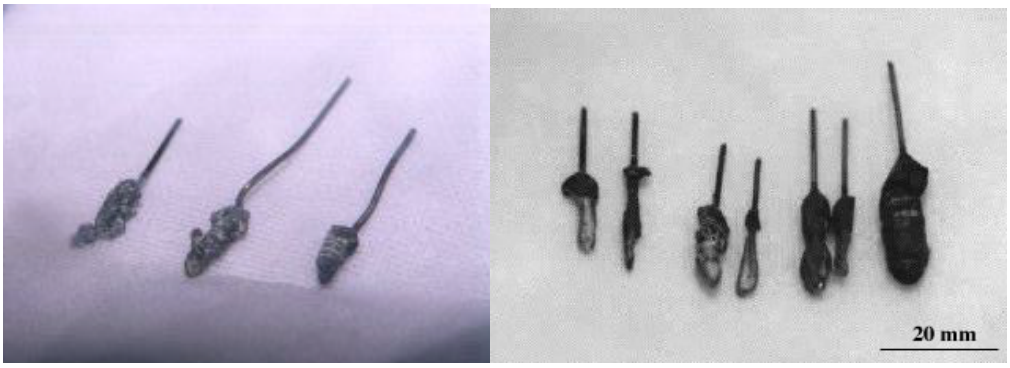

A typical result is shown in Figure 3, which shows that 90% of nitrogen in NdN was evolved from the salt. Considering the oxygen impurity in the NdN sample used in the experiments, it was evaluated that 95% of nitrogen could be recovered in this case. This result suggests that ^{15}N-enriched nitrogen gas may be recovered with high efficiency in the pyrochemical process of nitride fuel. In case of no recycle of $^{15}N_2$ gas(100% loss), the price of ^{15}N may be required to be lowered to around \$10/g-$^{15}N_2$(99.9% enrichment). However, if 90% of $^{15}N_2$ can be recycled, the required price of $^{15}N_2$ enrichment may be around \$100/g, which may be commercially achieved on the basis of the present technology.

Figure 3. **N2 evolution during exidation of NdN* by $CdCl_2$ in LiCl-KCl eutectic melt. Molar ratio, NdN/(LiCl-KCl) = 0.021, * 7.90 wt% N, 1.45wt% O, 0.063 wt% C.**

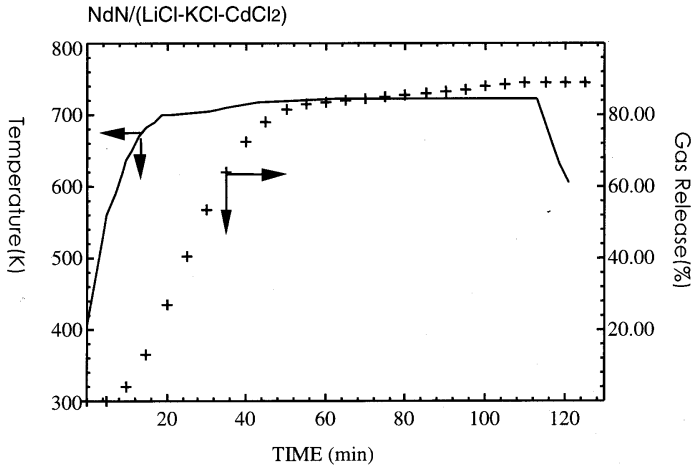

Database of fuel properties

Formation of Nitride Solid Solutions

The formation of the solid solution of actinide mononitrides can be pointed out as an advantage of nitride from the viewpoint of fuel stability under irradiation, contrary to oxide and metal fuels in which the solubilities of MAs are very limited. The binary solid solutions in the UN-NpN-PuN system were, therefore, prepared and the phases formed were checked by X-ray diffraction analysis. The procedure of sample preparation was described in earlier papers [9,14]. From the X-ray diffraction analysis no compound was observed except the NaCl-type cubic-structured mononitride and faint dioxides.

As shown in Figure 4, the lattice parameters of the solid solutions change continuously with the compositions, but deviate from the Vegard's law. It may be understood that the lattice parameters of the solid solutions deviate positively in the PuN-rich region, while negatively in the UN-rich region in a case of the UN-PuN solid solutions. Similar behavior can be seen in cases of the UN-NpN and NpN-PuN solid solutions as shown in the figure. The results indicate that the actinide mononitrides may form solid solutions in the whole composition range, but they are not ideal from thermodynamic aspects [11].

Figure 4 **Lattice parameters of UN-NpN-PuN solid solutions**

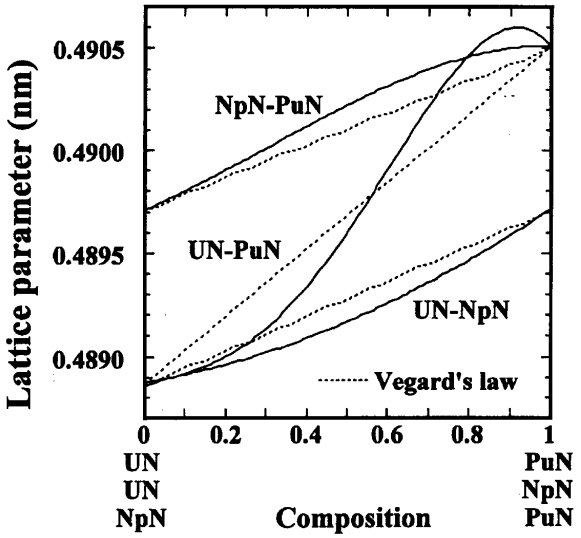

Thermal conductivity and evaporation behavior

The thermal conductivities of the binary solid solutions of the UN-NpN-PuN system were evaluated from the data on thermal diffusivity determined by a laser flash method, the specific heat capacity and the density [9,11,12]. The specific heat capacities were estimated from literature or by an additive method in case no literature datum was available. The theoretical density was calculated from the lattice parameters described above. The porosity correction to 100% theoretical density was made by use of the Maxwell-Eucken equation. The thermal conductivity of the solid solutions of the UN-NpN-PuN system was found to increase gradually with temperature like the respective mononitrides. Figure 5 shows the thermal conductivities of the binary solid solutions at 1273K. It can be seen that the thermal conductivities change continuously with the compositions, but the values for the solid solutions are lower than those evaluated by a simple additive law. Recently the PuN-ZrN solid solutions were prepared and the determination of the thermal conductivity is under way. A preliminary result indicates that the sold solutions show similar values to those of the respective mononitrides, PuN and ZrN.

The evaporation behavior of actinide mononitrides and their solid solutions has been investigated by Knudsen-effusion high temperature mass-spectrometry [10,16]. UN and NpN were confirmed to form liquid precipitations at evaluated temperatures and the pressures of the actinide metal vapours are close to those of the respective pure metals, while PuN evaporates congruently [16].

Figure 5 **Thermal conductivity of UN-NpN-PuN solid solutions**

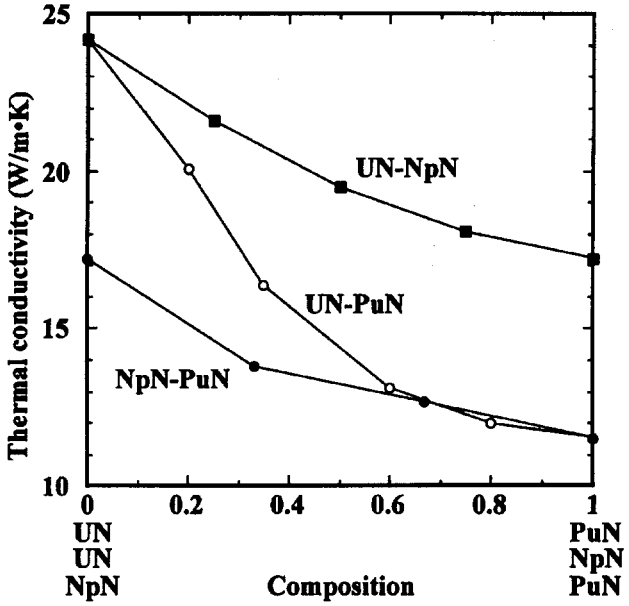

The binary solid solutions of the respective nitrides show relatively complicated evaporation behavior [10,11]. With regard to the solid solutions of UN and PuN, (U,Pu)N, the pressures of U(g) and Pu(g) depend on the composition of the solid solutions. It indicates that (U,Pu)N evaporates congruently and no liquid phase may form at least in the experimental conditions. In the system of NpN-PuN, the partial pressures of Np(g) over the solid solutions are close to that over pure metal, Np(l), and slightly depend on the PuN concentration. It suggests that a selective precipitation of a liquid phase containing Np may be occurred at evaluated temperatures. On the other hand, the pressure of Pu(g) depends on the PuN concentration in the solid solutions at higher temperatures. It may indicate that the liquid phase does not contain significant concentration of Pu. At lower temperatures, the formation of a liquid phase with Pu was suggested, because of the relatively high Pu vapour pressure.

Irradiation behaviour

The irradiation tests of uranium-plutonium mixed nitride fuel in JMTR show the advantages especially in the lowering of fission gas release by adoption of the cold fuel concept as described earlier [9,13]. It was confirmed from the puncturing tests that FP gas release of mixed nitride fuel irradiated up to 5.3-5.5%FIMA is 1.7-2.8% and the observed ratios of Xe/Kr agreed with calculated ones, 16. While most of FP gas was retained within fuel pellets, the increase in diameter of fuel pins was rather small; 0.4% at the maximum. The swelling rates evaluated from the porosity measurements were 0.6-0.8%/%FIMA. These results suggest that the observed swelling may be caused mainly from the accumulation of solid FPs. No chemical interaction was observed at the interface with cladding tubes and pellets.

Two (U,Pu)N fuel pins are under irradiation in JOYO with a collaboration with JNC(previously PNC) up to a target burnup of about 4%FIMA. According to the operation program of the JOYO, the irradiation will end in the middle of 1999 followed by post-irradiation examinations in the facilities of JNC and JAERI.

Concluding remarks

The recent progress of the research on nitride fuel cycle, which is the reference system for transmutation of MAs in JAERI, is described. The electrochemical studies in the LiCl-KCl eutectic melt have been carried out in order to establish the database for the design and evaluation of the pyrochemical reprocessing system of nitride fuels. The electrolysis of UN, NpN and PuN was examined at 773 K. The dissolution of actinides at the anode occurred around the theoretically evaluated potential and the respective actinide metal was found to deposit on the solid cathode. The other pyrochemical process, "LINEX", has been proposed for the reprocessing of nitride fuel. In the process, actinide elements in spent nitride fuel are dissolved in molten salt as chlorides and directly converted to the nitrides in the salt by the reaction with Li_3N. The evolution behavior of N_2 gas, which must be recycled in the nitride fuel system because of the utilisation of enriched N-15, was studied by use of lanthanide nitrides. The fundamental behavior of actinide elements in the molten salts, such as the distribution between the salt and molten metal and the electrodeposition, was also determined by electrochemical experiments.

The database of the properties of nitride fuel is also being prepared. The properties of actinide mononitrides such as thermal conductivity and evaporation behaviour have been determined. The quasi-binary system of NpN and the other actinide mononitride forms the solid solution, but is not considered to be thermodynamically ideal because of the deviation of the lattice parameters from the Vegard's law. The thermal conductivity of the solid solutions of actinide mononitrides was derived from the data on thermal diffusivity determined by a laser flash method. The evaporation behavior of the nitrides has been determined by high temperature mass spectrometry. From the irradiation tests of (U,Pu)N fuel in JMTR, the fuel shows excellent performance; the fission gas release was found to be very low, around a few percent, and there was no significant chemical interaction between fuel and cladding, at least up to the burnup of 5.5%FIMA.

REFERENCES

[1] Mukaiyama, M. Kubota, T. Takizuka, Y. Suzuki, T. Ogawa, T. Osugi, M. Mizumoto, Proceedings 4th OECD/NEA Int. Mtg. on Actinide and Fission Product Partitioning and Transmutation, Mito, Oct. 1996, p.80.

[2] Mukaiyama, M. Kubota, T. Takizuka, T. Ogawa, M. Mizumoto, H. Yoshida, Proceedings on *Evaluation of Emerging Nuclear Fuel Cycle System(GLOBAL'95)*, Versaille, Sept. 11-14, 1995, p. 110.

[3] I. Chang, Nucl. Technol., 88 (1989) 129.

[4] Ogawa, , M. Akabori, Y. Suzuki, F. Kobayashi, T. Osugi, T. Mukaiyama, Proceedings on *Future Nuclear Systems(GLOBAL'97)*, Yokohama, Oct. 5-10, 1997, p.812.

[5] Kobayashi, T. Ogawa, M. Akabori, Y. Kato, J. Am. Ceram. Soc., 78 (1995) 279.

[6] Shirai, T. Iwai, Y. Suzuki, Y. Sakamura, H. Tanaka, J. Alloys and Comp., 271-273 (1998) 680.

[7] Shirai, T. Iwai, K. Shiozawa, Y. Suzuki, Y. Sakamura, T. Inoue, submitted to J. Nucl. Mater.,

[8] Ogawa, M. Igarashi, EUCHEM Conf. on Molten Salts, Porquerolles Island, Jun.27-Jul.3, 1998.

[9] Arai, T. Iwai, K. Nakajima, Y. Suzuki, Proceedings on *Future Nuclear Systems (GLOBAL'97*), Yokohama, Oct. 5-10, 1997, p. 664.

[10] Nakajima, Y. Arai, Y. Suzuki, J. Alloys and Comp., 271-273 (1998) 666.

[11] Suzuki, Y. Arai, *ibid.*, 271-273 (1998) 577.

[12] Arai, K. Nakajima, Y. Suzuki, *ibid*., 271-273 (1998) 602.

[13] Suzuki, T. Ogawa, T. Osugi, Y. Arai, T. Mukaiyama, Proceedings 4th OECD/NEA Int. Mtg. on *Actinide and Fission Product Partitioning and Transmutation*, Mito, Oct. 1996, p.178.

[14] Suzuki, Y. Arai, Y. Okamoto, T. Ohmichi, J. Nucl. Sci. Technol., 31 (1994) 677.

[15] Tomczuk, D. S. Poa, W. E. Miller, R. K. Steunenberg, Trans. ANS, 50 (1985) 204.

[16] Nakajima, Y. Arai, Y. Suzuki, J. Nucl. Mater., 247 (1997) 33.

PREPARATION AND CHARACTERISATION OF TECHNETIUM METAL AND TECHNETIUM-RUTHENIUM ALLOYS

Kazuo Minato and Yoshiro Shirasu
Department of Materials Science
Japan Atomic Energy Research Institute
Tokai-mura, Ibaraki-ken 319-1195,
Japan

Abstract

Technetium metal and Tc-Ru alloys were characterised to build a database of the Tc metal target for transmutation. The lattice parameters of Tc-Ru alloys including Tc and Ru metals measured by X-ray diffraction decrease with increasing Ru concentration. The thermal conductivity of Tc-Ru alloys including Tc and Ru metals was determined by the thermal diffusivity measured by the laser flash method from room temperature to about 1 200 K. The thermal conductivity of Tc metal shows a minimum around 400 K, above which it increases with temperature. The thermal conductivity of Tc metal is smaller than that of Ru metal and the thermal conductivity of Tc-25% Ru, Tc-50% Ru and Tc-75% Ru alloys increases with temperature as well as Ru concentration.

Introduction

Technetium-99 is a long-lived fission product with a half-life of 2.111 x 10^5 years, which decays by beta emission with a maximum energy of 293.5 keV [1]. The cumulative yields for ^{99}Tc from thermal neutron fission of ^{235}U and ^{239}Pu are 6.11 and 6.16 %, respectively [2]. The yields for other long-lived technetium, ^{97}Tc and ^{98}Tc, are 1.2×10^{-10} and 8.7×10^{-7} % from ^{235}U and 4.7×10^{-9} and 2.7×10^{-7}% from ^{239}Pu, respectively [2].

In storage of high-level waste (HLW) from nuclear reactors, ^{99}Tc contributes dominantly to the beta radiotoxicity for a very long time. Since the transmutation of ^{99}Tc to stable ^{100}Ru is an attractive option to reduce the long-term risk of the storage of HLW, irradiation experiments for the transmutation, together with the related experiments, were performed [3-7]. The EFTTRA-T1 experiment revealed no technical limitations to the use of Tc metal as a target for transmutation [5].

We, JAERI, also started an experimental study concerning transmutation of Tc [8,9]. Based on the result of the EFTTRA-T1 experiment, Tc metal was placed in the reliable chemical form of the target to be transmuted. When the target of Tc metal is transmuted, the target will change to Tc-Ru alloy, whose Ru concentration increases with irradiation dose. Although the basic properties of Tc metal and some of its alloys were studied mainly in 1960s and 1970s, the data needed for a design of the target and for evaluation of the irradiation behaviour of the target are very limited.

The present paper describes results of out-of-reactor experiments on alloying behaviour of Tc-Ru and thermal conductivity of Tc-Ru alloys including Tc and Ru metals, which contribute to the formation of a database of the Tc metal target.

Preparation of Tc and Tc-Ru samples

Powder of Tc metal was purchased from Oak Ridge National Laboratory. The as-received powder was heated at 1 073 K in flowing hydrogen to reduce technetium oxide, if any, contained in the sample. The heat-treated powder was analysed by inductively coupled plasma-atomic emission spectrometry (ICP-AES) and inductively coupled plasma-mass spectrometry (ICP-MS). The main impurities were found to be iron and aluminium, and the total amount of impurities was about 15 ppm, as shown in Table 1.

Table 1. **Analysis of technetium powder by ICP-AES and ICP-MS**

Element	Amount (ppm)
Al	4.0
Ti	0.94
V	< 0.5
Cr	1.5
Mn	< 0.5
Fe	6.4
Co	< 0.5
Ni	1.9
Cu	< 0.5
Zn	< 0.5
U	< 0.5

The X-ray diffraction analysis of the powder was carried out at room temperature, using Ni-filtered Cu Kα radiation. The measured X-ray diffraction pattern of the powder from 25 to 140° was identical with the data of Tc metal reported by Muller *et al* [10]. The lattice parameters obtained were a = 0.27409 nm and c = 0.43983 nm, which were almost the same as the previously reported values [10-13]. The theoretical X-ray density was found to be 11.479 Mg/m^3 when an atomic weight of 98.913 was assumed [14].

For the characterisation of Tc-Ru alloys, five disk-shaped samples of Tc metal, Tc-25%Ru, Tc-50%Ru, Tc-75%Ru, and Ru metal were prepared by arc-melting technique. About 2 g of mixed powder of Tc metal and Ru metal (>99.9%) was pressed into a tablet of 10 mm in diameter and about 3 mm in thickness at room temperature and a pressure of 980 MPa. The tablet was then arc-melted to form a button on a water-cooled copper hearth in an atmosphere of purified argon. The button was remelted several times to assure homogenisation, followed by arc drop-cast to form a rod of 5 mm in diameter and about 10 mm in length. The rod was cut by a diamond cutter to obtain a disk of 5 mm in diameter and 1 mm in thickness.

The disk samples were then annealed at 1 573 K for 1 h in vacuum. The present annealing temperature was selected on the basis of the results of the annealing experiment by Spitsyn *et al* [15].

Characterisation of Tc and Tc-Ru alloys

Lattice parameters

The disk samples were analysed by X-ray diffraction method, using Ni-filtered Cu Kα radiation. Tc and Ru metals are isostructural, having a hexagonal close packed structure (space group $P6_3/mmc$), and form a complete solid solution [16].

The formation of a solid solution with a single phase was confirmed in each sample and the lattice parameters of the a- and c-axes of the five samples were obtained. Figure 1 shows the lattice parameters of the alloys as a function of Ru concentration. Both the lattice parameters of the a- and c-axes decrease with increasing the Ru concentration, which almost follow Vegard's law. The present result of the lattice parameters agreed well with the reported ones [16].

Figure 1. **Lattice parameters of Tc-Ru alloys including Tc and Ru metals**

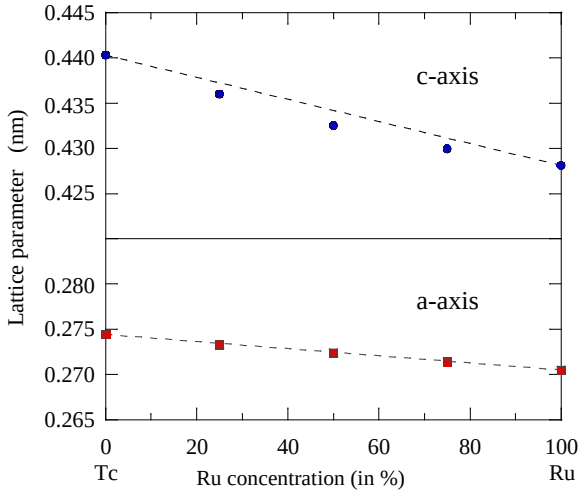

The immersion density of each disk sample measured with methylene iodide was found to be almost the same as the theoretical X-ray density.

Thermal diffusivity

The thermal diffusivity was measured on the disk samples from room temperature to about 1 200 K by the laser flash method. The measurements were performed in a vacuum below 3×10^{-3} Pa. The apparatus for the thermal diffusivity measurement was tested using a stainless steel sample as standard. The experimental uncertainties were less than 3%.

Since the samples had metallic luster, the surface of the disk samples was treated with carbon to absorb the laser beam efficiently. The influence of this treatment on the measured thermal diffusivity was less than 1%.

The sample was heated in an electric furnace to the desired temperatures and the sample temperature was measured with an R-thermocouple placed near the sample. The thermal diffusivity was determined from the temperature rise at the rear surface measured with an In-Sb infrared detector after the front surface of the sample was heated by the pulse of a ruby laser. The data of the temperature rise were analysed by the logarithmic method [17-18].

Figure 2 shows the thermal diffusivity of Tc metal, Tc-25%Ru, Tc-50%Ru, Tc-75%Ru, and Ru metal as a function of temperature.

Figure 2. **Thermal diffusivity of Tc-Ru alloys including Tc and Ru metals**

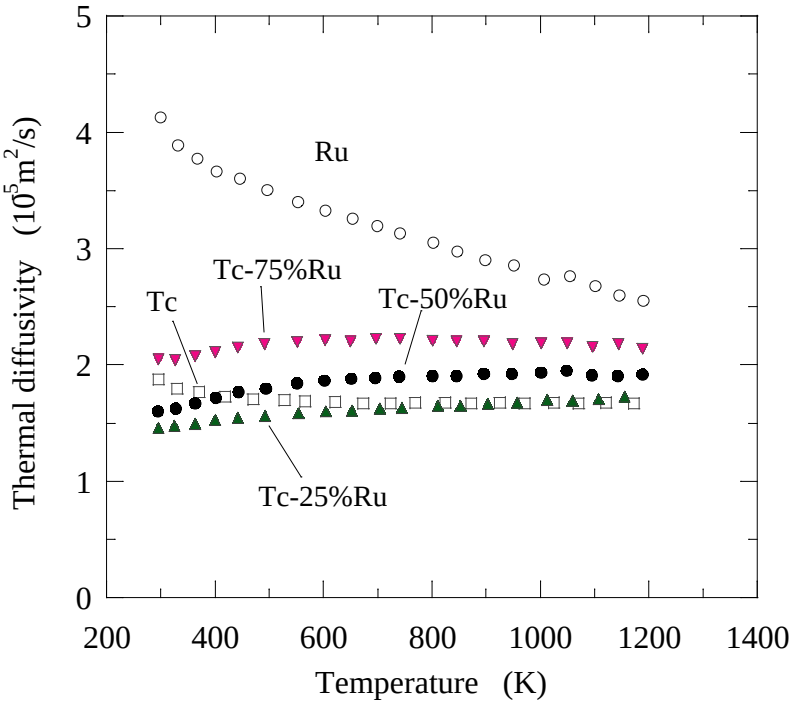

Heat capacity

When the thermal conductivity is determined from the thermal diffusivity, the specific heat capacity is needed:

$$\lambda = \alpha C_p \rho \text{ , (1)}$$

where λ is the thermal conductivity, α the thermal diffusivity, C_p the specific heat capacity and ρ the density of the sample.

As no specific heat capacity was measured in the present study, the data from the literature on the heat capacity of Tc [19-22] and Ru [21-23] are presented in Figures 3 and 4, respectively. For Tc, the data reported by Spitsyn *et al* [19] were experimental values, whereas others [20-22] were theoretically estimated ones. The recent compilation of the thermochemical data by Cordfunke and Konings [21] adopted the estimations by Guillermet and Grimvall [24]. Another recent compilation by Barin [22] adopted the same values as those of Stull and Sinke [23]. In the case of Ru, the compilation by Cordfunke and Konings [21] recommended the values based on their measurement, whereas the compilation by Barin [22] adopted the same values as those of Hultgren *et al* [25].

Figure 3. **Specific heat of Tc metal taken from the literature** [19-22]

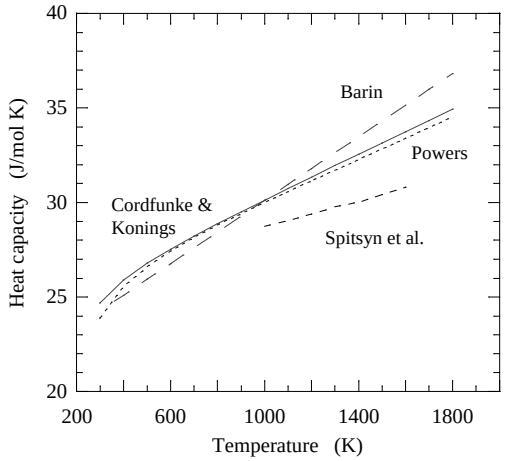

Figure 4. **Specific heat of Ru metal taken from the literature** [21-23]

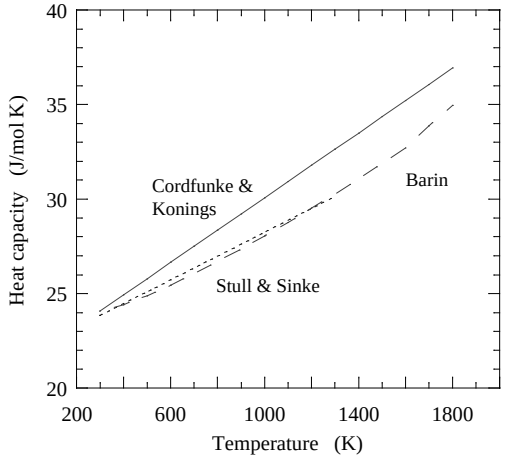

In the present study the values for heat capacity of Tc and Ru were taken from the compilation by Cordfunke and Konings [21] and those for Tc-Ru alloys were estimated by Neumann-Kopp rule.

Thermal conductivity

Figure 5 shows the thermal conductivity of Tc and Ru metals calculated through Eq.(1) as a function of temperature, together with the reported values [11,19,26-27]. It is noted that the thermal conductivity of Tc metal is smaller than that of Ru metal in the present temperature range. The thermal conductivity of Tc metal in the present experiment shows a minimum around 400 K, above which the thermal conductivity increases with temperature. The thermal conductivity of Ru metal, on the other hand, decreases with increasing temperature.

Figure 6 shows the thermal conductivity of the Tc-Ru alloys as a function of temperature, together with those of Tc and Ru metals. For Tc-25%Ru, Tc-50%Ru and Tc-75%Ru alloys, the thermal conductivity increases with temperature as well as Ru concentration.

Figure 5. **Thermal conductivity of Tc and Ru metals, together with the reported ones** [11,19,26-27]

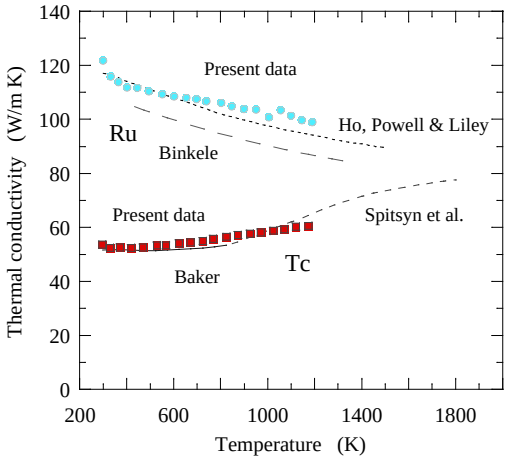

Figure 6. **Thermal conductivity of Tc-Ru alloys including Tc and Ru metals**

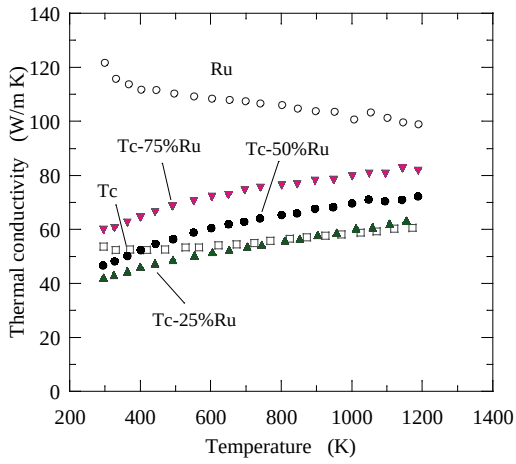

Conclusions

In order to build a database of the Tc metal target for transmutation, the lattice parameters of Tc-Ru alloys including Tc and Ru metals were measured by X-ray diffraction and the thermal conductivity of Tc-Ru alloys including Tc and Ru metals was determined by the thermal diffusivity measured by the laser flash method from room temperature to about 1 200 K. The following was concluded:

- The lattice parameters of Tc-Ru alloys decrease with increasing Ru concentration.
- The thermal conductivity of Tc metal shows a minimum around 400 K, above which it increases with temperature. The thermal conductivity of Tc metal is smaller than that of Ru metal.
- The thermal conductivity of Tc-25%Ru, Tc-50%Ru and Tc-75%Ru alloys increases with temperature as well as Ru concentration.

Acknowledgements

The authors wish to express their thanks to Dr. T. Ogawa, Department of Materials Science, JAERI, for his helpful advice, and to Dr. H. Katsuta, Director of the Department and Dr. T. Mukaiyama, Director of Center for Neutron Science, JAERI, for their interest and encouragement.

REFERENCES

[1] B. Firestone, *Table of Isotopes*, 8th ed. (John Wiley & Sons, New York, 1996) p. 695.

[2] F. Rider, NEDO-12154-3 (1981).

[3] W. Wootan, D. P. Jordheim and W. Y. Matsumoto, *Trans. Am. Nucl. Soc.*, 64 (1991) 125.

[4] J. M. Konings, W. M. P. Franken, R. P. Conrad, J.-F. Gueugnon and J.-C. Spirlet, *Nucl. Technol.*, 117 (1997) 293.

[5] J. M. Konings, A. D. Stalios, C. T. Walker and N. Cocuaud, *J. Nucl. Mater.*, 254 (1998) 122.

[6] Boucharat, J.-C. Spirlet, N. Cocuaud, J. Fuger and C. Prunier, in *Proc. GLOBAL '95*, Vol. 2, Versailles, France (1995) p. 1675.

[7] F Babelot, R. Conrad, W. M. P. Franken, J. van Geel, G. Gruppelaar, G. Muehling, C. Prunier, M. Rome and M. Salvatores, in *Proc. GLOBAL '95*, Vol. 1, Versailles, France (1995) p. 524.

[8] Minato, H. Serizawa and K. Fukuda, *J. Alloys Comp.*, 267 (1998) 274.

[9] Minato, H. Serizawa, K. Fukuda and M. Itoh, JAERI-Research 97-077 (1997).

[10] Muller, W. B. White and R. Roy, *J. Inorg. Nucl. Chem.*, 26 (1964) 2075.

[11] E. Baker, *J. Less-Common Metals*, 8 (1965) 435.

[12] L. Giorgi and E. G. Szklarz, *J. Less-Common Metals*, 11 (1966) 455.

[13] A. C. Marples and C. C. Koch, *Phys. Lett.*, 41A (1972) 307.

[14] G. Inghram, D. C. Hess, Jr. and R. J. Hayden, *Phys. Rev.*, 72 (1947) 1269.

[15] I. Spitsyn, Yu. N. Golovanov, O. A. Balakhovskii and A. A. Tsvetaev, *Doklady Akademii Nauk SSSR*, 205 (1972) 1421.

[16] B. Darby, Jr., D. J. Lam, L. J. Norton and J. W. Downey, *J. Less-Common Metals*, 4 (1962) 558.

[17] M. James, *J. Appl. Phys.*, 51 (1980) 4666.

[18] Takahashi, K. Yamamoto and T. Ohsato, *Netsu Sokutei*, 15 (1988) 103.

[19] I. Spitsyn, V. E. Zinov'ev, P. V. Gel'd and O. A. Balakhovskii, *Doklady Akademii Nauk SSSR*, 221 (1975) 145.

[20] A. Powers, *High Temp. Sci.*, 31 (1991) 105.

[21] H. P. Cordfunke and R. J. M. Konings, *Thermochemical Data for Reactor Materials and Fission Products* (Elsevier, Amsterdam, 1990).

[22] Ihsan Barin, *Thermochemical Data of Pure Substances* (VHC, Weinheim, 1989).

[23] R. Stull and G. C. Sinke, *Thermodynamic Properties of the Elements* (American Chemical Society, Washington, D. C., 1956).

[24] F. Guillermet and G. Grimvall, *J. Less-Common Metals*, 147 (1989) 195.

[25] Hultgren, P. D. Desai, D. T. Hawkins, M. Gleiser, K. K. Kelley and D. D. Wagman, *Selected Values of the Thermodynamic Properties of the Elements* (American Society for Metals, Ohio, 1973).

[26] Y. Ho, R. W. Powell and P. E. Liley, *Thermal Conductivity of the Elements: A Comprehensive Review, J. Phys. Chem. Ref. Data*, 3, Supplement No. 1 (1974).

[27] Binkele, Juel-2379 (1990).

TRANSMUTATION STUDIES OF MINOR ACTINIDES IN HIGH INTENSITY NEUTRON FLUXES

Gabriele Fioni, Teresa Bolognese, Michel Cribier,
Frederic Marie and Stefan Röttger
Commissariat à l'Énergie Atomique
CEA/Saclay, DSM/DAPNIA
91191 Gif-sur-Yvette
France

Herbert Faust and Philippe Leconte
Institut Max von Laue – Paul Langevin
38042 Grenoble
France

Abstract

Integral measurements of nuclear data and of the transmutation potential in specific neutron fluxes, constitute the fastest and essential way to overcome to the large uncertainties present in the nuclear data libraries. In the frame of the activities of the Directorate for Science of Matter (DSM) of the French Atomic Energy Authority (CEA), we propose a new project to carry out integral measurements relevant for nuclear waste transmutation systems.

A new beam tube will be installed to irradiate actinides and fission fragment samples at different distances from the fuel element of the ILL reactor. Variable neutron energy spectra could then be obtained by choosing the distance between the sample and the fuel element, opening the way to the determination of the ideal physical conditions to incinerate nuclear waste in hybrid transmutation systems.

Introduction

Social acceptability of nuclear energy is strongly related to the problem of long-lived nuclear waste produced during the burn-up of the nuclear fuel. By successive neutron captures, transuranic elements are formed from the initial uranium and plutonium isotopes, while by nuclear fission a large variety of light and medium mass isotopes are produced.

Several solutions aiming at the reduction of the long-term radiotoxicity by the transmutation of long-lived isotopes into stable or short living elements have been studied in the last years. A general consensus indicates that only neutron-induced reactions are adequate, due to the combination of high cross sections and to their lower energetic cost of production. Other options that were once suggested, as direct spallation by high-energy protons and gamma-ray induced reactions, seem to be economically non-viable, since the destruction of waste would require more energy than produced when generating this waste.

In principle any neutron source can be used for nuclear waste transmutation. Actinides can be transmuted by nuclear fission mostly into short living nuclei with a considerable gain in long term radiotoxicity. Long-lived fission products can be transmuted into stable isotopes by direct or successive neutron captures followed by beta decays. A clear example is constituted by the reaction.

$$^{99}Tc(n,\gamma)^{100}Tc \xrightarrow{T_{1/2}=15.8s} {}^{100}Ru$$

where the long-lived ($T_{1/2}$ =2.1 x10^5 years) ^{99}Tc is transmuted in 15.8 seconds into the stable ^{100}Ru.

Fission reactors constitute the most direct source of neutrons, and studies on the transmutation capabilities of thermal or fast reactors are being conducted in several countries. While the incineration of military plutonium seems to be possible in ordinary and fast reactors, nuclear waste transmutation is more difficult. In fact, ordinary PWRs do not have suitable neutron excess to transmute nuclear waste, unless the uranium enrichment is increased significantly. Fast reactors have a more favourable neutron balance, but safety considerations limit the amount of plutonium isotopes and minor actinide fuel that could be irradiated.

The neutron cross-sections for capture and fission reactions decrease significantly as a function of the neutron energy. Hence, a thermal neutron flux will provide higher transmutation rates for a given mass than epithermal and fast spectra. Nevertheless, as the transmutation of minor actinides is achieved by nuclear fission and not all isotopes are fissile at thermal energy, an essential parameter to be evaluated is the ratio between fission and capture cross-sections, which is larger in a fast neutron flux. Therefore fast spectra are preferable in order to avoid the generation of high Z actinides and to obtain higher neutron excess. The price to pay is a larger fuel inventory in the installation for a given thermal power.

Without going further into the details of this problem, it should be stressed that the choice of the most suitable neutron spectrum depends on the characteristics of each specific isotope and that systems where thermal and fast spectra coexist in the same installation are under study. To date no decision can be based on experimental bases, but only on computer simulations of the transmutation process.

The major problem in a clear assessment of the "ideal" neutron flux is constituted by the very poor knowledge of nuclear cross section data for most of the minor actinides and fission fragments concerned. Though a general agreement exists in the most widely used nuclear data library (JEF-2.2, ENDF-B/VI and JENDL 3.2) for nuclei that play a major role in the "conventional" fuel cycle, the situation concerning rarer isotopes like Am, Cm and Np is totally unsatisfactory. Large discrepancies exists in both thermal and fast energy regions, originating in large differences on the neutronics characteristics of the systems.

An extreme example is given by the ^{242gs}Am cross section where a difference of a factor of 20 existed between ENDF and JEF, making impossible any prediction on the possibility of transmutation of ^{241}Am in thermal fluxes. A recent experiment at ILL has been able to fix this large discrepancy [1].

An essential contribution to the solution of this scientific debate is constituted by integral measurements, where the evolution of a sample is measured for a specific neutron spectrum. In this frame the Mini-Inca project constitutes a unique experimental approach to carry out experiments in conditions which are representative of a thermal neutron based incineration systems.

The mini-Inca project

The Mini-Inca project aims to develop a set of experimental methods and computational procedures to carry out integral measurements to assess in a fast and reliable way the transmutation potential and the average nuclear parameters of specific isotopes in given neutron spectra. This will be achieved by measuring the isotopic composition of the sample after irradiation in a measured neutron flux. The evolution of a sample in a neutron flux is given by a linear system of differential equations [2]:

$$\frac{dN}{dt} = -MN \quad (1)$$

where : M is a square matrix where the non-diagonal elements give the reaction rates j->i and N is a vector giving the isotope population N_i for a given isotope i. The reaction rates Mij are given by the neutron induced reaction [$\sigma\,\phi$] or by the decay constants [$\lambda = \ln 2 / T_{1/2}$].

If the concentrations N_i and the neutron flux are known, a number of nuclear parameters can be obtained by a simple fit between the experimental data and the solutions obtained by solving the system (1).

To obtain valuable data, we have therefore to carry out a new type of integral experiments based on:

- Small mass samples, to avoid any problem related to corrections of the local flux due to the sample influence.
- A set of experimental methods from nuclear spectroscopy to mass spectrometry, to obtain in the fastest way the sample composition.
- The use of high intensity fluxes, to have access by multiple neutron capture to very short-lived isotopes.
- The possibility to carry out nuclear spectroscopy measurements shortly after the irradiation, when short-lived isotopes are still present.

- The use of neutron spectrum monitors irradiated together with the sample, and the use of on-line detectors to follow the variation of the flux intensity as a function of time.

Two type of measurements are foreseen:

1. Long irradiations of mono-isotopic or a known mixture of transuranic elements and fission fragments, to determine the transmutation rates in given high intensity neutron spectra. These type of measurements will not be very useful to determine nuclear parameters, but they will indicate the effective transmutation possibilities and the equilibrium compositions.
2. Short irradiations of high-purity mono-isotopic samples, for a precise determination of nuclear parameters as neutron cross sections, branching ratios and half-lives.

The isotopic composition will be obtained by a number of complementary techniques, from classical off-line mass spectrometry (TIMS and ICP-MS) to new quasi-on-line mass spectrometry with FEBIAD sources [3], and from alpha-(beta)-gamma nuclear spectroscopy [4].

A schematic view of the project is given in Figure 1, where most of the techniques that will be used and developed are indicated.

Figure 1. **Schematic view of the Mini-Inca project.**

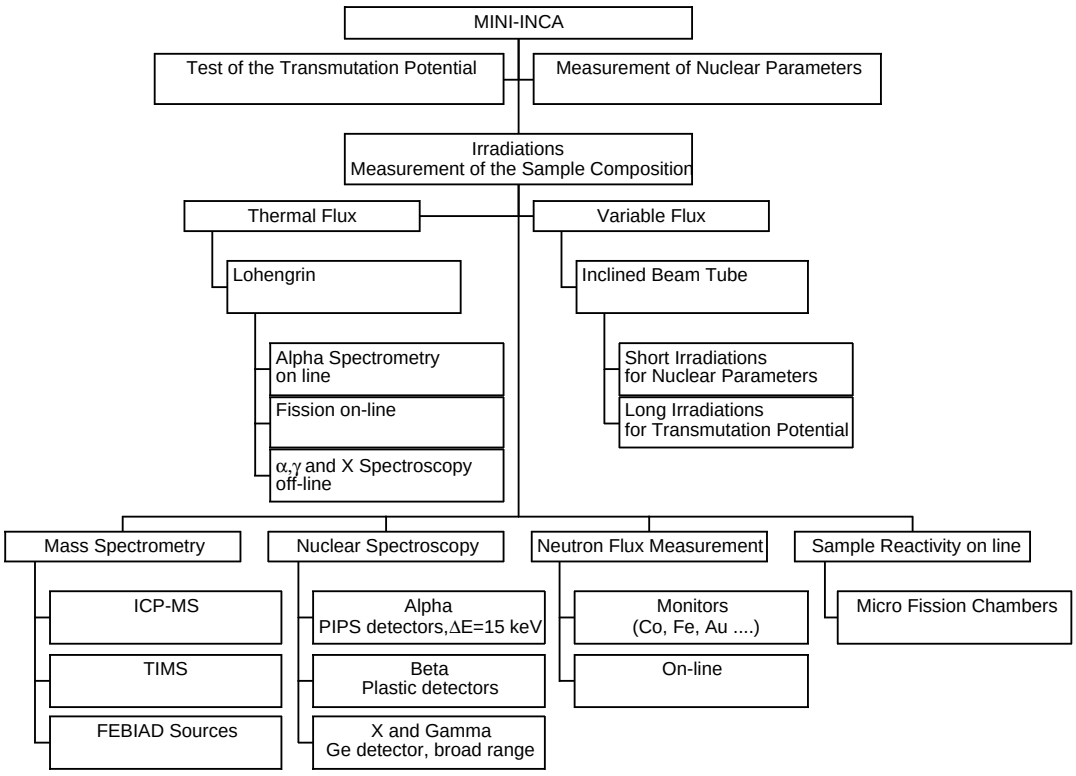

Dedicated irradiation facilities at ILL

The choice of the ILL reactor as the first facility to start the Mini-Inca project is mainly due to the unique possibility to dispose of several different neutron spectra, obtained by changing the distance between the sample and the fuel element. Additionally it provides the highest thermal flux in

the world, which makes possible high accuracy measurements in the thermal energy region and to carry out experiments in at the same intensities foreseen for a transmutation system which can approach $3*10^{15}$n/s/cm^2.

Variable flux facility

The energy distribution of neutrons generated by fission of ^{235}U can be parametrized as an evaporation spectrum with an average energy of about 2 MeV. Inside the reflector tank of the ILL reactor, neutrons are moderated by the heavy water, where the scattering length is about 20 cm. The moderator partly reflects the thermalized neutrons towards the fuel element. It is evident that different neutron spectra will be present at different distances from the fuel element, with an increase of the moderation as a function of the distance. Starting from about 60 cm from the fuel element edge, the spectrum is essentially a Maxwellian distribution at the moderator temperature.

In Figure 2, the neutron densities obtained at different distances from the axes of the reactor are given as a function of the neutron energy.

Figure 2. **Neutron Spectra at ILL for different distances from central axes of the reactor. The outer edge of the fuel element is located at 20.68 cm from the axes of the reactor.**

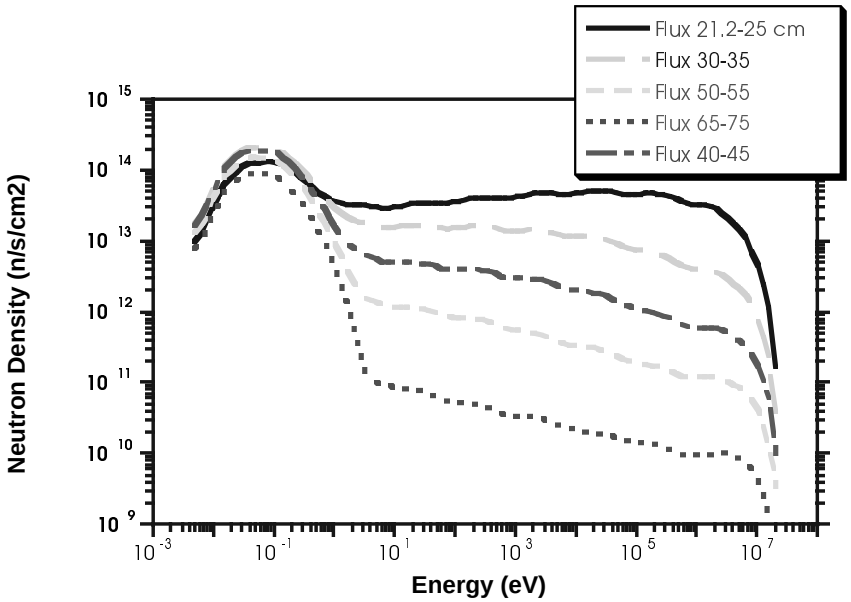

The plotted values correspond to an average flux $\langle\phi\rangle_i$ for a given energy interval $(E_i - E_{i-1})$ defined as:

$$\langle\phi\rangle_i = \int_{E_{i-1}}^{E_i} \phi(E)dE$$

with an energy bin such that:

$$\frac{\Delta E}{E} = cst$$

The spectra at about 30 cm, correspond both in intensity and in shape, to the one obtained for a strongly thermalized transmutation system [5]. The interest in making measurements in these kinds of thermal neutron fluxes is therefore evident. Additionally by measuring integral nuclear parameters with different spectra, we can have access to the average energy dependence of neutron cross sections.

A scheme of the installation of an inclined beam tube, which has been used for the MCNP code simulations, is given in Figure 3.

Figure 3. **Scheme of the installation of an inclined beam tube, which has been used for the MCNP code simulations**

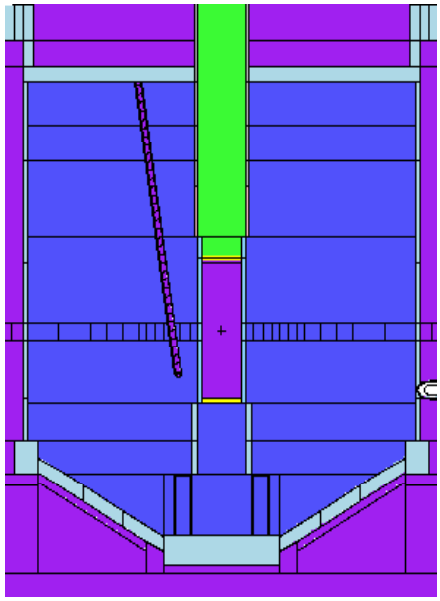

The goal is to install a very small channel of about 5 cm outer diameter, in order to minimise the anti-reactivity. Preliminary calculations indicate a loss of about 300 pcm for an Ag3Net (Al alloy) getting at 5 cm from the edge of the fuel element and filled with heavy water. This will correspond to a loss of about 12 hours of reactor cycle.

The samples have to be positioned at four different distances along the channel, to have access to three “epithermal” fluxes and to one thermal flux. At the closest position the total flux will be about 3×10^{15}n/s/cm^2, half of which is thermal. The pure thermal beam position will have a flux of about 5×10^{14}n/s/cm^2.

In order to minimise all manipulations of the irradiated sample, automatic irradiation systems are under study. The sample will be brought at the chosen irradiation position either by mechanical or by hydraulic systems. After irradiation it will go directly inside a dedicated hot-cell for conditioning either before shipping it to a radiochemistry laboratory or before being introduced automatically in a nuclear spectroscopy set-up.

Thermal flux position on H9

A valuable complement to the variable flux facility, is provided by the H9 beam tube which gives access to a neutron flux of about 5×10^{14}n/s/cm^2 with a thermalization coefficient higher than 98%. It is already equipped with a source changing facility to get a distance of about 60 cm from the edge of the fuel element. The beam tube is connected to the "Lohengrin" parabola mass spectrometer for unslowed fission fragments.

We also plan to use the H9 beam tube both for on-line measurements with Lohengrin and for off-line nuclear spectroscopy using a modified target changer.

The evolution of the composition of a minor actinide sample can be followed on-line by looking at the alpha particles emitted by decay of the isotopes formed during the irradiation. The formation and the decay rates of several isotopes could then be followed. The global fit of the obtained intensities will enable a comparison with the predictions obtained by solving the system (1) describing the sample evolution from different nuclear data libraries.

Another advantage of using Lohengrin lies in the possibility of also following the fission rate by looking at a given isotopic chain. In this case the target gives the main problem: beside the optimisation of the thickness and the geometry for the alpha and the fission spectrometry, the sputtering of the target material can constitute a major limitation. A new type of isotope deposition on titanium or graphite supports must be envisaged.

Another possibility of the H9 beam tube, is to use the target changer just to irradiate a sample and recover it to perform off-line nuclear spectroscopy. This requires a modification of the source changer and the installation of a "reaction chamber" on the changer tube. The chamber will be used under primary vacuum and it will house detectors to perform alpha-gamma spectroscopy. The main advantage of an installation of this type is that it will not be necessary to perform complicated manipulations of the sample and that the irradiation can continue after an intermediate spectroscopic measurement. Additionally, after the measurement the sample can be put into the waste container of Lohengrin.

A number of measurements are possible at this thermal energy position, with accuracies higher than 5 per cent.

Conclusions

The realisation of the proposed project will contribute significantly to the development of nuclear waste transmutation systems. It will provide the scientific and technical communities with a set of experimental procedures to assess in a fast and reliable way the transmutation potential and nuclear data for specific neutron fluxes.

Acknowledgements

We wish to acknowledge in the person of Mr. Bauer, the co-operation and the essential help of the ILL reactor department for the competent advice and the technical support in the definition of the project.

REFERENCES

[1] G. Fioni *et al*., *Transmutation of ^{241}Am in a high thermal neutron flux*, American Institute of Physics Conference Series 447(1998)43-51.

[2] M. Benedict, T.H. Pigford and H.W. Levi, *Nuclear Chemical Engineering*, Mc Graw Hill, New York, (1985).

[3] U. Koester, O. Kester and D. Habs, *Ion sources for fission fragment accelerators*, Review of Scientific Instruments, Vol. 69, 3 (1998) 1316-1321.

[4] F. Marie *et al.*, *Étude de la transmutation de plusieurs actinides d'intérêts à l'aide du spectromètre Lohengrin de l'ILL*, CEA-report, in press.

[5] F. Lelièvre, *Stratégies pour l'incinération de déchets nucléaires dans des réacteurs hybrides*, Ph.D Thesis, Université de Paris-Sud, December 1998.

THE INVESTIGATION OF THE TOTAL NEUTRON CROSS SECTION OF ^{237}NP

Vincent Gressier, Frank Gunsing, Alfred Leprêtre
CEA Saclay, DSM/DAPNIA/SPhN
91191 Gif-sur-Yvette
France

Antonio Brusegan, Klaus Burkholz, Zachary Hudson,
Egidio Macavero , Pierre Ribon, Peter Siegler
CEC-JRC-IRMM, Retieseweg
2440 Geel
Belgium

Abstract

Within the framework of a collaboration between the Institute for Reference Materials and Measurements (IRMM) and the Commissariat à l'Énergie Atomique (CEA), a project has been started to study neutron cross sections for nuclear waste transmutation purposes. We describe the measurements of the total neutron cross section of ^{237}Np, performed at the pulsed white neutron source GELINA of the IRMM. We used the time of flight method to obtain neutron spectra in the energy range from 0.3 eV to 2 keV. A preliminary list of new resonances under 120 eV is presented here. Besides these measurements, the Doppler effect has also been investigated for NpO_2. We will show how the use of an harmonic crystal model for Doppler broadening can explain some unexpected effects in the fit of the resonances.

Introduction

The nucleus ^{237}Np with a half-life of 2.144 .10^6 years is one of the most important minor actinides produced in conventional nuclear power plants: about 4 tons each year world-wide. After neutron capture, it becomes ^{238}Np which has a thermal fission cross section of 2000 b, much higher than the 0.02 b of the initial ^{237}Np, making it a good candidate for transmutation by neutron induced fission in thermal reactors.

Several measurements of the resonance parameters have been performed in the past [1,2,3,4] and several evaluations exist [5]. Nevertheless there is a strong demand for more precise resonance parameters [6].

Due to several large resonances at very low energy (starting at 0.49 eV), ^{237}Np is also a good candidate for Doppler effect studies.

Experimental set-up

The total cross section measurements of ^{237}Np were performed at the Geel Linear Electron Accelerator GELINA, using the time-of-flight technique. Three NpO_2 samples, with thicknesses 0.2, 1.0 and 2.0 g/cm^2 of ^{237}Np, have been used for the transmission measurements. For the two thinnest samples, the experiment covers the energy range from 0.3 eV to 40 eV at three different temperatures (15K, 50K and 290K) in order to investigate the Doppler effect. The neutron flight distance was 26.45 m. GELINA was providing a 15 ns electron bursts of 100 MeV average energy, a repetition frequency of 100 Hz and an average beam current of 12 μA. With a similar set-up, but at 49.33 m, we measured the transmission of the thickest sample covering the energy range from 0.3 to 120 eV at 290 K. The same sample was also used for the higher energy range from 45 eV to 2.6 keV at room temperature (290 K), but with GELINA running at 800 Hz, 70 μA and with a 2 ns pulse width.

The neutrons, produced via bremsstrahlung by the electron beam hitting a rotating uranium target, were moderated by water canned in two beryllium containers (4 cm thick). The neutrons enter into the flight paths through evacuated aluminium pipes of 50 cm diameter and are confined by collimators consisting of borated wax, lead and copper. In order to absorb slow neutrons, that otherwise overlap with the following GELINA pulse, a filter of cadmium (for experiments at 100 Hz) or a filter of ^{10}B (for the experiment at 800 Hz) was placed in the neutron beam.

The NpO_2 sample was mounted in an automatic sample changer at 12 m (for the experiments with the two thinnest samples) and at 23 m (for the thick sample). To determine the background, filters absorbing neutrons at specific energies (“black resonances”) were moved in and out of the beam with a sample changer controlled by the data acquisition system. In order to reduce systematic errors, these measurements sequences were recorded sequentially within a cycle lasting about one hour in total. The neutrons passing through the sample were further collimated and then detected by a NE912 lithium-glass detector. The signals from ^{6}Li(n,α) reaction were processed to provide the neutron time-of-flight and then stored by the data acquisition system FAST, upgraded at IRMM [7].

Analysis and results

The raw time-of-flight spectra were corrected for deadtime and background. The transmission was calculated as the ratio of these corrected spectra and normalised to the ratio of the time-integrated

incoming neutron fluxes of the sample «in» and «out», measured by neutron monitors located in the target hall. The in-house developed data processing package AGS [8,9] was used to carry out the various spectrum manipulations. A part of the transmission spectrum is shown in Figure 1.

Figure 1. **Transmission data of the 2 g/cm^2 thick NpO_2 sample measured at 49.33 m and at 290 K vs the neutron energy**

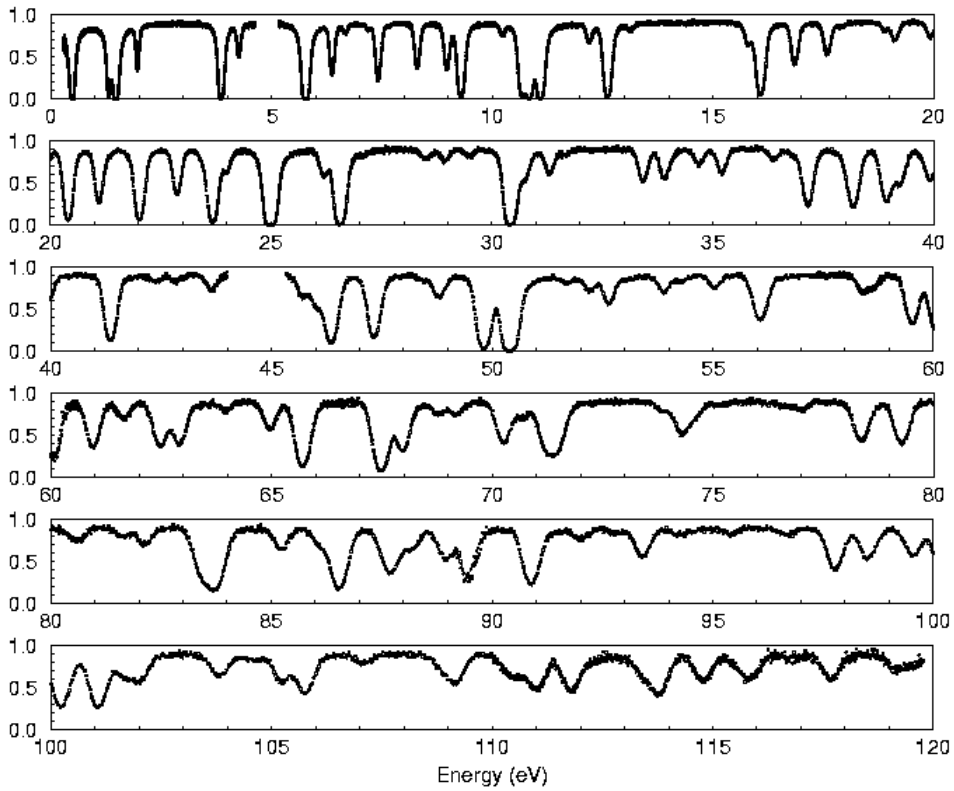

The R-matrix shape fitting program REFIT [10] was used in order to determine the resonance parameters like the resonance energy E_0, the neutron width Γ_n and the radiative width Γ_γ, which includes in our approximation the small fission width.

The given values of Γ_γ and Γ_n are still preliminary and demand further investigations. We find a good agreement between our Γ_n values and those of Auchampaugh [4] for the thinnest samples, but we have a systematic discrepancy of about 3% with the thick sample. This may come from an error on the quantity of neptunium. Therefore we only give in the following table the energies of the resolved resonances below 120 eV, those which are not present in the existing evaluations, all based on the results of D. Paya [1] or L.W. Weston [3]. In the table, our results are compared with the those of Auchampaugh given in the "BNL" [11]. Note that the two underlined resonances are only given in the evaluations and not in the reference 11.

Table 1. **Energies, in eV, of the resonances not given in the existing evaluations and comparison with the reference 11**

BNL	This work	BNL	This work	BNL	This work	BNL	This work
3.05		44.23	**44.29**	66.80	**66.80**	89.94	
7.68	**7.66**	44.95	**44.94**	69.35		91.02	
14.41	**14.38**	48.87	**48.90**	72.30		94.57	**94.53**
15.94	**15.92**	49.23	**49.29**	73.08		94.92	**95.08**
	17.05	50.34		75.66			**102.07**
17.94	**17.93**	56.15	**56.14**	76.21	**76.24**	103.40	
24.78	**24.79**	56.57	**56.55**	77.55	**77.58**	104.05	**103.96**
28.63	**28.61**	56.87	**56.87**	77.83			**106.91**
32.49	**32.49**	57.40		78.50	**78.50**	108.28	
34.07	**34.09**	61.67		79.90		109.84	**109.84**
38.04	**38.04**	62.49	**62.51**	82.39		112.65	**112.64**
39.02	**39.03**	63.42	**63.42**	83.80	**83.84**	113.03	**113.02**
43.20		66.40	**66.40**	87.79	**87.77**		

Doppler effect study

In the code REFIT, the Doppler broadening of the resonances is taken into account by the use of a "high-energy" Gaussian approximation to the free gas model with an effective temperature instead of the thermodynamic temperature.

The fit of the transmission data show that REFIT is unable to reproduce exactly the shape of the resonances, mainly at low energy. This effect is highlighted by the shape of the residual (see second spectrum of Figure 3) which are the ratio (fit-data)/σ_{data}.

A second observation is the behaviour of the effective temperature as function of the energy. If we adjust during the fitting procedure the effective temperature, this is lower than the thermodynamic temperature for the resonances at low neutron energy, as shown in Figure 6. Such a result is not allowed in the theory of the free gas model.

To determine if the cause of these disagreements is the description of the Doppler effect, we use the program DOPUSH developed by D. Naberejnev [12,13] which describe the Doppler broadening based on a more realistic model derived from the Lamb's crystal model [14].

As we are missing information on the phonon spectrum of the NpO_2 crystal, we are using the known phonon spectrum of UO_2 (Figure 2), which has a similar crystal structure and mass.

Figure 2. **The UO_2 crystal phonon spectrum**

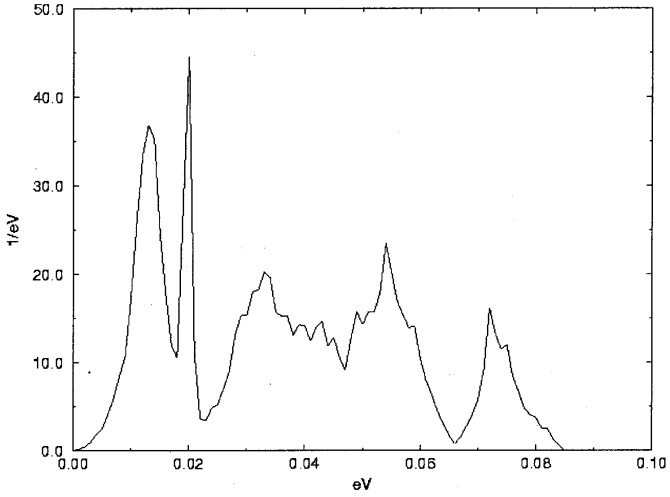

With a given set of resonance parameters E_0, Γ_n, Γ_γ, two Doppler broadened cross sections are calculated by the DOPUSH programme, one with the harmonic crystal description, the other using the exact free gas model. Then the corresponding transmissions are deduced, for a given flight distance, adopting experimental errors bars. Then REFIT is used to fit these transmissions with its free gas model. In Figure 3, we compare the residuals obtained from the experimental transmission and the two simulated transmissions. As a result, the residual of the data "generated" with the harmonic crystal model show the same behaviour as the residuals of the experimental data. On the other hand, the residuals of the data "generated" with the exact gas model do not produce a significant structure. In this indirect way we could infer that the data "generated" with harmonic crystal model reproduces the experimental data better than with the free gas model.

Figure 3. **Comparison between the residuals calculated by REFIT**

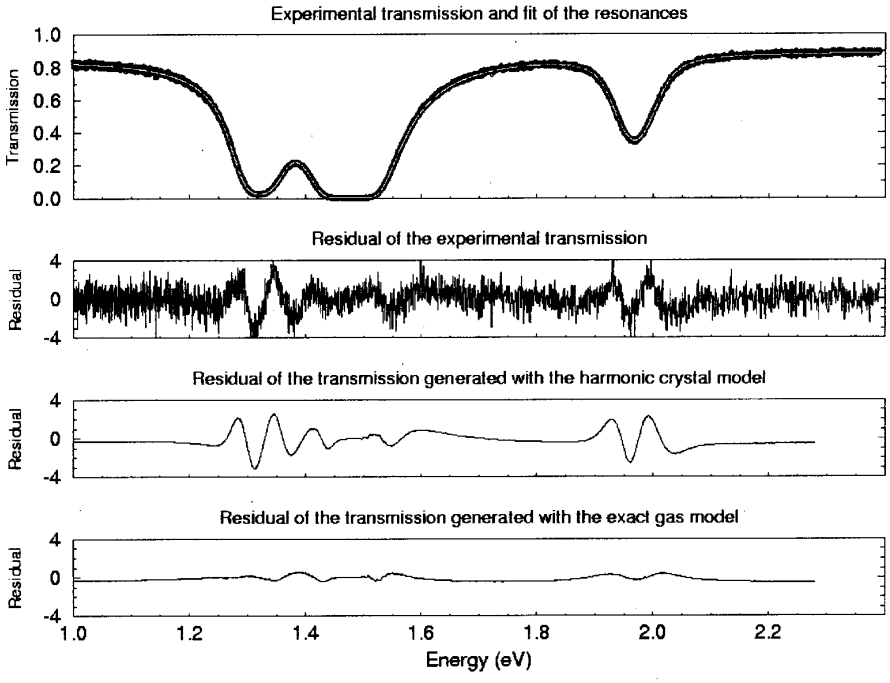

To verify this hypothesis, the following procedure of a “manual fit” has been developed:

For an isolated resonance with known parameters coming from the evaluations, a transmission spectrum is “generated” using DOPUSH with the harmonic crystal model. This spectrum is then fitted by REFIT with its gas model and the resulting parameters are compared to the initial parameters. The resulting differences are then used to correct the REFIT resonance parameters obtained from the analysis of the experimental data. The results are then assumed to be “real” resonance parameters which DOPUSH uses with the harmonic crystal model to generate a new transmission. Figure 4 shows in the residuals that the use of the “real” resonance parameters within the harmonic crystal model of DOPUSH creates a much better representation of the experimental data.

In Figure 5, the description of the resonance shape by REFIT is compared to the “generated” transmission of DOPUSH (with adjusted resonance parameters and harmonic crystal model). The harmonic crystal model seems to be able to reproduce the right shape of the resonances, because of its more accurate description of the Doppler broadening.

Figure 4. **Comparison between the fit by Refit and the simulated fit with the “generated” transmission based on the harmonic crystal model for Doppler broadening**

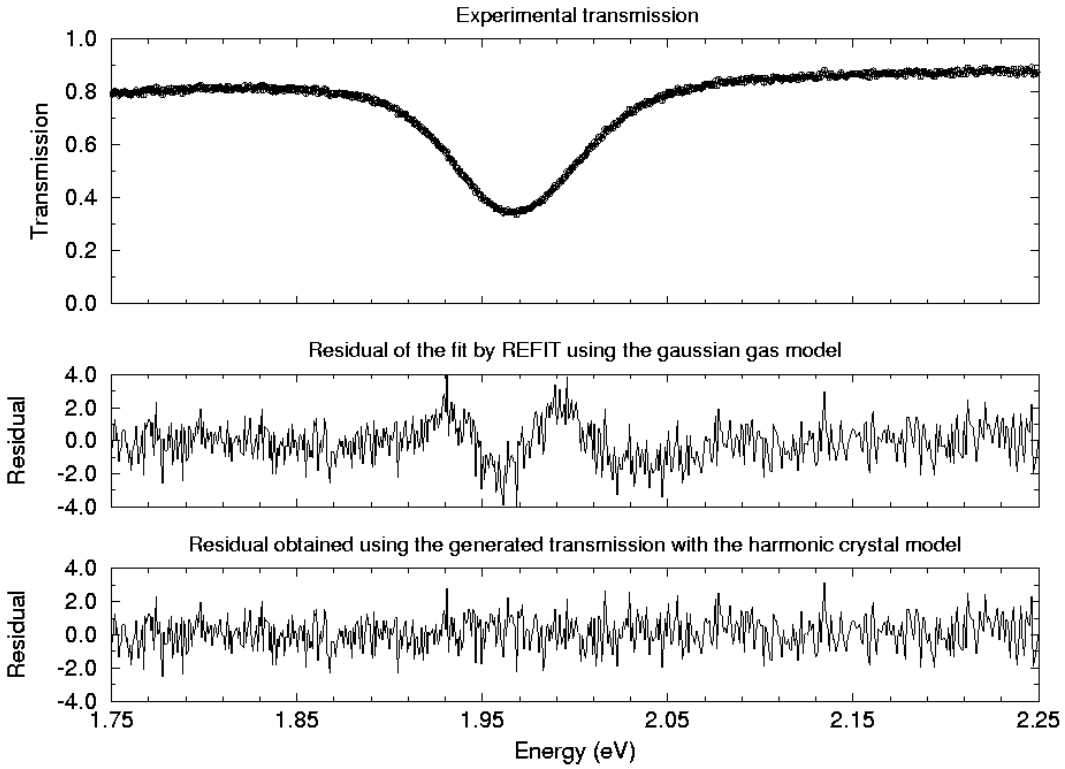

Figure 5. **Comparison between the fit by Refit and the "generated" transmission based on the harmonic crystal model for Doppler broadening with adjusted resonance parameters**

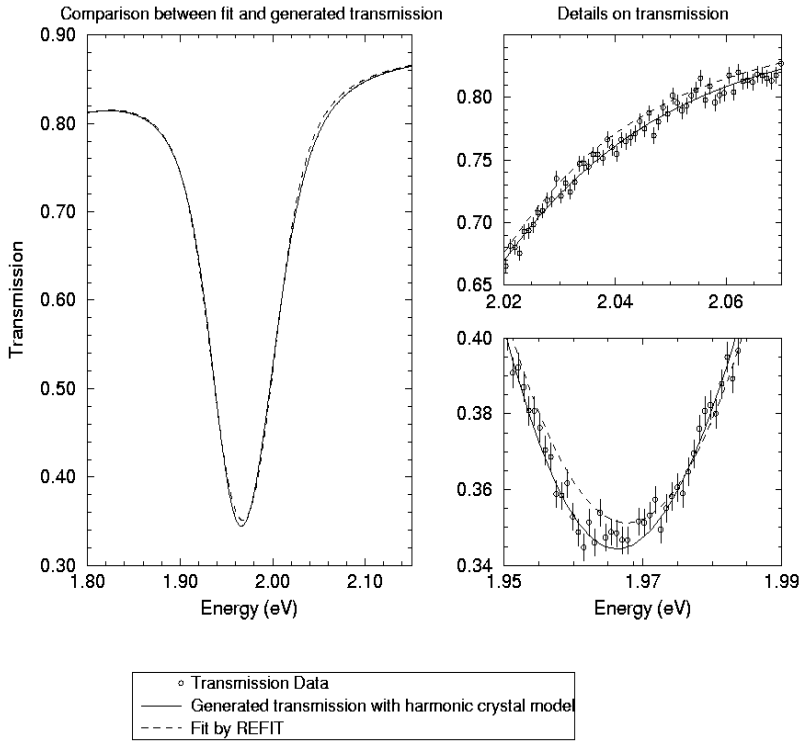

By adjusting the effective temperature on the transmission "generated" with the exact gas model, we observe in Figure 6 that the effective temperature stays constant as expected.

On the other hand, the effective temperature resulting from the transmission data "generated" by DOPUSH with the harmonic crystal model and fitted by REFIT shows the same behaviour as the fit to the experimental data.

We conclude that for molecules like NpO_2 and in the temperature/energy range under investigation, the structures seen in the residuals of the fits and the variation of the effective temperature in function of the neutron energy may be attributed to the the gas model, which is inadequate to describe the physical process of the Doppler broadening of the resonances.

The harmonic crystal model should be implemented in REFIT in order to improve the description of Doppler broadening for chemical compounds as NpO_2.

Figure 6. **Variation of the effective temperature adjusted on different data by Refit for a real temperature of 290 K**

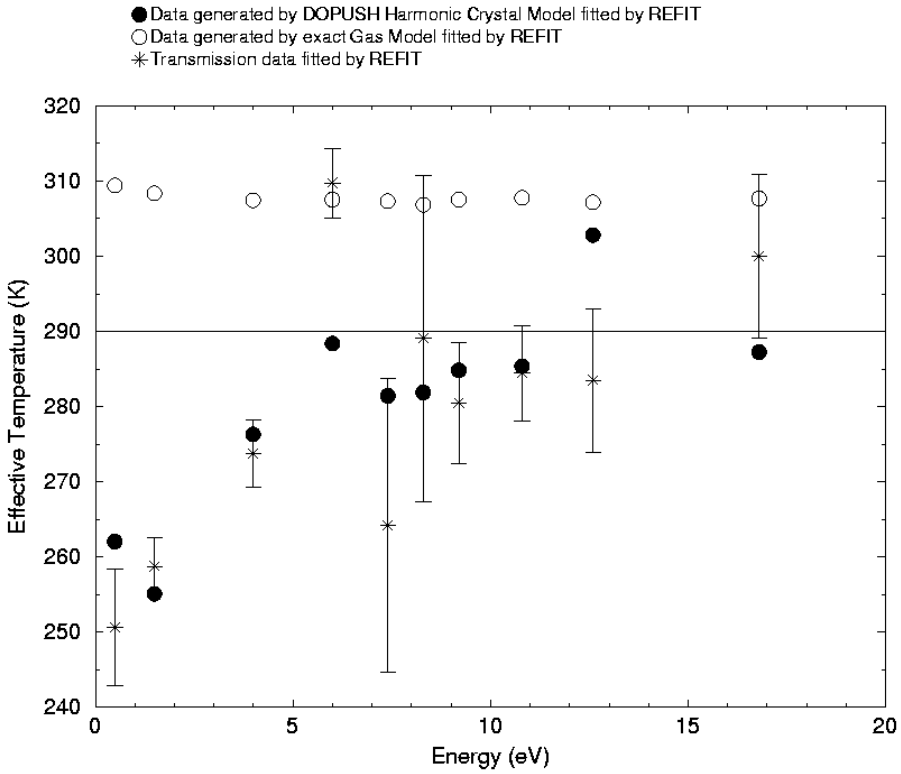

Acknowledgements

The authors would like to thank C. Ingelbrecht of the IRMM for preparing the samples, J.M. Salomé and the IRMM Linac operators for their assistance, H. Weigmann, C. Mounier and D. Nabrejnev for their precious help.

REFERENCES

[1] D. Paya, *Mise en Évidence et Étude d'une Structure Intermédiaire dans la Section Efficace de Fission de ^{237}Np*, FRNC-TH-431, PhD Thesis, Orsay (1972).

[2] Mewissen *et al*., Nucl. Sci. Eng.70 (1979) 155.

[3] L. W. Weston and J. H. Todd, Nucl. Sci. Eng. 79 (1981) 184.

[4] G. F. Auchampaugh and al., Los Alamos National Laboratory, Report LA-9756-MS (1983).

[5] H. Derrien and E. Fort, *Evaluation of the ^{237}Np Neutron Cross sections in the Energy Range from 10-5 eV to 5 MeV*, Int. Conf. On Nuclear Cross Sections for Technology, Knoxville, Tenn, USA (1979).

[6] NEA Nuclear Science Committee, *The NEA High Priority Nuclear Data Request List*, NEA/NSC/DOC(97)4 (1997) 50.

[7] A. Brusegan, E. Macavero, J. Gonzales, *Private Communication*.

[8] C. Bastian, IEEE Trans. Nucl. Science 43(4), (1996) 2343.

[9] C. Bastian, in Proc. Int. Conf. *On Neutron Research and Industry*, Crete, Greece 611.

[10] M. C. Moxon and J. B. Brisland, REFIT, *A least squares fitting program for resonance analysis of neutron transmission and capture data computer code*, version 12TN (United Kingdom Atomic Energy Authority, Harwell, 1991).

[11] S. F. Mughaghab, Neutron Cross Sections Vol 1. Part B *Neutron Resonance Parameters and Thermal Cross Sections*, National Nuclear Data Center, Brookhaven National Laboratory, Upton, New York, Academic Press(1984).

[12] D. Naberejnev, É*tude de l'influence des liaisons cristallines sur l'absorption et la diffusion des neutrons aux* énergies *des résonances*, PhD Thesis, Aix-Marseille (1998).

[13] D. Naberejnev, C. Mounier, and R. Sanchez, *On the Influence of Crystalline Binding on Resonant Absorption and Reaction Rates*, Nucl. Sci. Eng. (February 1999).

[14] W. E. Lamb, Phys. Rev. 55 (1939) 190.

EXPERIMENTAL MEASUREMENTS OF ^{99}TC AND ^{129}I TRANSMUTATION IN TARC AT CERN

E. González on behalf of the TARC collaboration
CIEMAT, Dept. Nuclear Fission, Avda. Complutense 22 Edif. 17
28040 Madrid,
Spain

The TARC collaboration

A. Abánades[n,(§)], J. Aleixandre[b], S. Andriamonje[c,a], A. Angelopoulos[j], A. Apostolakis[j],. H. Arnould[a], E. Belle[g], C.A. Bompas[a], L. Brillard[f], J. Bueno[b], S. Buono[c,h,(†)], F. Carminati[c], F. Casagrande[c,e,(¶)], P. Cennini[c], J.I. Collar[c], E. Cerro[b], R. Del Moral[a], S. Díez[m,(§)], L. Dumps[c], C. Eleftheriadis[l], M. Embid[i,d], R. Fernández[c,d], J. Gálvez[i], J. García[n,d], C. Gelès[c], A. Giorni[g], E. González[c,d], O. González[b], I. Goulas[c], D. Heuer[g], M. Hussonnois[f], Y. Kadi[c], P. Karaiskos[j], G. Kitis[l], R. Klapisch[c], P. Kokkas[k], V. Lacoste[a], C. Le Naour[f], C. López[i], J.-M. Loiseaux[g], J.M. Martínez-Val[n], O. Méplan[g], H. Nifenecker[g], J. Oropesa[c], I. Papadopoulos[l], P. Pavlopoulos[k], E. Pérez[i], A. Pérez-Navarro[m,(§)], M. Perlado[n], A. Placci[c], M. Poza[i], J.-P. Revol[c], C. Rubbia[c], J.A. Rubio[c], L. Sakelliou[j], F. Saldaña[c], E. Savvidis[l], F. Schussler[g], C. Sirvent[i], J. Tamarit[b], D. Truber[f], A. Tzima[l], J. B. Viano[g], S. Vieira[i], V. Vlachoudis[a,l], K. Zioutas[l].

a) *CEN, Bordeaux-Gradignan, France*
b) *CEDEX, Madrid, Spain*
c) *CERN, Geneva, Switzerland*
d) *CIEMAT, Madrid, Spain*
e) *Dip. di Fisica e INFN, Univ. di Padova, Italy*
f) *IPN, Orsay, France*
g) *ISN, Grenoble, France*
h) *Sincrotrone Trieste, Italy*
i) *Universidad Autónoma de Madrid, Spain*
j) *University of Athens, Greece*
k) *University of Basel, Switzerland*
l) *University of Thessaloniki, Greece*
m) *Univer. Alfonso X el Sabio, Madrid, Spain*
n) *Universidad Politécnica de Madrid, Spain.*

(§) Present address at LAESA, Zaragoza, Spain. Present address MIT, Cambridge, USA
(†) Present address CRS4, Cagliari, Sardegna, Italy

Abstract

A short description of the set-up of the TARC experiment at CERN and the ARC principle is presented. This is followed by a very brief overview of the flux measurements and their comparison with the MC prediction. Then the method and specific set-up used for the integral transmutation of ^{99}Tc and ^{129}I measurements will be shown, indicating some of the actions taken to minimise systematic uncertainties. With this set-up the transmutation rate of ^{99}Tc and ^{129}I was measured in many positions around the lead block, corresponding to different neutron spectra and flux intensities. The experimental results and the excellent agreement with the MC predictions are discussed. Finally, the CeF_3 measurements of the energy dependence of the neutron capture on ^{99}Tc targets are explained. All these measurements confirm the ARC effect and its potentiality for LLFF transmutation.

Introduction

The TARC experiment conducted at CERN by an international collaboration including more than 14 institutions from different European countries and partially financed by the DGXII of the EU and some national agencies, is the second phase of the experimental program of the Energy Amplifier [1], EA. The objectives of the experiment can be grouped in two main lines: first, the measurement and simulation of the production of neutrons in large volumes of lead and their diffusion and moderation in this medium, and second, the measurement and simulation of the Transmutation by Adiabatic Resonance Crossing, ARC, of some of the most relevant long lived fission fragments, LLFF, mainly ^{99}Tc and ^{129}I.

The ARC principle is based on the lead properties. Lead is a material highly transparent to neutrons (very low absorption cross section from the MeV region down to very low energies) but with a moderate elastic neutron cross section that in addition is nearly energy independent in a large energy range (mean free path close to 3 cm) and with a high atomic mass that limits the maximum energy transfer in a neutron elastic collision (the minimum fraction of the original neutron energy after a collision is $\alpha \equiv ((A-1)/(A+1))^2 = 0.981$ for natural lead). Taking into account these properties it is easy to realise that if a neutron source, producing neutrons in the MeV region, is introduced in a large lead volume a high neutron flux will be developed with a neutron energy spectra nearly isoletargic. In other words neutrons produced at high energies will moderate very slowly their energy, moving over long distances without substantial change in their energies (high flux intensity) and, because of the low absorption, the total number of neutrons is conserved down to very low energies. The scattering cross section being constant provides in this way a nearly isoletargic flux, when integrated over the whole volume covered by the neutron flux. For any particular position this distribution is slightly modified depending on the spatial distribution of the neutron source.

The main element to achieve that high intensity flux is the very small energy loss per collision, for this reason we describe that process as *Adiabatic* neutron moderation. The isoletargic energy distribution of the flux allows to take full advantage of the resonances in the cross section of the transmutation process. In the case of LLFF, the transmutation takes place by neutron capture. For example when ^{99}Tc ($t_{1/2} = 2\times10^5$ y) captures a neutron produces ^{100}Tc that decays, with a half live of 15.8 s, to the stable ^{100}Ru. Several of the most offending LLFF in the nuclear wastes present important neutron capture resonances, Figure 1 for ^{99}Tc, making resonance capture in an adiabatic neutron flux, TARC, a promising method for the elimination of those wastes.

The verification of the TARC principle requires both the measurement of the neutron flux energy and space distribution and the experimental determination of the transmutation rates. In the following sections the experimental set-up, a brief description of the flux measurements techniques and results, the measurements of transmutation rates and their comparison with Monte Carlo simulations will be presented.

TARC experimental set-up

The main elements of the TARC experiment are a large lead block, the proton beam, and the DAQ system.

Figure 1 **^{99}Tc capture cross section**

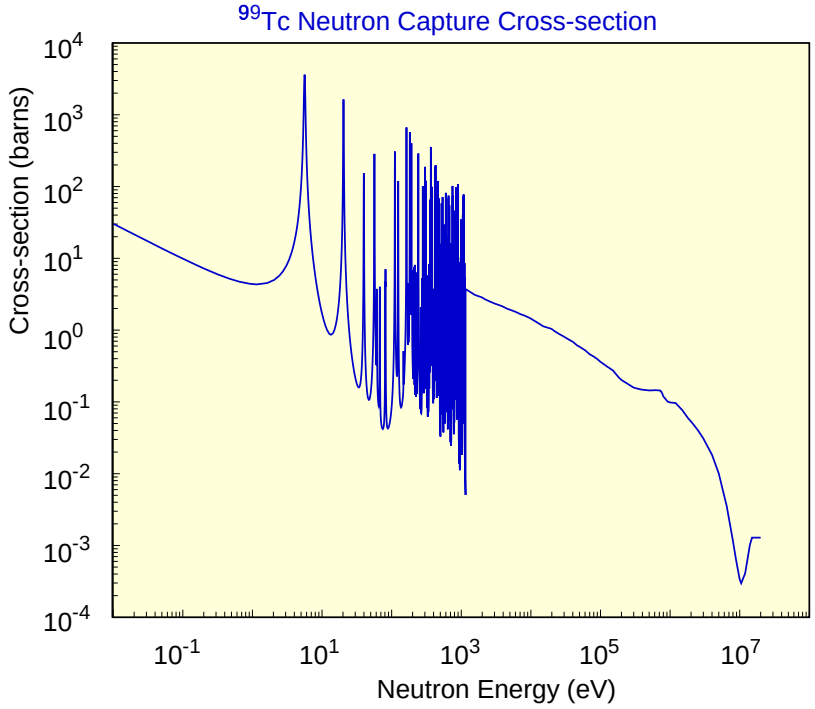

Figure 2 shows the arrangement of the 334 tons of pure lead where the neutrons, produced by spallation by the proton beam and diffused by the collisions with the lead nuclei make up the neutron flux. Lead has been commercially obtained with a nominal purity of 99.99%. This Lead purity has been exhaustively verified for nearly every element in the periodic table, by several techniques. The only relevant contaminations found were 19±2 ppm of Bi and 3.6±0.6 ppm of Ag. The block shape is close to a square parallelepiped, 3.3×3.3 m^2 of base and 3 m long, with the corners removed. It includes a 120 cm deep longitudinal beam hole, in the centre of the front face, and 12 full length longitudinal instrumentation holes.

A very flexible pulsed proton beam, extracted from the PS accelerator complex at CERN, has been used. The kinetic energies ranged from 200 MeV to 2.75 GeV, and the beam intensities varied from 10^3 to 10^{10} protons per shot. The beam intensity has been measured, shot by shot, by two systems. The first one, for high intensities, was based on a pair of beam transformers, Figure 3, which provided an intrinsic resolution of 1%. The absolute calibration was based on the irradiation of Al foils. A global uncertainty of 5% was achieved on the beam intensity determination. The beam instrumentation included also multiwire proportional chambers, MWPC, that measured the position and angle of the beam. For very small beam intensities a scintillators hodoscope allowed to count the actual number of particles arriving to the lead beam hole at each shot.

The advanced DAQ system was based on VME and CAMAC modules, recorded more than 200 Gbytes of data and allowed the on-line monitoring of the data quality.

Figure 2 **TARC lead block, transverse view**

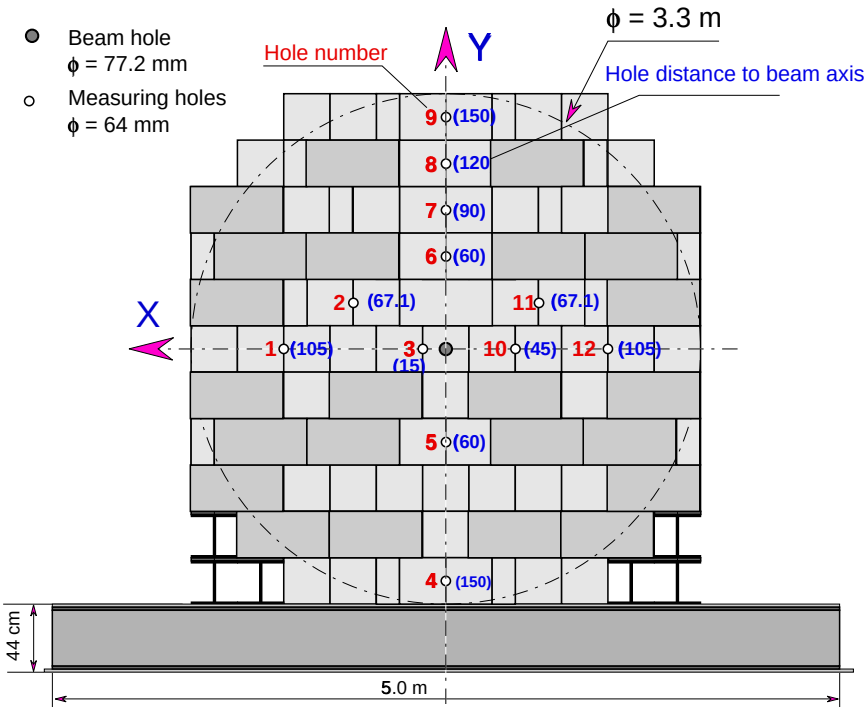

Figure 3 **Longitudinal view of the beam instrumentation close to the experimental area**

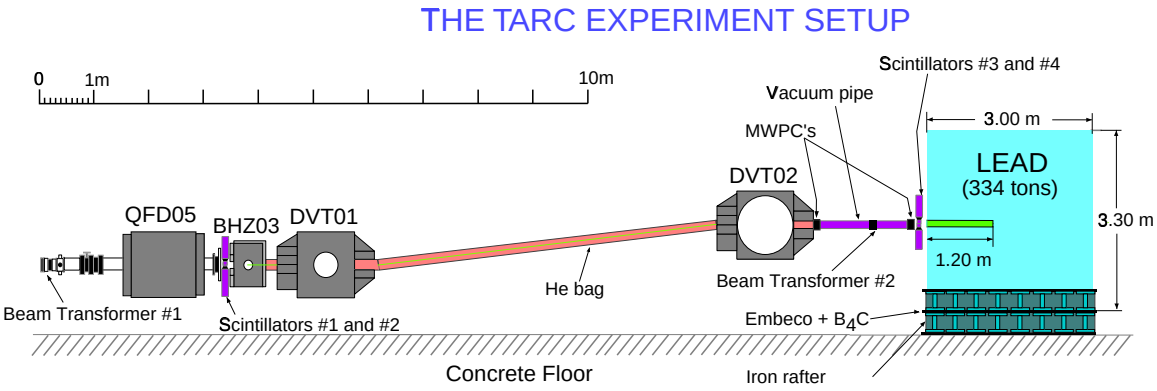

Neutron flux measurements

A large panoply of neutron detectors, including ^{3}He (ionisation and scintillation), ^{6}Li + Si detectors, Activation foils, Thermoluminiscense detectors and Track etching detectors, placed in successive measurements at different positions inside the instrumentation holes, has provided a very detailed map of the neutron flux for the full neutron energy range, from thermal energies to few MeV. The details of the different detectors can be found somewhere else [2,3,4,5]. From the point of view of the LLFF transmutation experiments, the most relevant energy region, 0.1 eV to 1000 eV, is covered by the ^{3}He scintillation detector and the (^{6}Li, ^{233}U)+ Si counters. Both detectors rely on the time to energy relation, characteristic of the neutrons moving in a slowing down lead spectrometer [6] to compute the energy of the detected neutrons. This relation has been calibrated in TARC with the

help of a CeF_3 scintillator and samples with known resonances. As an additional verification, the neutron fluence has been measured at precise energies in a completely independent way, using activation foils. Foils of ^{115}In (1.457 eV), ^{107}Au (4.9 eV) and ^{186}W (18.8 eV) have been used in TARC.

Figure 4 shows the measurements, from all detectors, of the neutron fluence, as a function of the neutron energy, at the instrumentation hole #10 and at co-ordinate Z=+7.5 cm, for a proton kinetic energy of 1.73 GeV. The detector redundancy together with the repetition of measurements at symmetrical positions and different beam energies, and the excellent agreement of measurements from different detectors have provided a very strict control of systematic uncertainties.

Figure 4 **Neutron fluence neutron energy spectra measured at TARC**

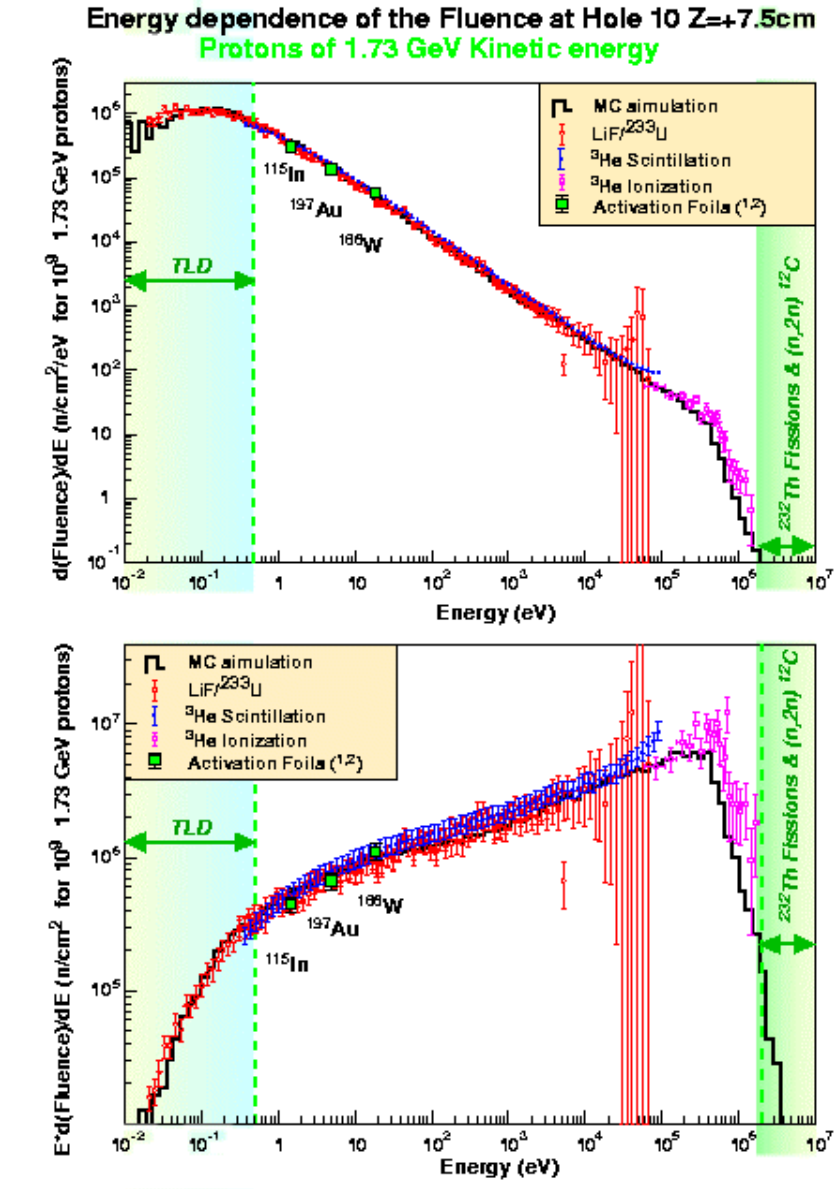

Notes: 1) Data scaled from 2.75 GeV kinetic energy. 2) Data scaled from different (close) position.

Many measurements where made with those detectors at different positions. Maps of the fluence at different energies have been built from these measurements. Figure 5 shows the space distribution of the fluence, for energies from 0.1 eV to 180 KeV, for a proton kinetic energy of 2.75 GeV, versus the distance to the lead block centre multiplied by the sign of the Z co-ordinate. Even when a perfect spherical symmetry is not expected, the data can be approximately described by a simple gaussian function of this distance, as expected from the Fermi age theory for a punctual source in an infinite lead volume.

Figure 5 **Experimental spatial distribution of the neutron fluence for different energies**

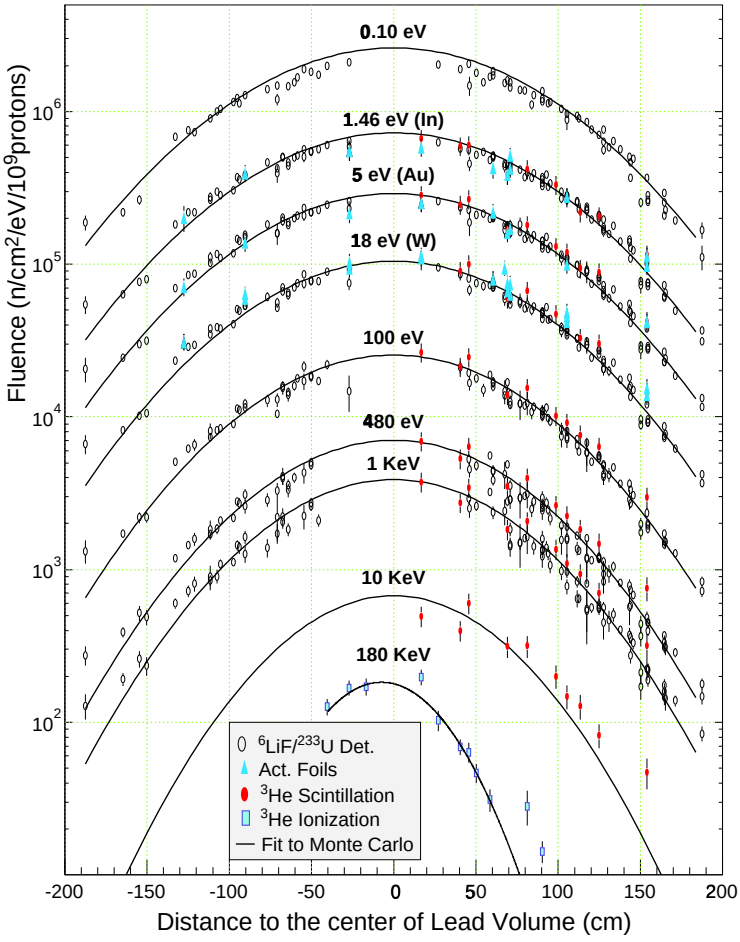

Both figures show the excellent agreement of the Monte Carlo predictions, for all the positions and energies, with differences to the data of the order of 10 to 15%, in the energy range most relevant to ARC.

Transmutation of ^{99}Tc

In the TARC experiment the ^{99}Tc transmutation was directly measured for macroscopic samples (close to 1 gram) in different conditions both of the sample and of the neutron flux energy spectra and intensity. In addition to the interest of the direct data by themselves, they allow to verify the available evaluated cross sections and the simulation tools. The ability to study situations with largely different contributions of the resonance region to the ^{99}Tc transmutation and the study of situations with large selfshielding effects was especially interesting.

Figure 6, shows a simplified scheme of the ^{99}Tc transmutation process. ^{99}Tc, already radioactive with a half live of 2.111×10^{5} years, after capturing a neutron becomes ^{100}Tc, usually in an excited state. This state decays very fast (typically in few ns) into ^{100}Tc ground state, by emitting the so-called *prompt* photons. At a much slower rate, half-live of 15.8 s, ^{100}Tc decays by a β^- transition to ^{100}Ru, about 7% of the cases into excited states of this isotope. Then, these ^{100}Ru excited states decay very fast, in less than 1 ns, into the ^{100}Ru ground state, emitting the so-called *delayed* photons.

The absolute transmutation rate is determined at TARC from the measured rate of these delayed photons. The measurement is integral in the sense that it includes the contribution from the transmutation produced by neutrons of all the energies. Because of the uncertainty on the fraction of ^{100}Tc decays including one or more photons, our measurement of the transmutation rate has a systematic error of 14%. This has become the dominant component of the TARC measurement of the ^{99}Tc transmutation rate. However special care has been applied to keep all the other systematic errors at their minimum level, in such a way that, whenever more precise information on the ^{100}Tc decay is available, the TARC data resolution can be improved.

Figure 6 **Simplified scheme of the ^{99}Tc transmutation process**

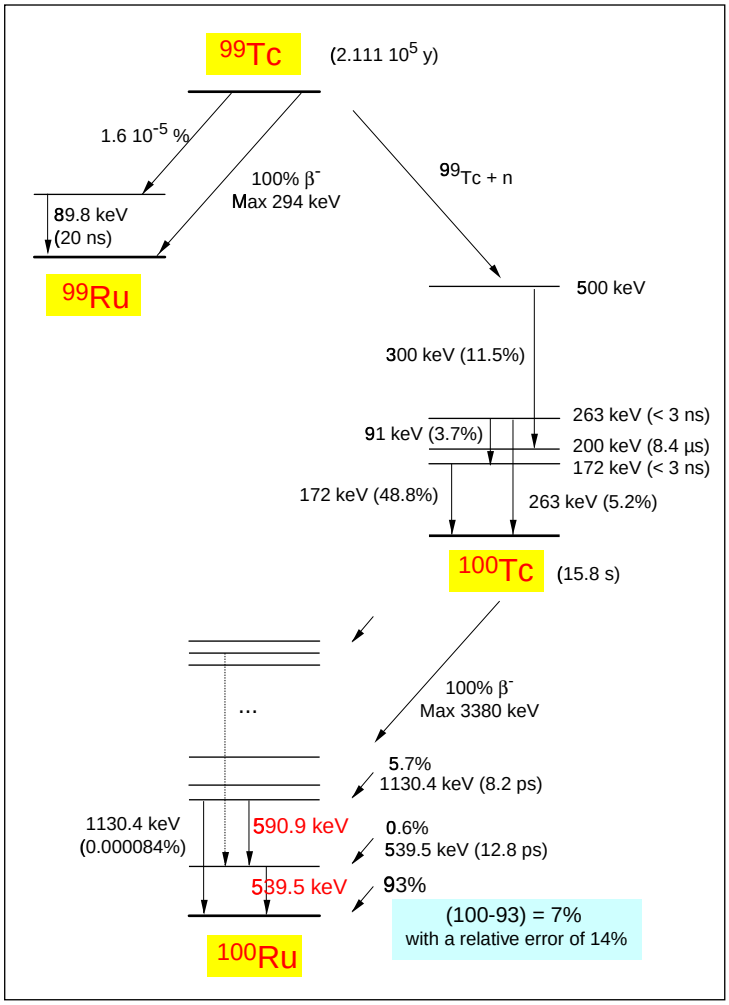

Figure 7 **Experimental determination of the ^{99}Tc half-live**

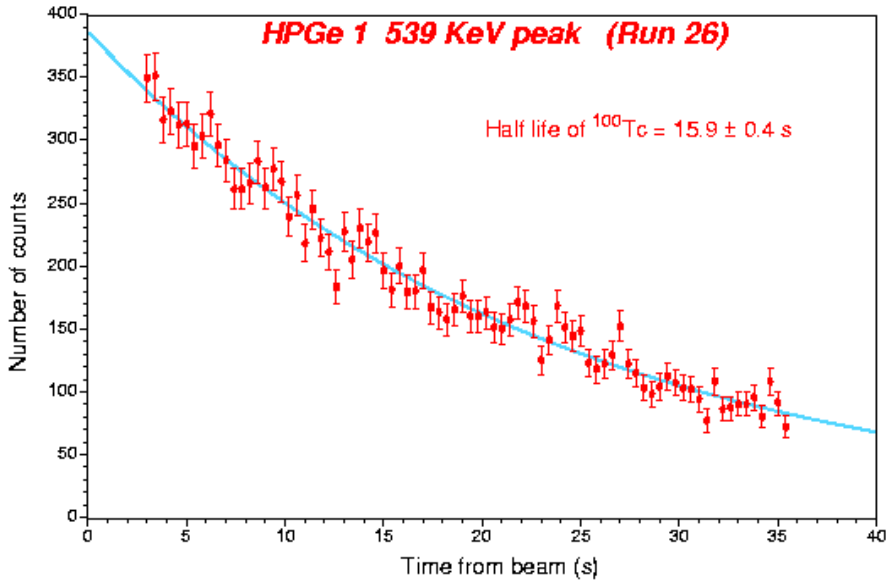

The short half live of ^{100}Tc, verified at TARC in a special experiment, Figure 7, makes difficult the accumulation of the large statistics required to achieve the 1% statistical precision of TARC. This difficulty is overcome by using a pneumatic system, called *Rabbit* and described schematically at Figure 8, that transfer cyclically the sample between the irradiation position and the measuring station after each pulse of the CERN-PS proton accelerator. In this way and with a precise measurement of the beam intensity, pulse by pulse, it was possible to accumulate as much statistic as required with modest mass samples and neutron flux intensities. This figure also shows the shape of the container and sample used in most of the ^{99}Tc transmutation experiments, that consist on 441 mg of $KTcO_4$ powder.

Figure 8 **Scheme of the TARC Rabbit system**

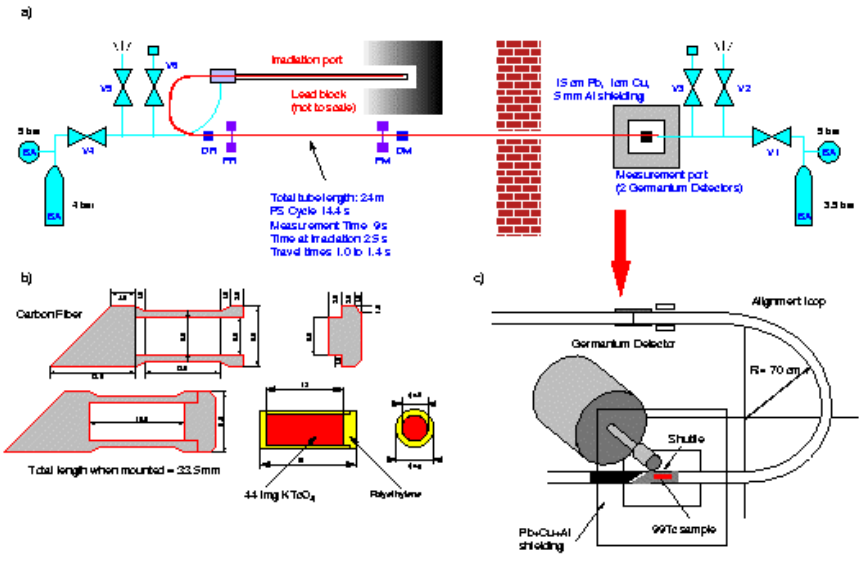

Figure 9 shows a transverse view of the *Rabbit* measuring station. All the elements of this station have been carefully set-up to reduce the instrumental systematic errors. This includes a very large detector shielding with more than 15 cm of lead and the use of redundant instrumentation by installing two large independent HPGe counters. In addition detailed studies and appropriated correction had been applied for every single aspect of the experiment, including: the samples masses, the calibration of the HPGe detectors, the photon absorption in the sample itself and in the transport capsule, the beam intensity and quality, the position of the sample during the measurement at each *Rabbit* cycle, the accidental and correlated pileups, the system dead time, the electronic failures and the procedure for evaluation of the number of signals inside each photon line. As a result of these efforts we estimate in 8% the total instrumental systematic error of the ^{99}Tc transmutation rate measurement at TARC.

Figure 9 **Transverse view of the *Rabbit* measuring station**

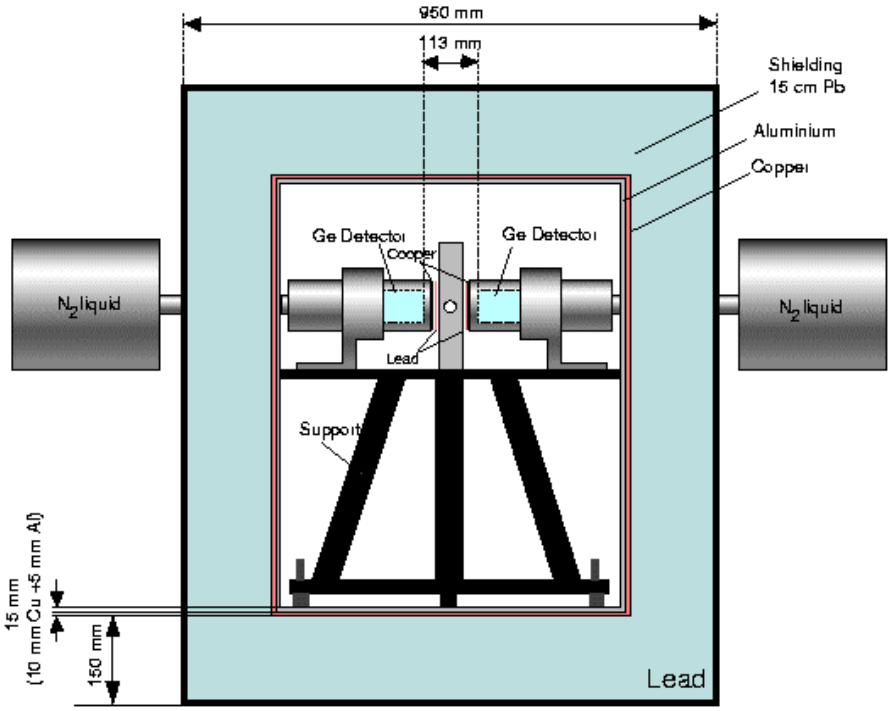

Figure 10 shows the spectrum of photons collected by one of the HPGe counters from the sample during one set of irradiations. The spectrum shows the characteristic set of lines corresponding to the decay of ^{100}Tc into the excited states of ^{100}Ru. Two prominent lines can be found at 539 KeV and at 590 KeV. The resolution of the HPGe counter at these energies is of 2-3 KeV and even when the background is very small, note that the vertical scale in Figure 10 is logarithmic and that the detail in the corner shows the 539 peak in linear scale, this background has been carefully discounted from the activity on the line. Both photon lines had been used independently to compute the transmutation rates, and combining this fact with the use of two detectors, a four-fold redundancy in the ^{99}Tc transmutation rate determination was available at TARC. This redundancy has provided an exceptional control of the possible instrumental systematic effects. In the Figure there are a few lines produced from the impurities in the sample, ^{137}Cs and ^{98}Tc, the intensity of these peaks is independent of the irradiation and this fact has also been used to control the data quality.

Figure 10 **Spectrum of delayed photons from the ^{99}Tc sample after irradiation**

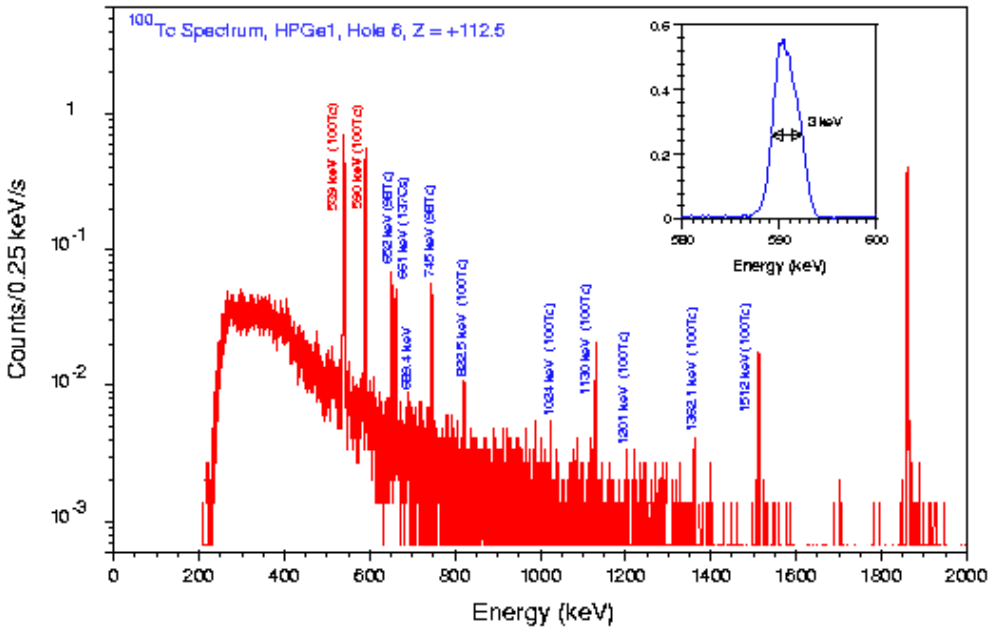

Figure 11 **^{99}Tc transmutation rate, for a sample with 216.1 mg of ^{99}Tc and for 2.75 GeV kinetic energy protons, as a function of the irradiation position in the TARC lead block**

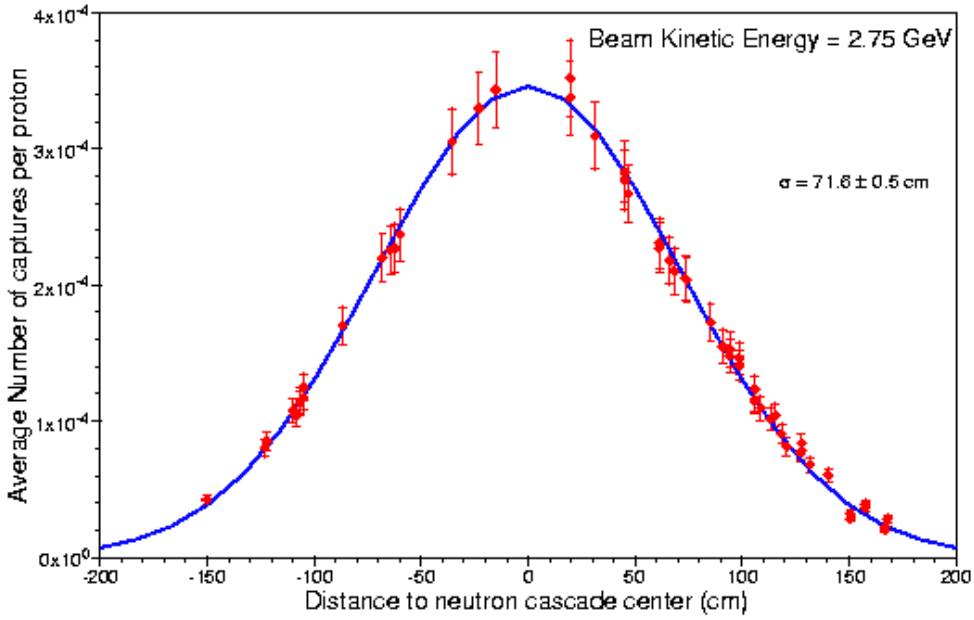

With this system and careful analysis, a large set of measurements had been performed irradiating the sample at more than 50 positions distributed all around the TARC lead block. Figure 11 shows the average number of captures in ^{99}Tc, or ^{99}Tc transmutations, per proton in the different positions, as a function of the distance to the neutron cascade centre times the sign of the Z co-

ordinate. The transmutation rate for a sample with 216.1 mg of ^{99}Tc, placed at 45 cm from the lead block centre, is 2.67×10^{-4} transmutation per 2.75 GeV proton and the total error is 16%. The different data are very coherent one to each other, show a high degree of isotropy (except for the farthest points that are too close to the lead block surface) and can be approximately described by a gaussian function with parameters very close to those corresponding to the neutron flux distribution in the range from 1 to 100 eV. This behaviour is expected from the large contribution of the two main capture resonances (5.9 and 20 eV) to the ^{99}Tc transmutation in the TARC experimental conditions.

Figure 12 **Ratio of the transmutation rates measured by the two different HPGe counters from the 590 KeV photon line as a function of the irradiation position**

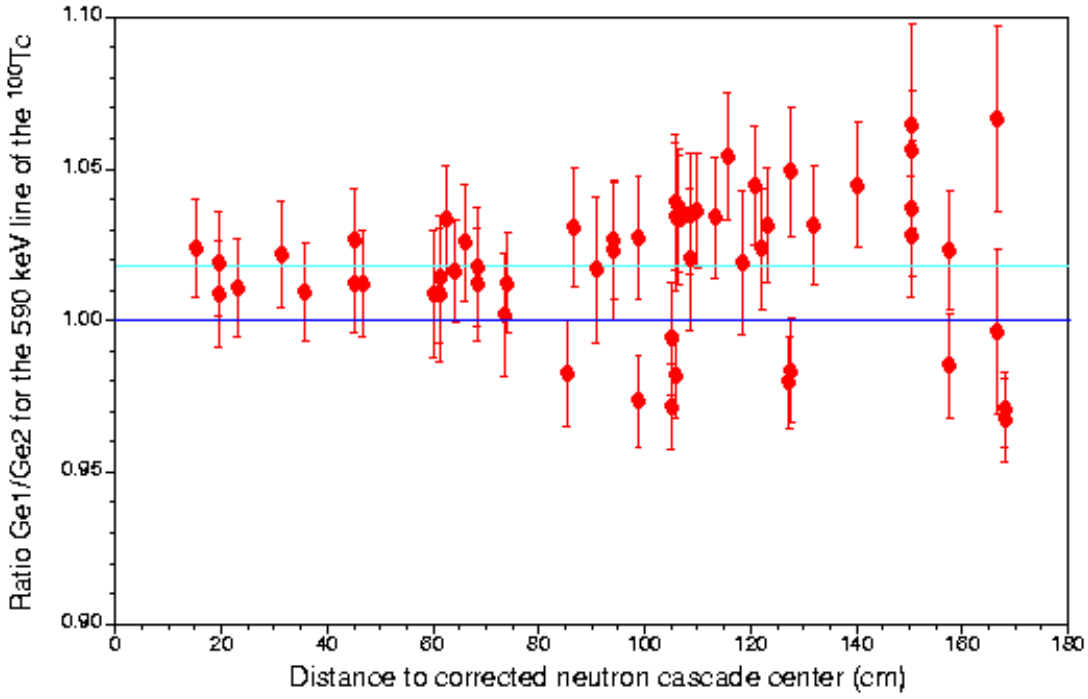

A verification of the low level of systematic errors is provided by the Figures 12 and 13. The first figure shows the ratio of transmutation rates obtained from the data of the two different HPGe counters from the same ^{100}Tc photon line (590 KeV). This figure is sensible to the systematic errors on the efficiency and dead time of the counters, an all the points are compatible within errors with a constant ratio corresponding to 2% systematic error. On the other hand, Figure 13 shows the ratio of the estimated ^{99}Tc transmutation rates by using the two photon lines for the same HPGe counter as a function of the irradiation position. This figure, that will show systematic errors on the angular correlation corrections, photon absorption in the instrument materials, peak reconstruction and relative probability of the two lines, is also compatible within errors with a constant value corresponding to a systematic error of 3%.

Figure 13 **Ratio of the transmutation rates measured by using the two photon lines for the same HPGe counter as a function of the irradiation position**

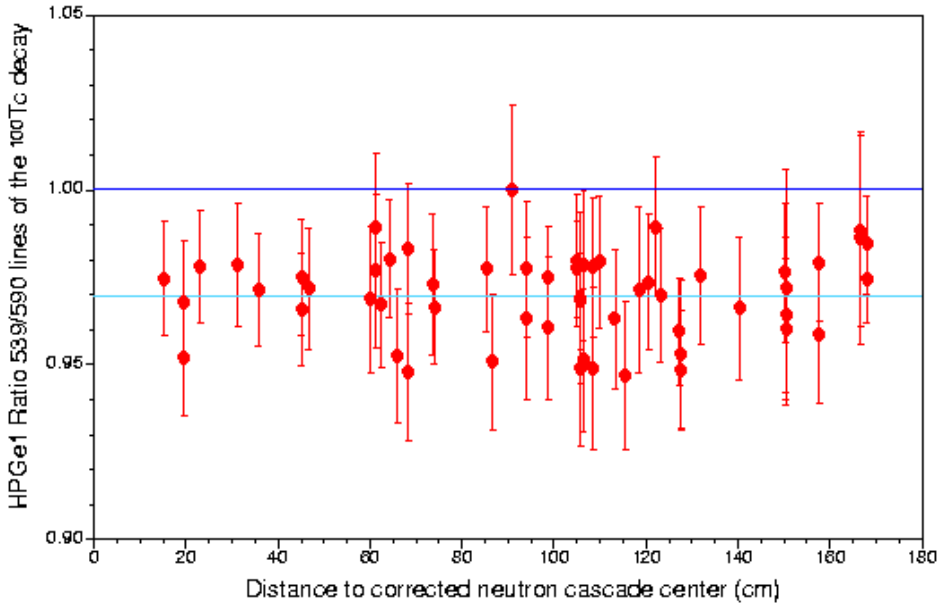

Previous graphs have shown the quality of the data, Figure 14 shows the comparison of the experimental data with the predictions of a complete Monte Carlo simulation of the ^{99}Tc transmutation process at the TARC experiment, using the Energy Amplifier simulation system [7,8,9] and the JENDL 3.2 nuclear data libraries. An excellent agreement is found for all the positions, with an average deviation smaller than 5% well below the 14% uncertainty on the fraction of ^{100}Tc decays with photons. All the points are consistent with this deviation within the errors bars displayed in the figure that include only the statistical and instrumental systematic uncertainties.

Figure 14 **Ratio Data/Monte Carlo for the ^{99}Tc transmutation rate as a function of the irradiation position**

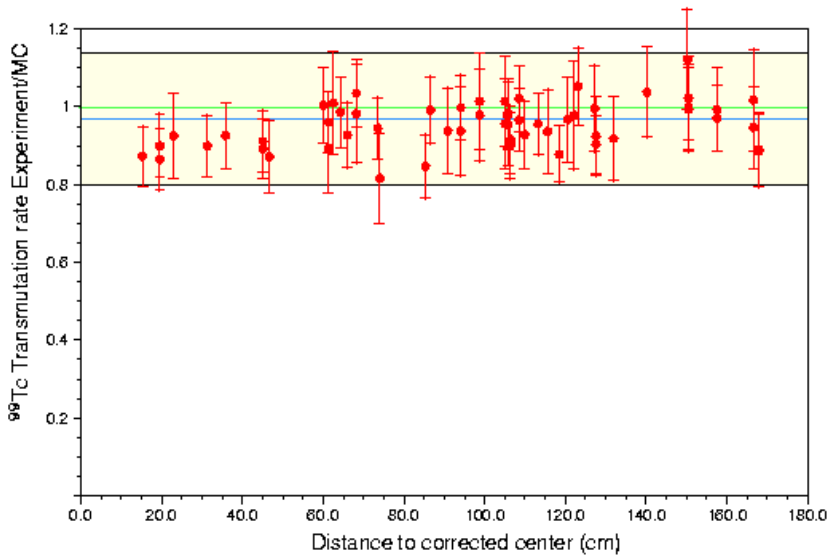

The complexity of the simulation and the relevance of the agreement are clarified by Figures 15 and 16. Figure 15 shows the fraction of ^{99}Tc transmutation produced by neutrons of different energy ranges: thermal region (0-3 eV), the main resonances region (3-100 eV) and the fast region (100 eV-20 MeV) as a function of the irradiation position, according to the Monte Carlo simulation. These graphs show the substantial change in the contributions from resonance and fast neutrons to the ^{99}Tc transmutation, from the centre to the periphery of the lead block, as a consequence of the neutron energy spectrum evolution with the position inside the lead block.

Figure 15 **Monte Carlo estimated contributions from the different neutron energy ranges as a function of the irradiation position**

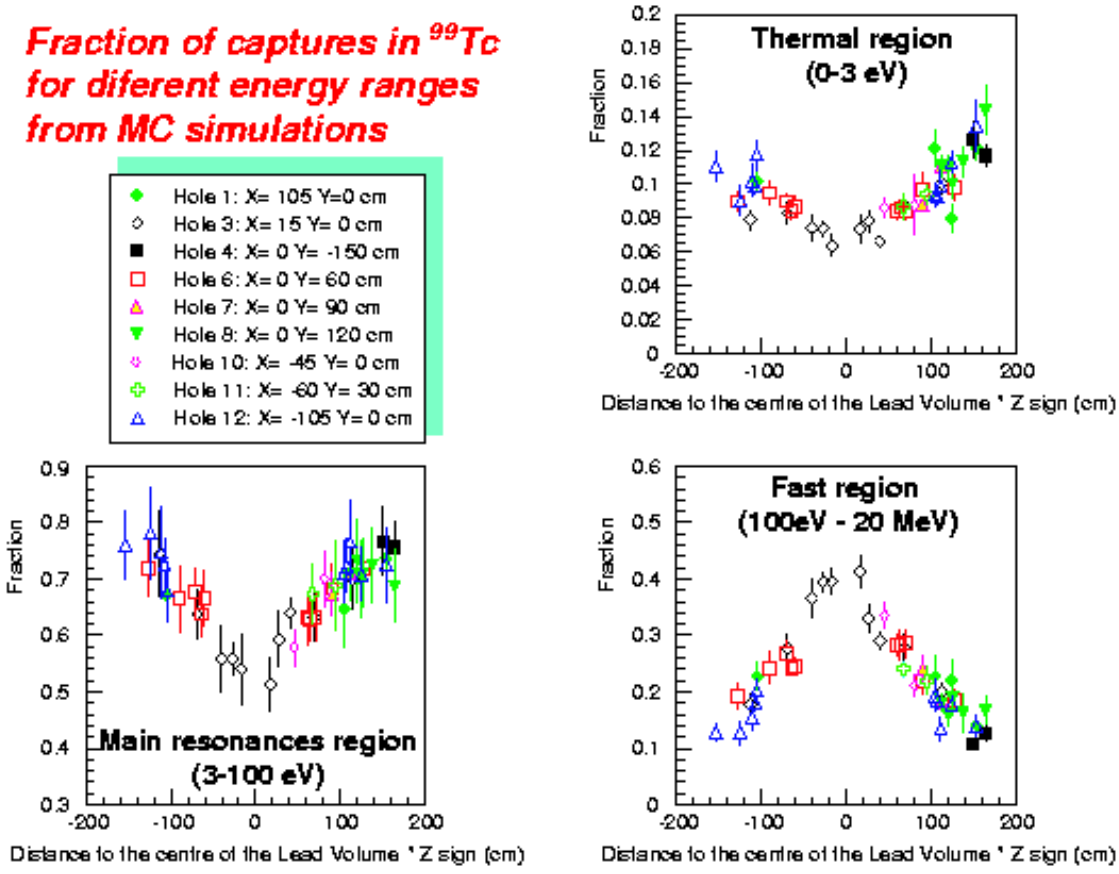

On the other hand, Figure 16 shows the experimental data of the transmutation rates, at a fixed irradiation position, for three different samples of ^{99}Tc. The samples have different masses, density and chemical form (2 samples are $KTcO_4$ and one is a very thin Tc metallic foil). The data show that shelfshielding levels as high as 50% are suffered by the heavier sample. The figure also presents the Monte Carlo simulation, in excellent agreement with the data. Shelfshielding is a function of the neutron spectra and consequently of the irradiation position, changing the magnitude from point to point in Figure 14, the agreement at all the position shows a correct description of the effect by the Monte Carlo with the JENDL 3.2 database. Further details on the integral measurements of the ^{99}Tc transmutation can be found at [10,8,9].

Figure 16 **Experimental data and Monte Carlo predictions for the ^{99}Tc transmutation rate, normalised to the sample mass, for three different samples with different masses and chemical compositions**

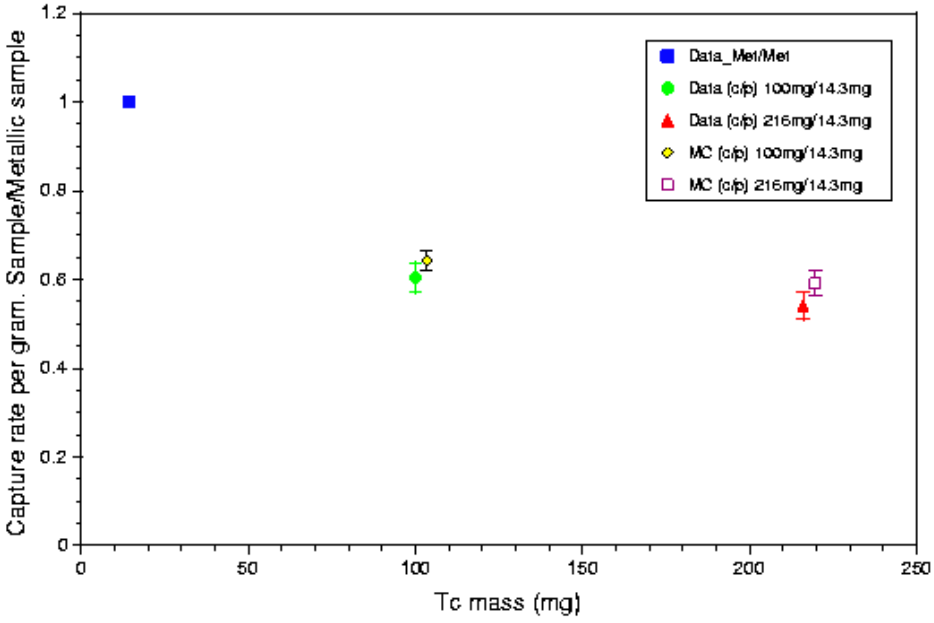

Figure 17 **^{99}Tc transmutation rate as a function of the neutron energy and ^{99}Tc apparent neutron capture cross section**

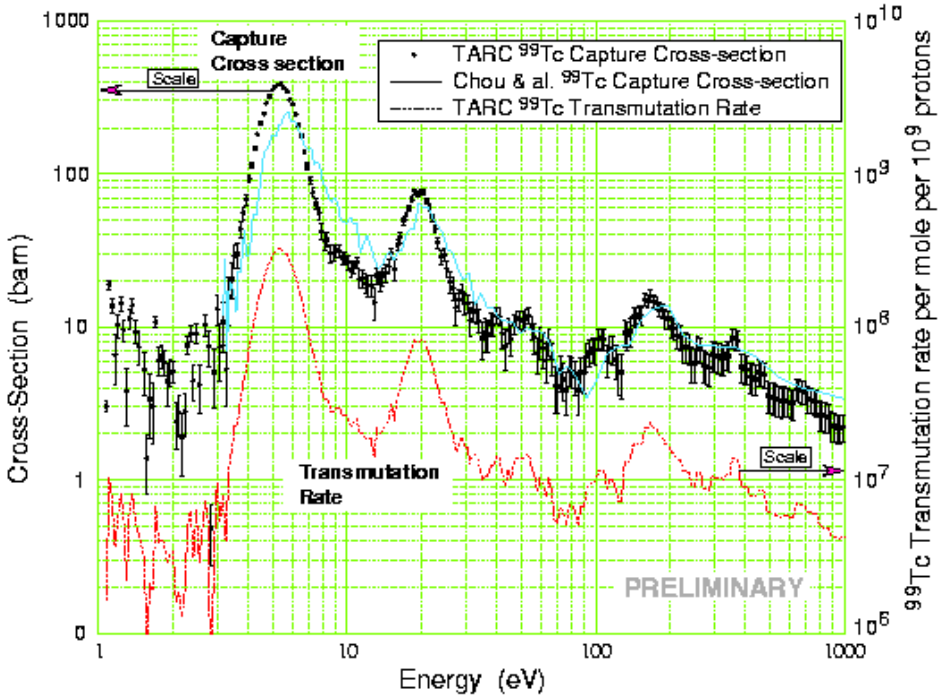

In addition to the integral measurements, the dependence of the transmutation rate with the neutron energy was measured from the prompt photons emitted after the neutron capture, with the help of a CeF_3 scintillator and using the characteristic relation between detection time and neutron energy of lead slowing down spectrometers, already mentioned. Figure 17 show this dependence for a ^{99}Tc sample irradiation position at 45 cm from the lead centre and a proton kinetic energy of 2.75 GeV. The apparent neutron capture cross section of ^{99}Tc, obtained from this curve and the neutron flux energy spectra experimentally measured, is also shown in the figure in comparison with the previous Chou et al measurements [11]. Much better statistics and resolutions had been obtained at TARC. This apparent capture cross section is an additional element for cross checking the available nuclear data libraries. Further details on the integral measurements of the ^{99}Tc transmutation can be found at [8,9].

Transmutation of ^{129}I

The ^{129}I fission fragment with a half live of 1.57×10^7y, is together with ^{99}Tc, one of the most offending isotopes in the nuclear wastes at very long times. The measurement technique used for iodine is simpler than for technetium because the half-lives of the resulting isotopes are long enough and no *Rabbit* was required. On the other hand the analysis is more difficult. Figure 18 shows the scheme of nuclear reactions taking place in the sample during the ^{129}I transmutation. When ^{129}I captures a neutron produces ^{130}I excited states, but as ^{130}I has two isomers, a fraction of the reactions will decay immediately to the ground state but another part will populate the ^{130m}I isomer. Then the ^{130m}I can either decay to the ground state or directly decay to ^{130}Xe. Finally, the ^{130}I ground state nuclei will also decay to ^{130}Xe. The delayed photons produced in the last 3 decays have been used at TARC to evaluate the transmutation rate of the sample.

Figure 18 **Scheme of nuclear reactions taking place in the TARC ^{129}I sample during its transmutation**

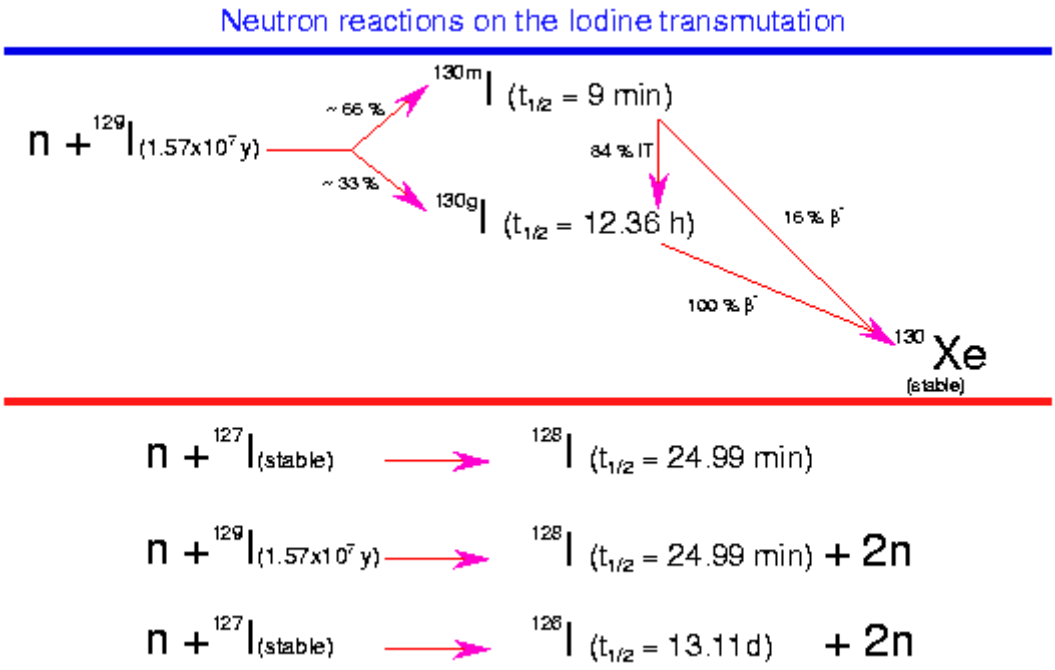

Figure 19 **Geometry and characteristics of the ^{129}I sample used at TARC**

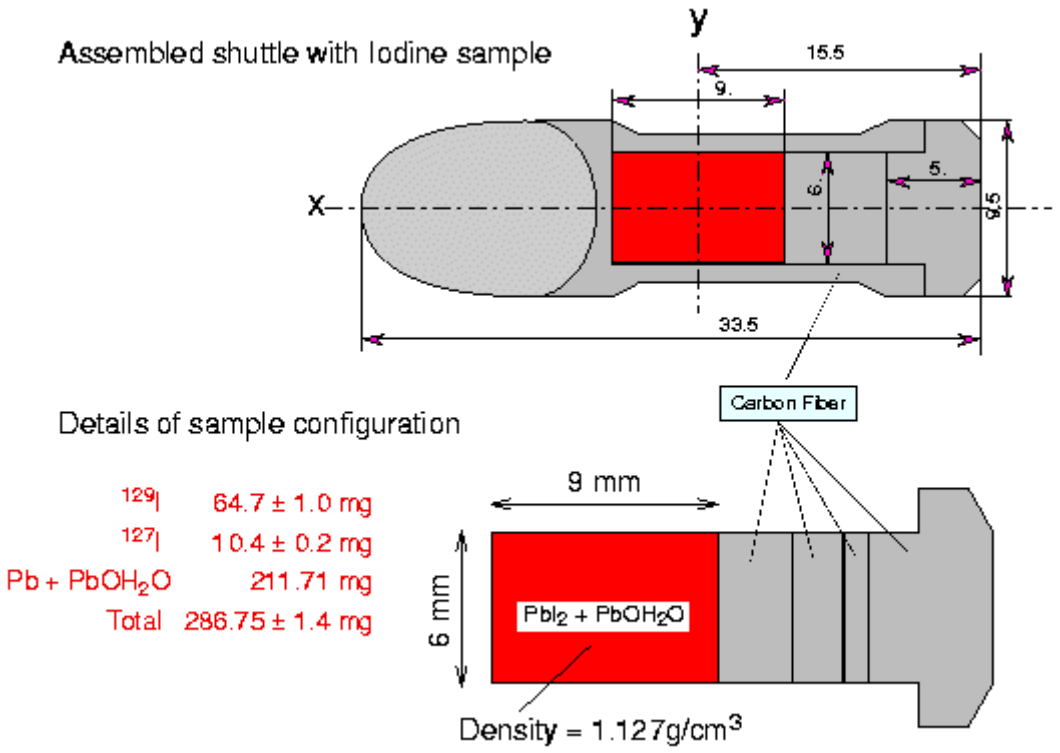

Figure 20 **Photon spectra collected from the ^{129}I sample at two different times after irradiation**

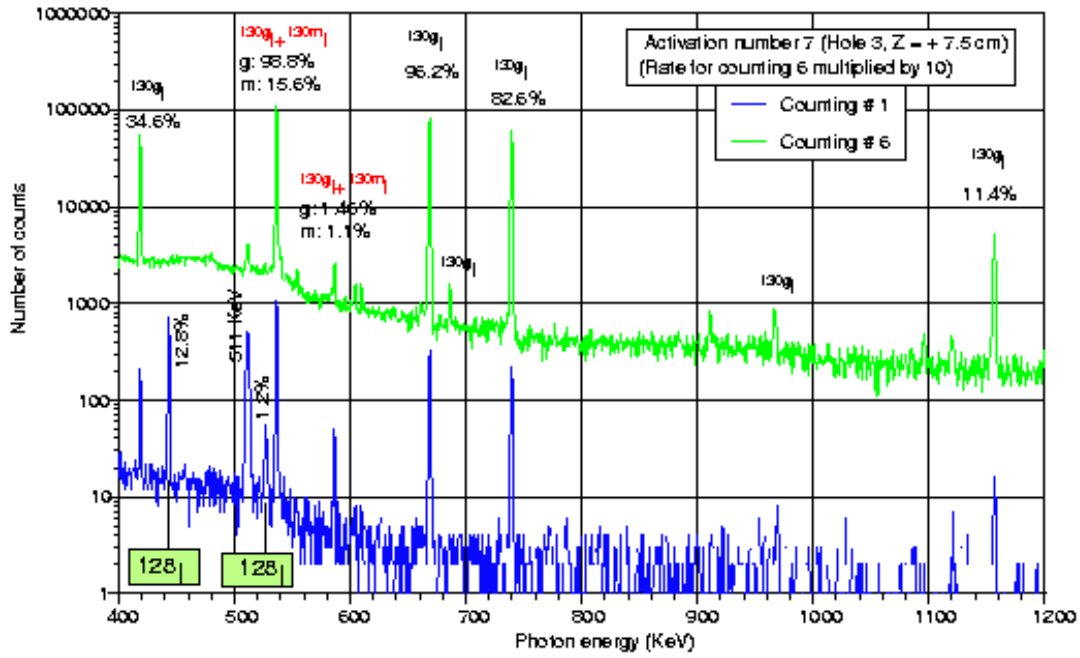

In addition to ^{129}I, the sample whose geometry and characteristics are shown at Figure 19, contains the stable isotope ^{127}I and, in consequence, ^{128}I is also produced during the irradiation. Figure 20, shows two photon spectra obtained from the PbI_2 sample after irradiation. The bottom one, correspond to a short counting taken shortly after irradiation and include the contribution from the ^{130m}I ($t_{1/2}$ = 9 min). In the upper spectra, taken several hours later, the contribution from ^{130m}I is negligible and all the peaks are only populated by ^{130g}I, with a half-live of 12.36 h. Using several counting measurements at different times after irradiation it was possible to compute the production probability of each isomer of the ^{130}I in the neutron capture by ^{129}I. There is very little experimental information on this parameter and certainly no previous data for the TARC neutron spectra.

Figure 21 **Ratio of ^{130m}I/^{130g}I production in the ^{129}I transmutation measured at TARC (a) and comparison with previous values of this parameter (b)**

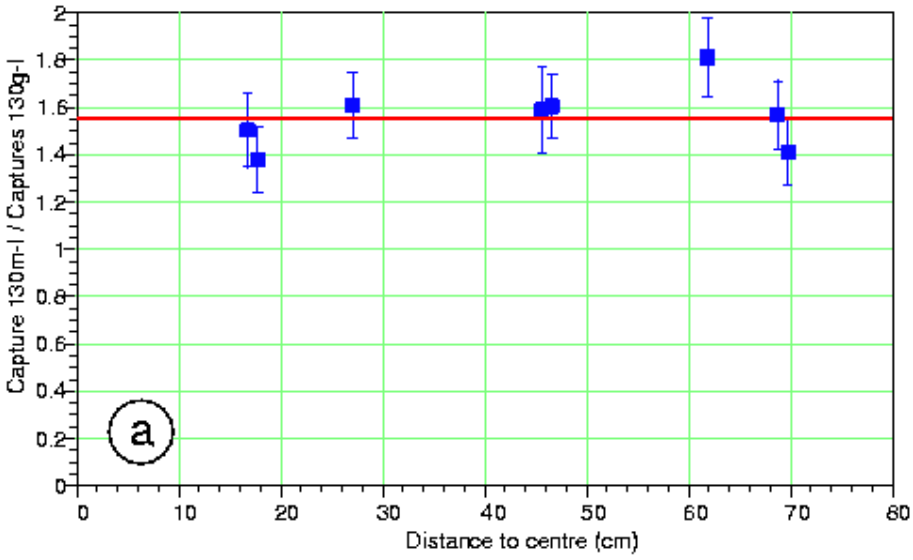

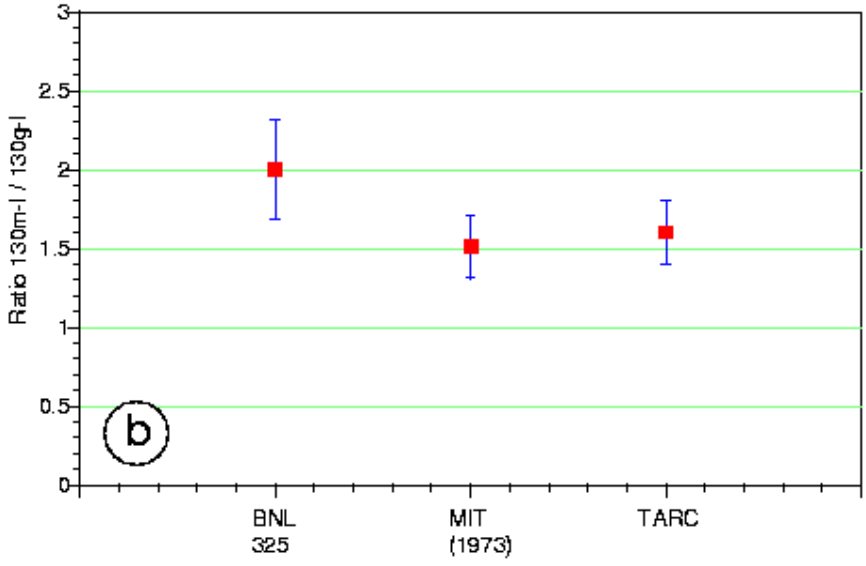

Figure 21a shows the values obtained for this parameter in irradiations performed at different positions inside the lead block. All the data is consistent with a constant value of $^{130m}I/^{130g}I = 1.55$, that, as can be seen at Figure 21b, is in good agreement with the only 2 previous data available, to our knowledge, from MIT [12] and BNL [13].

Using this value of the isomers production ratio, it was possible to compute the absolute ^{129}I transmutation rate. Figure 22a shows the dependence of this transmutation rate with the position of the sample for a kinetic energy of the protons in the beam of 2.75 GeV. The shape of this curve is similar to the one obtained for ^{99}Tc, the systematic error 10% is also similar, but the absolute transmutation rate value is 2.5×10^{-5} per 2.75 GeV proton, for a sample with 64.7 mg of ^{129}I placed at 45 cm from the lead block centre, is smaller than for the ^{99}Tc, taking into account the different masses of the samples. Finally, Figure 22b presents the ratio between the measured data and the Monte Carlo simulations. As in the ^{99}Tc case, an excellent agreement is found validating both the simulation program and the used nuclear data libraries. Further details on the ^{129}I transmutation measurements can be found at [14,8,9].

Figure 22 **^{129}I transmutation rate, for a sample with 64.7 mg of ^{129}I and protons with 2.75 GeV kinetic energy, as a function of the irradiation position (a), and ratio data/Monte Carlo (b)**

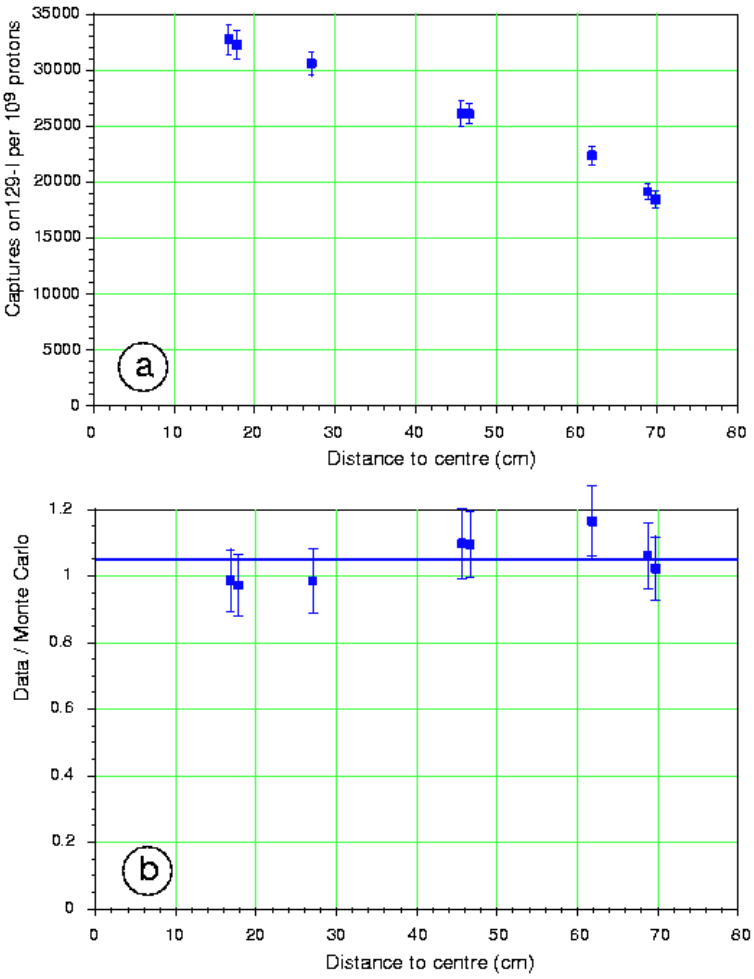

Conclusions

The TARC experiment has performed a comprehensive set of measurements for the characterisation of the neutronics in lead and of the adiabatic resonance crossing method for transmutation of long lived isotopes. I this last respect, a large set of direct measurements of the transmutation rates of ^{99}Tc and ^{129}I has been obtained at different irradiation positions inside the TARC lead block, corresponding to different neutron flux energy spectra. These spectra are similar to the ones foreseen for the EA reflector zone where the transmutation of those isotopes could take place. The special efforts on the setting up and analysis of the experiment has allowed to achieve a complete control of systematic effects and absolute resolutions close to 15%.

The TARC experiment do not correspond to the optimum situation for transmutation of these isotopes, however it has demonstrated the adiabatic resonance crossing principle, whose corollary is that the neutron cross section resonances can be used to improve the transmutation efficiency for these isotopes. In addition, because of the excellent agreement between the experimental data and the simulation, the TARC experiment has validated both the Monte Carlo program and the nuclear data libraries used to simulate the experiment, within the experimental resolution. These validated tools can be used to design specially optimised transmutation devices, either for specific isotopes or for isotope families, taking into account all the requirements of each installation.

Acknowledgements

The enthusiastic and professional support from CERN, in particular from the PS and TIS Divisions and the ECP group, that made possible the experiment are greatly appreciated. We would like to thank the DGXII of the European Union for their financial support, and to express our acknowledgement to the other funding institutions: Centre National de Recherche Scientifique and IN2P3 in France and Empresa Nacional de Residuos Radioactivos S.A., Comisión Interministerial de Ciencia y Tecnología and the Agrupación Eléctrica para el desarrollo de la Tecnología Nuclear in Spain.

REFERENCES

[1] Rubbia *et al*., *Conceptual design of a fast neutron operated high power energy amplifier.* CERN/AT/95-44 (ET), (1995).

[2] Gonzalez *et al*., Update of the TARC experiment results. Presented at the *Technical Committee Meeting on Feasibility and Motivation for Hybrid Concepts for Nuclear Energy Generation and Transmutation* organised by IAEA at CIEMAT. Madrid, 1997.

[3] P. Pavlopoulos *et al., Low Energy flux Measurements (at TARC).* Workshop on P&T strategy studies and transmutation experiments. Karlsruhe, 1998.

[4] Gonzalez *et al*., *High energy flux measurements and high energy neutron studies (^{3}He ionisation, fission measurements, (n,2n) reactions on ^{12}C and ^{232}Th and temperature measurements).* Workshop on P&T strategy studies and transmutation experiments. Karlsruhe, 1998.

[5] Arnould *et al., Experimental Verification of Neutron Phenomenology in Lead and Transmutation by Adiabatic Resonance Crossing in Accelerator Driven Systems*. Submitted to Physics Letters on Dec. 1998.

[6] Bergmann *et al*., Proceedings 1st Int. Conf. Peaceful Uses At. Energy, 4,135 (1955). L.E. Lazareva et al., J.E.T.P. 29,381 (1955)

[7] F. Carminati *et al*., TARC General Purpose Monte Carlo, CERN/LHC/EET 96-011, (1996).

[8] The TARC Collaboration, Neutron Driven Nuclear Transmutation by Adiabatic Resonance Crossing. To be submitted to Nucl. Instrum. and Meth. (1999)

[9] The TARC Collaboration, Final Report of Contract F141-CT96-009 of the EU in the 4th Framework Program. Neutron Driven Nuclear Transmutation by Adiabatic Resonance Crossing. In preparation.

[10] Abanades *et al., ^{99}Tc Capture Rate Measurements with Spallation Neutrons in a Large Lead Block.* CERN/ET/Internal Note 97-14, (1997).

[11] Chou and H. Werle, J. Nucl. Energy, 27,811. (1973).

[12] *Hopke et al*., Phys. Rev**.** C8 (1973).

[13] BNL 325 Report on ^{129}I neutron capture cross-section (1973).

[14] Andriamonje *et al*., *Measurement of the Neutron Capture Rate on 127-I and 129-I with the TARC Experiment.* CERN/ET/Inertal Note (1997).

THE NEUTRON CAPTURE AND TOTAL CROSS SECTION OF ^{99}TC IN THE RESONANCE REGION

Caroline Raepsaet
CEA Saclay
DRN/DMT/SERMA
91191 Gif-sur-Yvette
France

Franco Corvi
CEC-JRC-IRMM
Retieseweg 1
2440 Geel
Belgium

Alfred Leprêtre
CEA Saclay
DSM/DAPNIA/SPhN
91191 Gif-sur-Yvette
France

Claude Bastian
CEC-JRC-IRMM
Retieseweg 1
2440 Geel
Belgium

Jorge Gonzalez
CEC-JRC-IRMM
Retieseweg 1
2440 Geel
Belgium

Egidio Macavero
CEC-JRC-IRMM
Retieseweg 1
2440 Geel
Belgium

Antonio Brusegan
CEC-JRC-IRMM
Retieseweg 1
2440 Geel
Belgium

Frank Gunsing
CEA Saclay
DSM/DAPNIA/SPhN
91191 Gif-sur-Yvette
France

Claude Mounier
CEA Saclay
DRN/DMT/SERMA
91191 Gif-sur-Yvette
France

Abstract

In order to improve nuclear data for nuclear waste transmutation purposes, measurements of the neutron radiative capture and total cross sections of ^{99}Tc in the resonance region have been performed, using the time-of-flight method at the pulsed white neutron source GELINA of the Institute for Reference Materials and Measurements (IRMM) in Geel, Belgium. A neutron capture experiment has been set up and samples of thickness 0.10, 0.26 and 1.0 g/cm^2 have been measured. For the total cross section, a transmission experiment was carried out on samples of thickness 0.16, 0.44 and 4.0 g/cm^2. For both measurements, the total energy range covered was from 3 eV to 100 keV. The neutron resonance shape fitting programme REFIT was used to derive the neutron resonance parameters. The results up to 2 keV are presented here.

Introduction

During the period of irradiation of the fuel assemblies in the core of a nuclear reactor, noxious waste is produced by fission and activation. In order to reduce the amount of the fission products and minor actinides which could induce very long-term radioactivity, transmutation techniques using reactors (fast or thermal) or hybrid systems are under study. One of the most harmful fission products is ^{99}Tc. Produced in very large quantities in the Pressurized Water Reactors (about 1 ton is extracted per year from spent fuel in France), ^{99}Tc has a very long β^- half-life of 2×10^5 years. It also has the ability to migrate in any kind of material, including the storage glasses, which could, in a worst-case scenario, lead to its release in the environment during long-term storage. But, after neutron capture, ^{99}Tc becomes ^{100}Tc, decaying to the stable isotope ^{100}Ru with a half-life of 16 s. Therefore, ^{99}Tc is a very good candidate for transmutation.

Several measurements of the neutron cross sections of ^{99}Tc have been performed in the past [1-5] concerning limited energy ranges and providing a reduced number of resonance parameters. Two existing evaluations, JEF2.2 [6] and ENDF/B6-r3 [7] have also been considered, containing respectively parameters for 89 resonances up to 1.114 keV and 68 resonances up to 800 eV. As more precise parameters were needed over a wider energy range, new measurements of the total and capture cross sections of ^{99}Tc have been required in the High Priority Nuclear Data Request List [8] of the OECD, from 1 eV to 100 keV, with an accuracy of 5%.

Apart from the transmutation purposes, the improvement of the cross sections of ^{99}Tc is of great interest for the reactivity calculations of power reactors. According to the large quantities produced, its absorption near the end of the fuel cycle is noticeable, specially in the epithermal range.

Experimental details

In the framework of a collaboration between the Commissariat à l'Energie Atomique (CEA, Saclay, France) and the Institute for Reference Materials and Measurements (IRMM, Geel, Belgium), radiative capture and transmission measurements have been performed at the pulsed white neutron source GELINA (Geel Linear Accelerator) of the IRMM. The samples have been made at the sample preparation group of the IRMM. Two sets of measurements have been carried out and the experimental details are given in Table 1.

Table 1. **Experimental details**

Energy range	Low energy measurements 3 → 800 eV		High energy measurements 50 eV → 100 keV	
	Capture	Transmission	Capture	Transmission
Sample thickness (g/cm^2)	0.10 0.26	0.16 0.44	1.0 2.0	4.0
Total acquisition time (h)	250	230	380	450
Mean energy of e^- (MeV)	100		100	
Pulse width (ns)	15		2	
Average beam current (μA)	20		60	
Repetition rate (Hz)	200		800	
Sample composition	$^{99}Tc_4Al_{11}$		metallic Tc	

Capture Set-up

Figure 1. **Schematic view of the capture set-up**

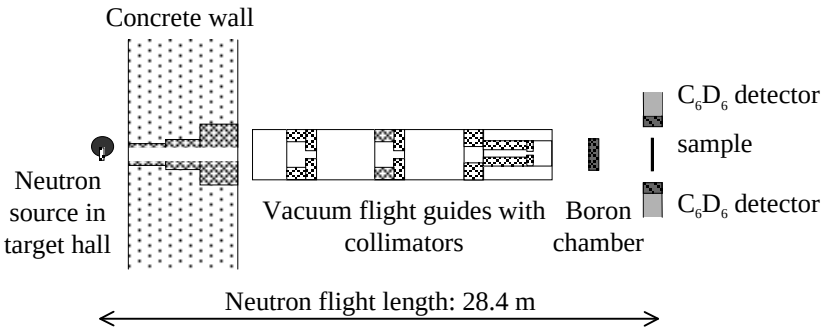

The neutron beam produced by the neutron source was collimated in the evacuated flight tubes before reaching the sample. The prompt gamma rays emitted after the $^{99}Tc(n,\gamma)^{100}Tc$ reaction were detected by two total energy C_6D_6 detectors, placed at 90° on both sides of the sample. At the same time, the incoming neutron flux was measured with a boron chamber placed in the beam before the sample. The efficiency of the capture detectors was made independent of the gamma decay mode using a pulse height weighting method: the experimental weighting function used was determined experimentally at Geel [9,10]. The background on the incoming neutron flux was measured using the black resonance method, placing filters at 10 m from the neutron source. The background on the capture detectors was determined by iterations between the reduction and analysis programmes. The acquisition of the capture data was made in list-mode, using a dedicated package [11] developed at IRMM and complemented with a set of post-acquisition programmes. This post-treatment of the data for each cycle of measurement allows to check possible modifications of the experimental conditions, which could induce systematic uncertainties on the results. It also reconstructs the summed histogrammes from the lists of all the cycles of the whole measurement.

Transmission set-up

Figure 2. **Schematic view of the transmission set-up**

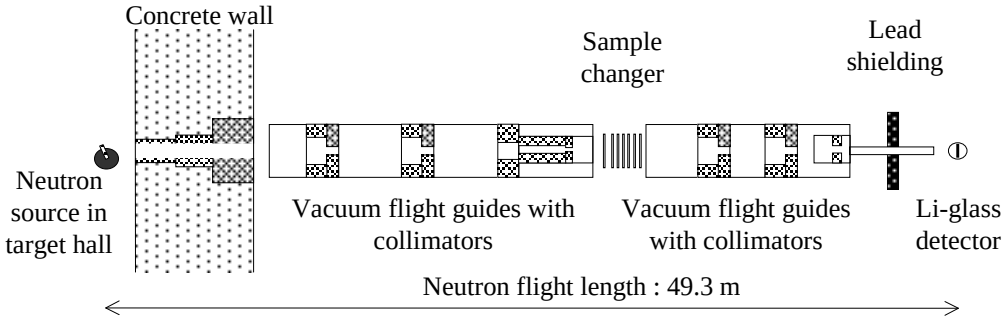

The collimated neutron beam was attenuated by the sample placed at a distance of 23 m from the neutron source. The neutrons which did not react in the sample were further collimated before being detected by a lithium glass, placed at a flight distance of 49.3 m. The transmission set-up is provided

with a sample changer, driven by the acquisition system. Each measurement cycle was composed of four sequences, recorded alternatively in order to reduce systematic uncertainties. In the first two sequences, data were recorded with the sample in and out of the beam. In the two last sequences, filters were added in the beam with and without the technetium sample, in order to derive the background. The acquisition system, from the trademark FAST [12], was used in histogramme-mode.

Data reduction

The experimental data coming from the capture and transmission acquisition systems, composed of different histogrammes and scalers, were combined and corrected for experimental effects. The data reduction package [13,14] used has been developed at IRMM, in collaboration with CEA. It calculates propagation of the uncertainties [15], statistical and correlated induced by the different parameters used at each stage of the data reduction. The spectra, the associated uncertainties and a description of the action performed at each step are gathered in a unique file. The results of the data reduction are the experimental transmission and capture yield, and the total associated covariance matrices.

The dead time correction was applied to the transmission experimental spectra. The backgrounds were determined and subtracted from the spectra with and without the technetium sample in the beam. The transmission is obtained as the ratio of these two spectra. The transmission factor was normalised the flux monitors located in the uranium target hall.

Concerning the capture measurements, the pulse height weighting function was applied to the bi-dimensional C_6D_6 spectra. The histogrammes, after dead time correction and background subtraction, were normalised at present to the capture area determined for the resonances from the transmission experiment.

The results of the capture and transmission measurements are presented in Figure 3 at the end of the data reduction. The capture yield is represented in the upper parts of the graphs for the sample of 1.0 g/cm^2 thickness and the transmission in the lower part for the sample of 4.0 g/cm^2 thickness.

Analysis

The analysis of the data was made with the neutron resonance shape analysis programme REFIT [16], using the least squares method.

Preliminary resonance parameters obtained from the analysis of the transmission data have been used as a starter file for the capture yield analysis and until now, capture and transmission have been processed separately. For each measurement, the different thicknesses were first analysed separately before being processed simultaneously in the common energy ranges.

The systematic uncertainties are still under study. The errors presented in all the tables here are calculated by the data reduction programme, as the result of the propagation of the contribution of the statistical uncertainties and the contribution of the correlated uncertainties induced by the parameters used during the reduction.

Figure 3. **The capture yield and transmission spectra derived from the measurements up to 90 keV, at the end of the data reduction**

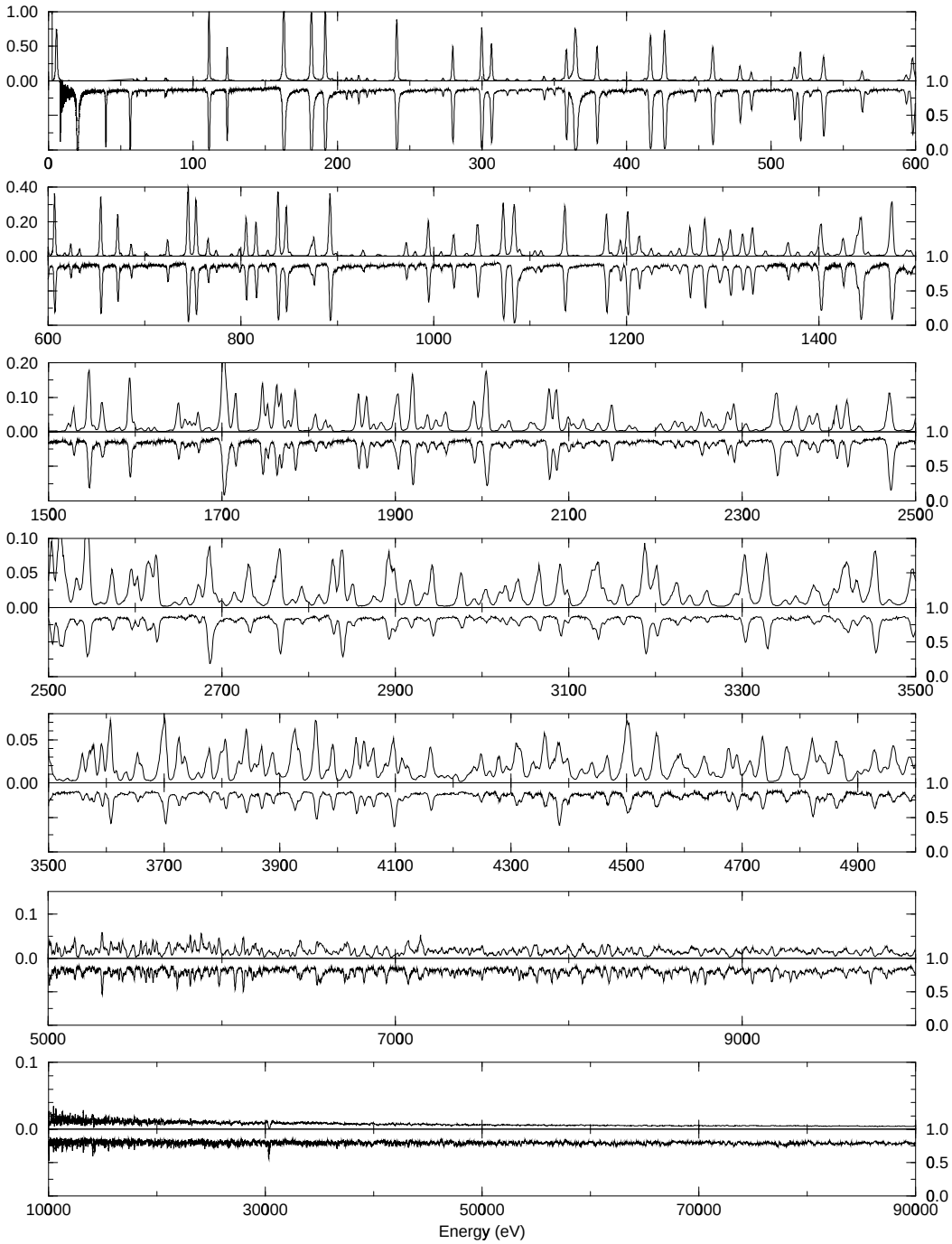

Figure 4. **The capture yield and transmission resulting from the analysis up to 2 keV on the same energy scale**

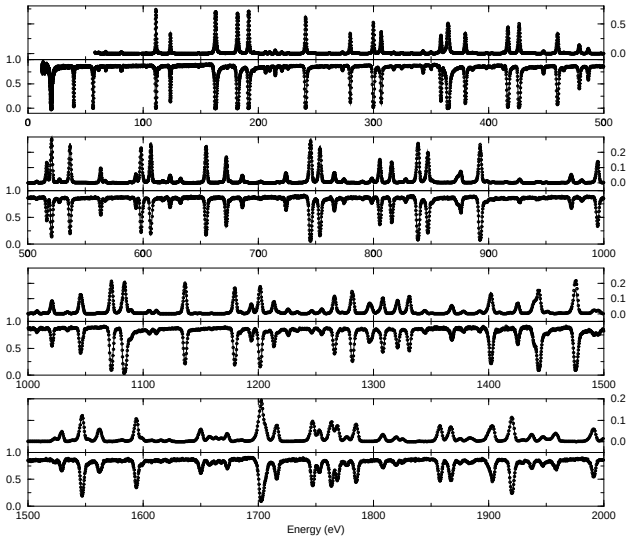

In addition to the capture and transmission study, a measurement of the prompt gamma capture decay spectra was done with a Ge-detector at IRMM, and the spin of 51 *s*-resonances was determined. A parity assignment was also performed to separate ℓ=0 and ℓ=1 resonances up to 1 keV (assuming that higher total angular momentum resonances are not detected in our energy range). The results of these studies [17] have been introduced in the analysis.

Up to 2 keV, capture yield and transmission resulting from the adjustments are shown in Figure 4, for the sample of thickness 1.0 g/cm^2 and 4.0 g/cm^2, for capture and transmission, respectively. The experimental points are represented by small circles with the uncertainty resulting from the data reduction, the result of the adjustment by the plain line.

Figure 5. **Distribution of the adjusted G_g for capture and transmission on *s*-resonances below 200 eV and comparison of the values given in references [1,2,6,7,18] and obtainedfrom the present study**

	$\overline{\Gamma}_\gamma$ (meV)
Watanabe et Reeder [1]	112
Adamchuck et al. [2]	174 ± 8
Mughabghab [18]	160
ENDF/B6-r3 [7]	130
JEF2.2 [6]	160.4
Present study: capture	141.6 ± 11
Present study: transmission	147.4 ± 12

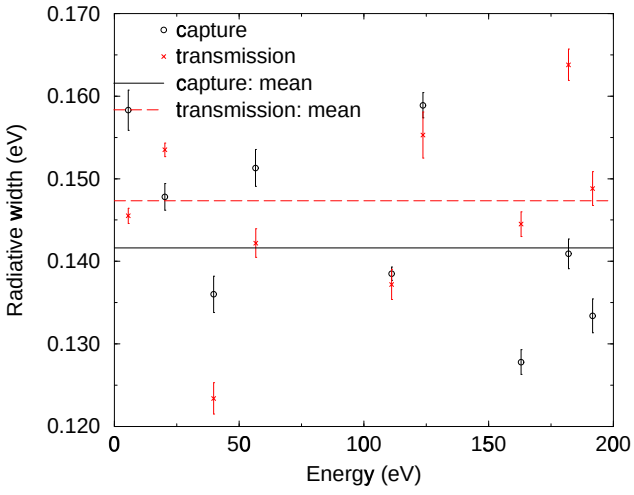

The value of the resolution function, due mainly to the Doppler effect and in a minor part to the experimental set-ups (machine + detectors), allowed us to deduce the radiative width Γ_γ for both measurements, on 9 *s*-resonances below 200 eV. As the distribution of Γ_γ shows little variations in energy, and as the adjustment was not possible for *p*-resonances, which are much smaller than *s*-resonances, the means of the distributions have been assigned to all other *s*- and *p*-resonances. Figure 5 shows the distribution of the adjusted Γ_γ and the mean values for capture and transmission. For both measurements, the dispersion of the distribution is 8%.

Figure 6. **Comparison of the potential scattering radius, for references [6,7,18] and the present study and comparison of the corresponding total cross sections of ^{99}Tc at 300 K**

	R (fm)
JEF2.2	6.00
ENDF/B6-r3	7.91
Mughabghab	6.00 ± 0.50
Present study	7.20 ± 0.30

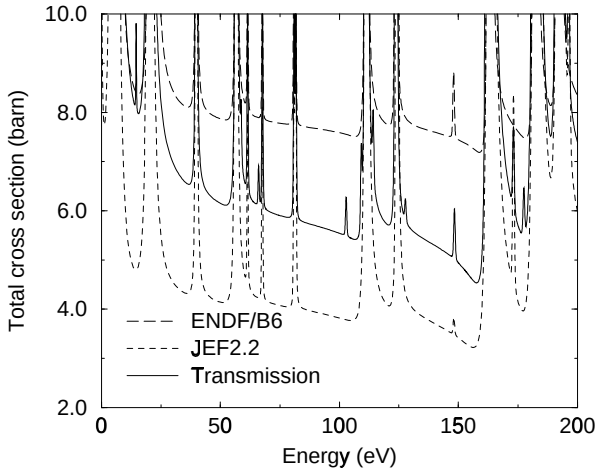

The potential scattering radius was deduced from the transmission measurement of the thickest sample (4.0 g/cm^2). Figure 6 gives a comparison between the values given in the evaluations JEF2.2 [6] and ENDF/B6-r3 [7], and the present study. Our result is situated between the two evaluations. It can be seen on the graph, which shows the total cross sections calculated at 300 K with NJOY for the evaluations and with REFIT for the experimental results. The value of the total cross section between the resonances is very sensitive to the potential scattering.

The high resolution of GELINA allowed to detect small resonances, unreported before. A total of 224 resonances have been fully analysed from the transmission results up to 2 keV. As the capture measurements are more sensitive to small resonances, 245 resonances are reported from the capture measurements in the same energy range. An example of new resonances is given in Figure 7, as a comparison between the capture cross sections calculated with NJOY [19] for the two evaluations [6,7] and from the present results of the transmission measurements.

Figure 7. **Comparisons of the capture cross sections of ^{99}Tc, calculated at 300 K with NJOY [19] for the two evaluations [6,7] and from our results. In the left graph, capture and transmission coincide.**

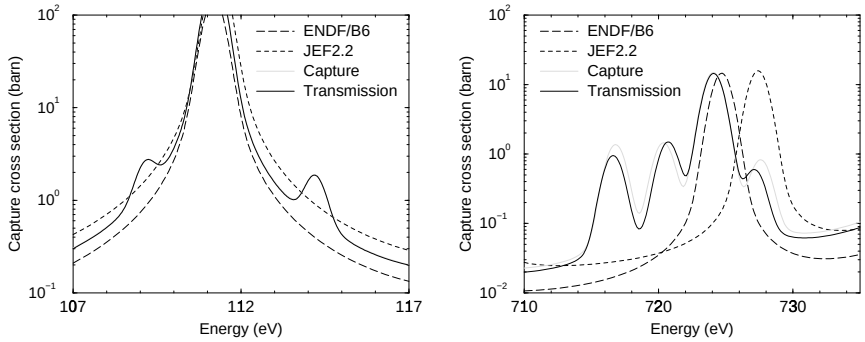

Table 2. **Resonance parameters of the first and second *s*-resonances of ^{99}Tc, from the present work, the evaluations [6,7] and previous measurements [1,2,3,4]**

	First *s*-resonance			Second *s*-resonance		
	E (eV)	$2gG_n^0$ (meV)	G_g (meV)	E (eV)	$2gG_n^0$ (meV)	G_a (meV)
Watanabe et Reeder [1]	5.6	1.84 ± 0.15	134 ± 4	20.3	1.66 ± 0.03	140 ±7
Adamchuck *et al.*[2]	5.6	-	-	21.1 ± 0.02	1.61 ± 0.26	150 ± 30
Chou *et al.*[3]	5.65	1.29 ± 0.36	263 ± 6.5	20.3	1.58 ± 0.41	263.9 ± 9.8
Fischer *et al.*[4]	5.59 ± 0.01	1.45 ± 0.07	171.5 ± 4.5	20.32 ± 0.01	1.49 ± 0.015	176.0 ± 3.9
JEF2.2[6]	5.6175	1.481	177	20.333	1.599	147
ENDF/B6-r3[7]	5.60	1.902	134	21.100	1.611	150
Present analysis: capture	5.5837 ± 0.0007	1.6186 ± 0.02	158.3 ± 2.4	20.272 ± 0.0007	1.7303 ± 0.02	147.8 ± 8.7
Present analysis: transmission	5.5835 ± 0.0003	1.6098 ± 0.007	145.5 ± 0.91	20.273 ± 0.0005	1.6719 ± 0.005	153.5 ± 0.82

The first *s*-resonances of ^{99}Tc, of energies 5.6 and 20.3 eV, are the most important ones. Our resonance parameters are compared to the values of different references [1-4,6-7] in Table 2, and the total cross sections are plotted in Figure 8, for the transmission measurements and two evaluations [6,7]. Concerning the first resonance, the present study is situated between the two evaluations, which presents a large difference in size. Concerning the second one, at 20.3 eV, there was an important discrepancy in the energy and our results seem to be in good agreement with the JEF2.2 data.

Figure 8. **Total cross section of ^{99}Tc at 300 K, obtained with NJOY [19] for the evaluations [6,7] and calculated with the results of the present study**

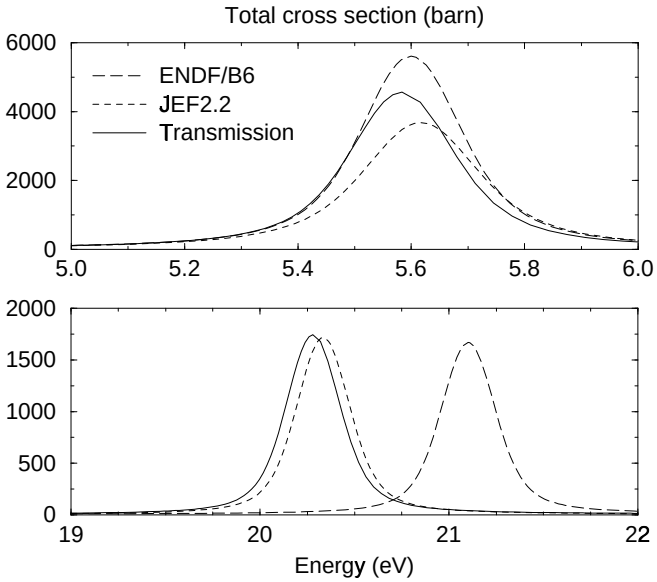

Conclusion and perspectives

The present work adds a considerable amount of consistent information to the existing one. Transmission and capture measurements have been performed on a large energy range and with different sample thickness. The analysis of the experimental data has been made up to 2 keV at the present time and adds a noticeable number of new information concerning the resonance region of ^{99}Tc.

The analysis of both measurements is still going on. Resonances will be resolved for both measurements at least up to 5 keV, probably more. A simultaneous adjustment of capture and transmission measurements will be done, and a new parity assignment will be performed on the resulting resonance parameters. From theses parameters and the results of the measurements, average parameters will be derived in the unresolved range up to 100 keV. At the present time, the systematic uncertainty has not been determined and is not taken into account in the results presented here. A first evaluation shows that, for both measurements, it will be situated between 4% and 5%.

Acknowledgments

The authors would like to thank the following people: J. C. Spirlet (ITU Karlsruhe) for providing the technetium, C. Ingelbrecht (IRMM) for preparing the samples, J. M. Salomé and the LINAC team for their assistance, H. Weigmann, D. Paya and H. Tellier for valuable discussions.

REFERENCES

[1] T. Watanabe, S. D. Reeder, *Nucear Science Engineering*, 41 (1970) 188.

[2] Y. V. Adamchuck, G. V. Muradyan, Y. G. Shchenkin, M. A. Voskanyan, in *Neutron resonance parameters of ^{99}Tc*, report IAE-2335, (1973).

[3] J. C. Chou, H. Werle, *Journal of Nuclear Energy*, 27 (1973) 811.

[4] P. Fischer, U. Harz, H. G. Priesmeyer, *Atomkern. Kerntech*. 38-1 (1981) 63.

[5] R. L. Macklin, *Nuclear Science Engineering* 81 (1982) 520.

[6] C. Nordborg, M. Salvatores, *Status of the JEF Evaluated Data Library*, Proceedings of International Conference on Nuclear Data for Science and Technology, Gatlinburg, Tennessee, United Stattes, (1994) 680.

[7] V. Mac-Lane, *ENDF-201 supplement: ENDF/B-VI summary documentation*, BNL-NCS-17541, supplement 1 (1996).

[8] *The NEA High-Priority Nuclear Data Request List - Status In June 1997*, NEANSC/DOC-4 (1997).

[9] F. Corvi, A. Prevignano, H. Lieskien, P. B. Smith, *Nuclear. Instrum. Methods*, A265 (1988). 475.

[10] F. Corvi, G. Fioni, F. Gasperini, P. B. Smith, *Nuclear Science Engineering*, 107 (1991) 272.

[11] C. Bastian, *IEEE Trans. Nucl. Sci*., 43-4 (1996) 2343.

[12] *Data Acquisition System Manual*, CMTE-FAST Daten System GmbH, Munich, Germany (1990).

[13] C. Bastian, *AGS, A Set of UNIX Commands for Neutron Data Reduction*, *Proceedings of International Conference on Neutrons in Research and Industry*, Crete, Greece, (1996).

[14] C. Bastian, *AGS Manual on The Web*, *http://www.irmm.jrc.be/inf/ags_manual.html*.

[15] C. Bastian, *General Procedures and Computational Methods for Generating Covariance Matrices*, Proceedings of International Symposium on Nuclear Data Evaluation Methodology, New York, USA, (1992) 642.

[16] M. C. Moxon, J. B. Brisland, *REFIT, A Least Squares Fitting Program for Resonance Analysis of Neutron Transmission and Capture Data Computer Code*, version 12TN, UKAEA, Harwell, Great Britain (1991).

[17] F. Gunsing, A. Lepretre, C. Mounier, C. Raepsaet, A. Brusegan, F. Corvi, E. Macavero, L. Zanini, H. Postma, *Investigation of ^{99}Tc Neutron Resonances*, Proceedings of 6th International Seminar on Interaction of Neutrons with Nuclei, Dubna, Russia, (1998).

[18] S. F. Mughabghab, M. Divadeenam, N. E. Holden, *Neutron Cross Section, Neutron Resonance Parameters And Thermal Cross Section, Part A, Z=1-60*, Academic Press Inc., New York, (1981).

[19] R. E. MacFarlane, R. W. Muir, *The NJOY Nuclear Data Processing System, Version 91*, LA-12740-M, (1994).